A STIRLING ENGINE FOR USE WITH LOWER QUALITY FUELS

By

Christopher J. Paul

A DISSERTATION

Submitted to
Michigan State University
in partial fulfillment of the requirements
for the degree of

Mechanical Engineering - Doctor of Philosophy

2014

ABSTRACT

A STIRLING ENGINE FOR USE WITH LOWER QUALITY FUELS

By

Christopher J. Paul

There is increasing interest in using renewable fuels from biomass or alternative fuels such as municipal waste to reduce the need for fossil based fuels. Due to the lower heating values and higher levels of impurities, small scale electricity generation is more problematic. Currently, there are not many technologically mature options for small scale electricity generation using lower quality fuels. Even though there are few manufacturers of Stirling engines, the history of their development for two centuries offers significant guidance in developing a viable small scale generator set using lower quality fuels.

The history, development, and modeling of Stirling engines were reviewed to identify possible model and engine configurations. A Stirling engine model based on the finite volume, ideal adiabatic model was developed. Flow dissipation losses are shown to need correcting as they increase significantly at low mean engine pressure and high engine speed. The complete engine including external components was developed. A simple yet effective method of evaluating the external heat transfer to the Stirling engine was created that can be used with any second order Stirling engine model. A derivative of the General Motors Ground Power Unit 3 was designed. By significantly increasing heater, cooler and regenerator size at the expense of increased dead volume, and adding a combustion gas recirculation, a generator set with good efficiency was designed.

Zu meinem Vater,
Eines Tages, werden wir uns wiedersehen.

ACKNOWLEDGMENTS

I would like to thank my mother and sister. They both provided the support through the years that allowed me to underatake such a journey. This arduous, long journey would have never even begun, were it not for their encouragement and assistance.

I would like to thank Dr. Abraham Engeda. I am grateful for the opportunities that he made possible. Also, he was always able to offer that extra insight and experience to get over the biggest humps.

I would like to thank my guidance committee, Dr. Craig Somerton, Dr. Norbert Müller, and Dr. Wei Liao. I thank them for the advice, constructive criticism, and direction they provided.

TABLE OF CONTENTS

LIST OF TABLES

LIST OF FIGURES

KEY TO SYMBOLS

Symbol	Definition
a	Sonic Velocity
A	Area
bsfc	Brake specific fuel consumption
B_n	Beale Number
c	Empirical constant
C	Courant Number
Cp	Constant pressure specific heat
d	Displacement
D	Diameter
e	Total energy per mass
f	Frequency
f_f	Fanning friction factor
f_r	Reynolds friction factor
F	Force per unit length per unit area
h	Specific enthalpy
K	Loss coefficient
L	Length
LHV	Lower heating value
LMTD	Log-mean-temperature-difference
m	Mass
M	Mach number

n	Empirical exponent
NTU	Number of transfer units
Nu	Nusselt number
P	Static pressure
Pe	Peclet number
Pr	Prandtl number
Q	Heat transfer
r	Radius
R	Gas Constant
Re	Reynolds number
St	Stanton number
t	Time
T	Temperature
u	Velocity
U	Heat transfer convection coefficient
V	Volume
w	Specific work
$\dot{W}$	Power
W_n	West Number
x	Postion

Symbol	Definition
α	Thermal diffusivity
β	Bulk viscosity

γ	Ratio of specific heats
ε	Effectiveness
η	Efficiency
θ	Crank angle
μ	Shear or dynamic viscosity
ρ	Density
σ	Ratio of free-flow area to frontal area
ϕ	Phase angle between pistons
ω	Angular velocity

Subscript	Definition
ω	Angular velocity
a	Appendix gap
air	Air
amp	Amplitude
avg	Average
b	Bend
c	Compression space
CGR	Combustion Gas Recirculation
b	Bend
D	Diameter
e	Expansion space
fuel	Fuel
h	Heater

hyd	Hydraulic
hys	Hysteresis
H	High
in	Inlet
loss	Loss
L	Low
max	Maximum
mean	Mean
mid	Mid-stroke
min	Minimum
new	New
o	Reference
old	Old
out	Outlet
PP	Power Piston
s	Surface
w	Wall
x	Axial

Superscript	Definition
$\dot{}$	Time rate of change
$\tilde{}$	Normalized
'	Per unit length
$\bar{}$	Average

CHAPTER 1

Introduction

1.1 Motivation

Currently there is a lot of interest in increasing the use of renewable fuels from biomass and unconventional fuels such as biogas from waste and garbage as alternatives to fossil fuels. Gas or steam turbines are usually employed in large scale generation of electricity, while at smaller scales, internal combustion engines, whether compression or spark ignition, are often employed. They all operate acceptably well at higher temperatures that fossil fuels can reach. At lower temperatures and smaller scales the advantages of these modes of generation are significantly diminished. Additionally, they are more susceptible to problems caused by the particulates generated by the use of unconventional fuels. An external combustion engine such as the Stirling engine offers the ability to use lower quality fuels without these drawbacks. Lower quality fuels are fuels that have higher levels of impurities and poorer combustion characteristics.

1.2 Small Scale Electrical Generation

There are many ways to produce electrical power. At large scales, conventional steam and gas turbines are used with a wide variety of fuels such as coal and natural gas. Alternative sources of fuel can be used with steam turbines since the combustion system is separated from the turbine working fluid, water or steam. Internal combustion gas turbines can be used with clean burning alternative fuels or fuels that have been gasified or liquefied. Externally fired gas turbines can be used where fuel gasification is impractical by employing a secondary combustion cycle similar to the combustion system used with a steam turbine. A high temperature heat exchanger is then used to transfer the heat to the working fluid of the primary cycle. (Ferreira and Pilidis, 2001)

Small scale generation of electricity can be done in many different ways. (Gaderer *et al*, 2010) Table 1.1 lists some of the possibilities for use with biomass. The highest efficiencies are for those systems where the fuel is gasified: piston engine, internal combustion gas turbine and fuel cells. The efficiency of the externally fired gas turbine is comparable to the gasified, internal combustion gas turbine. If the fuel cannot be gasified easily, e.g. waste, there are four choices: organic Rankine, steam piston, Stirling engine and externally fired turbine. Limiting the size to 25 kWe, leaves few good choices that have extensive availability and operational experience. While current availability and operational experience with Stirling engines is minimal, Stirling engines or “regenerative hot-air piston engines” do have a strong history to build on. See for example Finkelstein, 1959 and Hargreaves, 1991. Additionally, many of the technical advancements in internal combustion piston engines can be incorporated into Stirling engines since they share many features.

	Size (kWe)	Efficiency based on fuel LHV (%)	Availability and Operational Experience
Organic Rankine	6-2000	10-15	Extensive (> 200 kWe)
Steam Piston	25-200	8-14	moderate
Stirling Engine	1-35	5-20	minimal
Piston Engine using gasified fuel	20-2000	10-36	extensive
Turbine using gasified fuel	30-100	8-23	minimal
Externally fired Turbine	50-100	8-25	minimal
Fuel cell using gasified fuel	1-250	20-50	minimal

Table 1.1
Small-Scale Power Production Using Biomass
(Gaderer *et al*, 2010)

1.3 Fuels

There are many different fuels for generating electricity. Large scale electricity generation uses natural gas and coal. At smaller scales, a wide variety of fuels are possible. Fossil fuels include clean burning gasoline, diesel and natural gas. Conventional fuels that are not clean burning are coal and wood. Alternative fuels can be from biomass, such as crop residues or wood waste, biogas from the digestion of waste, or directly burned municipal solid waste. Biogas can have its impurities removed so that it can be used in systems that burn clean fuels. Some biomass may be gasified for use in systems that use clean burning fuels as well. (Easterly and Burnham, 1996)

The alternative fuels that cannot have their impurities removed are such fuels as wood waste, crop residue, municipal solid waste and poor quality coal. Table 1.2 lists the properties of these fuels along with methane for comparison. These alternative fuels are considered to be of lower quality due to their impurity content and lower heating values.

Fuel	Higher Heating Value (kJ/kg)	Lower Heating Value (kJ/kg)	Moisture Content (% by weight)	Ash Content (% by weight)
Methane[1]	55528	50016	-	-
Eastern bituminous coal[2]	30471	-	6.0	9.7
Western subbituminous coal[2]	18655	-	30.4	9.2
Hardwoods[2]	19771	9885	50	2.1
Agricultural[2]	18841	13188	30	5.9
Municipal waste[3]	10467	-	30	36

Table 1.2
Properties of Lower Quality Fuels
[1] Turns, 2000
[2]Easterly and Burnham, 1996
[3]Wiltsee *et al*, 1993

1.4 Application

A possible application of such a Stirling based generator set is the Self-Sustaining Solar-Bio-Nano Based Wastewater Treatment System. (Liao, 2012) This small-scale wastewater treatment system would integrate nano-reverse osmosis and biological treatment to generate potable water from blackwater sources. The energy needed for water treatment would be generated by employing solar-thermal collection and biogas produced from the biological treatment of the blackwater and food wastes. The biogas would supplement the solar-thermal energy, providing continuous water treatment and supply in darkness and inclement weather when solar energy may not be available in sufficient quantity.

One potential user of such a system would be the US Military. This self-sustaining wastewater treatment system would reduce the logistical burden of supplying water to forward operating bases (FOB). Typically 35 gallons of potable water at $50 per gallon are needed per soldier per day with an equivalent amount of generated wastewater to be disposed. A further reduction in the logistical burden would be achieved by using an on-site wastewater treatment system that is energy-neutral.

Figure 1.1 shows the on-site wastewater treatment system and its various components. These components are: solar-dish heat collector, Stirling engine, thermophilic anaerobic digester, biogas storage tank, aerobic clarification reactor, nano-reverse osmosis along with the necessary pumps, generators and control systems. The solar-dish heat collector would employ a focusing solar collector to provide thermal energy to the Stirling engine. The Stirling engine would use the thermal energy supplemented by biogas to drive an electric generator. The thermophilic anaerobic digester would use the blackwater and food wastes to produce the necessary biogas as well as solid and liquid digestate. The solid digestate would further be processed into fertilizer or fuel for combustion. The liquid digestate would be processed by the aerobic clarification reactor into reclaimed water. The reclaimed water would be made potable through nano-reverse osmosis.

Figure 1.2 shows the solar dish heat collector and Stirling engine. The entire assembly rotates to track the sun, with the pivot being the pedestal of the solar magnifier. The Stirling engine is located at the focal point of the solar magnifier. The Stirling engine moves laterally (left/right in Figure 1.2) and vertically (up/down in Figure 1.2) to remain at the focal point of the solar magnifier.

Figure 1.3 shows the energy conversion subsystem. It is composed of the Stirling engine, a compressor, a heat exchanger used as a recuperator, the solar dish receiver, combustor, and fuel pump. Included within the Stirling engine are the alternator, engine heater and cooler and water-to-air heat exchanger.

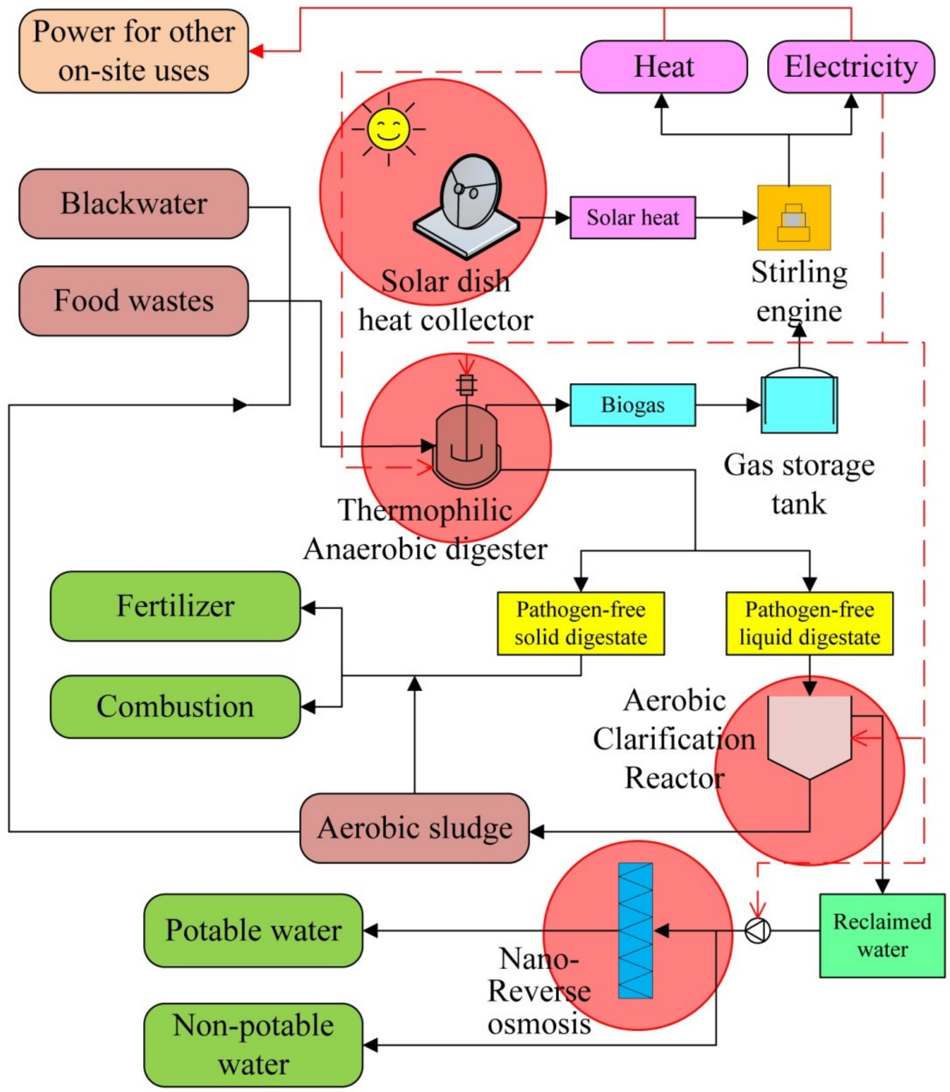

Figure 1.1
Self-Sustaining Solar-Bio-Nano Based Wastewater Treatment System
(Liao, 2012)

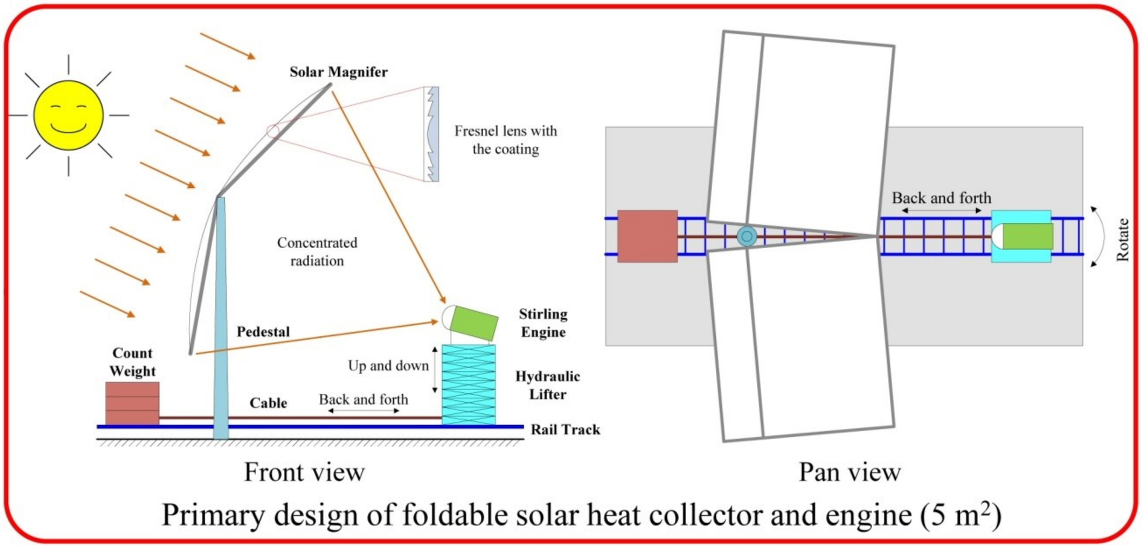

Figure 1.2
Solar Heat Collector and Stirling Engine
(Liao, 2012)

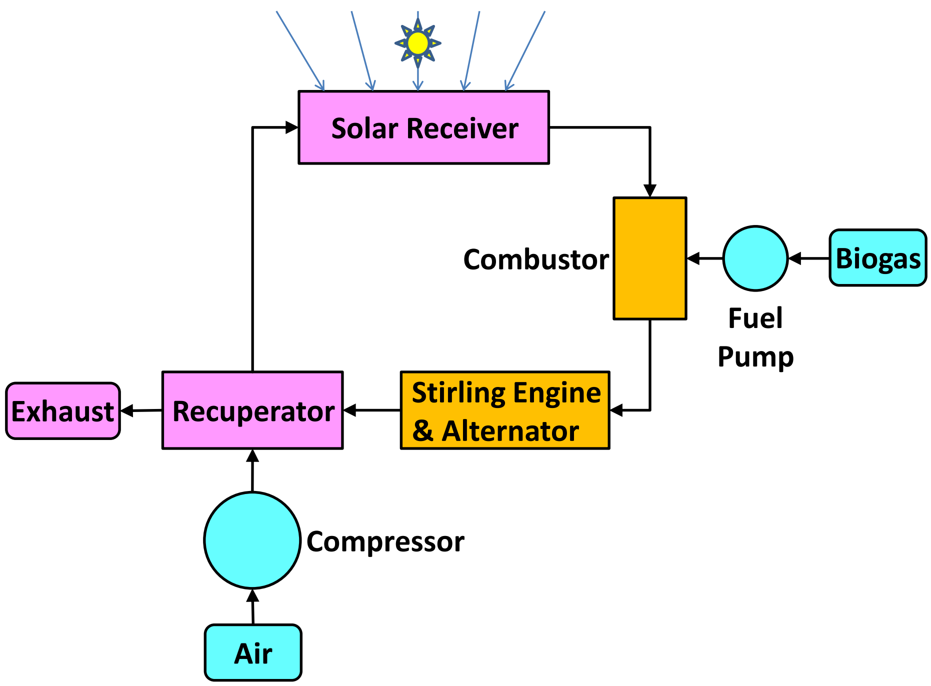

Figure 1.3
Energy Conversion Subsystem

1.5 Objectives

Stirling engines have been around for nearly 200 years, almost 100 years longer than internal combustion engines. Yet, Stirling engine prime movers have not found any commercially viable applications. The sole exception being the Stirling cryogenic cooler, which is the engine reversed. This lack of commercial application is due to three influences. These three influences are the internal combustion engine, the Stirling engine itself and the applications in which the Stirling engine is used.

Firstly, this problem of usefulness is due in part to the internal combustion engine. The internal combustion engine has some advantages over other prime movers. These advantages are ease of use, compactness, and good specific power. Additionally, they are well understood, being readily amenable to scaling techniques based off of well-functioning, built engines. In order to design a good engine, there is no need to resort to design methods that start from first principals. Finally, internal combustion engines are viable as long as there is ready access to petroleum based fuels.

Secondly, the Stirling engine itself is part of the problem. Theoretically, the Stirling engine is simple to understand. Practically, it is another matter. Scaling techniques have defied being applied successfully to Stirling engines. This leaves design from first principals. Even after 40 years of using computer simulations, designing a well-functioning Stirling engine is a minefield of potential problems. The history of Stirling engines is littered with many attempts at building Stirling engines that had inadequate performance. (Hargreaves, 1991)

Finally, most of the applications in which Stirling engines have been used are not necessarily best suited to Stirling engines. As already noted, most of the applications where Stirling engines have been tried, are better performed by internal combustion engines as long as petroleum based fuels are available. Stirling engines are only viable in situations where petroleum based fuels are not easy to obtain logistically. Other types of heat sources being the only source of power make the Stirling engine attractive.

The goal of this research is to develop a small scale Stirling engine based electricity generation system that uses existing, mature technologies, does not rely on high quality petroleum based fuels, and is intended for use in military applications. One such application is part of the self-sustaining wastewater treatment system for forward operating bases. Various fuels maybe used, including biogas, wood, pellets made from other biomass, coal, and garbage. It may also be used with solar heating. The specific fuel would necessitate a unique combustor and possibly a particulate filter. The complete system needs to be truck transportable. This is exactly the sort of application that is best suited to the employment of Stirling engines. In this context, the objectives of this dissertation are to add to the limited body of knowledge in open sources in modeling the systems employing Stirling engines.

This dissertation is concerned with the design of a generator set employing a Stirling engine for use with lower quality fuels. Chapter 2 provides the fundamentals of Stirling engines. Chapter 3 reviews the current state of study in the modeling of Stirling engines and their associated systems. Chapter 4 delves into the methodology to be employed in modeling the Stirling engine and the other system components. Chapter 5 presents the results of validating the Stirling engine and system modeling. Chapter 6 covers the analysis of the complete system. Chapter 7 finishes with conclusions drawn from the results.

CHAPTER 2

Fundamentals of Stirling Engines

2.1 Brief History of Stirling Engines

The origins of the Stirling engine began in 1816 when Rev. Robert Stirling, D.D filed patent No. 4081 titled, “Improvements for Diminishing the Consumption of Fuel, and in particular an engine capable of being Applied to the Moving of Machinery on a Principle entirely New.” The patent describes the machine including the regenerator, its working cycle and prospective applications. The first known engine built was made in 1818 to drive a water pump. Further developments by Rev. Stirling and his brother James resulted in the patents of 1827 and 1840 The three engine patents are described in detail in section 2.4.1.

Stirling engines or more generically, hot air engines became commonplace during the second half of the 19^{th} century. They could be used wherever a source of shaft power was needed, for example to drive a pump. Some of the more notable makers were Bailey, Robinson, Lehman and Heinrici to name a few. A notable addition was made by A.K Rider, when he used two pistons instead of a displacer and piston as used by Stirling. The primary advantages of the Stirling engine over the steam engine of the same era were higher efficiency, less likelihood of explosion, and less water usage. Despite these advantages, the Stirling engine never supplanted the steam engine. The number of configurations, sizes and applications are too numerous to list briefly (Finkelstein, 1959).

The invention and development of the internal combustion engine at the end of the 19^{th} century meant the end of widespread use of other types of engines such as Stirling engines as well as steam engines. Internal combustion engines have the advantages of good power-to-weight ratio and reliability that make them superior to steam and Stirling engines. By the beginning of World War One, Stirling engines were only used in small niche applications such as the paraffin fueled fan, "Kyko" for use in the tropics. Little work was done on Stirling engines between the world wars.

But just before the Second World War began, research into Stirling engines was started at the Physical Research Laboratories at Eindhoven Belgium. Philips was interested in finding a better way to power radios than using batteries. This work led to the development of the first modern Stirling engines. The first experimental high speed Stirling engine, the Type 1, appeared in 1938. It produced 16 W at 1000 rpm. The Type 1 was developed into the Type 3, which was used to drive a fan. Further work on Stirling engines continued through World War Two. One of the best engines was the 1941 Type 10 engine (described in detail in section 2.4.2). A variant of the Type 10 engine was developed to drive an electric generator for small electrical equipment for use in underdeveloped areas using such fuels as kerosene and gasoline. The advent of the transistor and thus lower power requirements made this generator uneconomic. (Hargreaves, 1991)

The development work at Philips on Stirling engines continued regardless. Engines ranging in size from a few watts to a few hundred were designed and built. They were single-cylinder and multi-cylinder engines intended for many different uses, including marine and automotive applications. Some innovative drive mechanisms were also developed such as the rhombic drive and the swashplate. Philips also came up with the Stirling refrigerator by simply driving the Type 10 engine instead of heating it – this resulted in the only commercially successful application of Stirling cycle machines to date. Philips licensed its Stirling technology to a variety of companies. General Motors, Ford, MAN-MWM, United Stirling Sweden (USS), and DAF are the most notable. By 1978, Philips had ceased its work on Stirling engines (Hargreaves, 1991).

The work done by the licensees of Philips has either been terminated or been carried on by in various ways. General Motors and Ford stopped their programs in the late 1970s. United Stirling Sweden worked on Stirling engines through the 1980s. R.J. Meijer, who invented the rhombic drive for Philips, founded Stirling Thermal Motors (STM) in Ann Arbor, Michigan after retiring from Philips. MAN-MWM continued developing Stirling engines until the early 1990s; their last program to develop a Stirling engine for submarines was terminated with the breakup of the Soviet Union (Walker *et al*, 1994).

The USS work has branched into a few areas. Kockums of Sweden (now part of Saab) makes Stirling engines for use in submarines (Saab, 2014). The USS 4-95 automotive demonstration engine was further refined and developed by Mechanical Technology, Inc (MTI) (Ernst and Shaltens, 1997). Stirling Energy Systems (SES), now bankrupt, used a variant of the USS 4-95 engine as part of their concentrated solar power (CSP) dish-Stirling system. Another USS engine, the V 160 has been further developed into the SOLO 161. The SOLO 161 has been used in a different CSP dish-Stirling system, the Eurodish (Mancini *et al*, 2003) and is produced by Cleanergy of Sweden for use in yet another CSP dish-Stirling system (Cleanergy, 2014).

During the 1960s, an alternative to the Stirling engines with drive mechanisms was invented: the free-piston Stirling engine. One of the earliest researchers of the free-piston Stirling engine was William Beale of the University of Ohio. He founded the company Sunpower located in Athens Ohio. Sunpower is one of the leading manufacturers of free-piston Stirling cryocoolers. Infinia, recently bankrupt, used free-piston Stirling engines in its CSP dish-Stirling system as well.

2.2 Stirling Engine Principles

The Stirling engine is an external combustion piston engine, being named after its inventor. A generic name would be “a regenerative hot-gas engine.” The basic working principle of the Stirling engine is simply that a gas expands when heated and contracts when cooled, the difference between the work of expansion and the work of compression can be used to drive a pump, electric generator or another device. Additionally, the Stirling engine can be designed to accept power input and be used in refrigeration or as a heat pump.

Stirling engines have some unique characteristics that make them attractive. It uses an external heat source meaning that a wide variety of heat sources can be used, including gaseous, liquid and solid fossil fuels, nuclear heating, solar heating and biofuels. Low quality fuels can be used because Stirling engines can be made to work on small temperatures differences, as small as 85ºC. (Senft, 1993) Pollution from exhaust gases can be reduced since combustion takes place in a more easily controlled environment. The heat rejected from the cycle is more readily available for use in supplementary systems like cogeneration. The fuel consumption of a Stirling engine may be lower due to the potential to reach higher efficiencies. The operation of a Stirling engine tends to be more silent and have less vibration due to its smoother pressure variations and lack of explosive combustion. (Urieli, 1984)

The Stirling engine also has some characteristics that traditionally have made it more difficult to make it competitive with other engine types, most notably the internal combustion engine. The first problem is the sustained high temperature from the heat source requires the use of materials that have good high-temperature characteristics.

These materials are available, many being developed for gas turbines, but they are prohibitively expensive. The second problem is difficulty in designing adequate seals to keep the fluid contained in the working spaces, while allowing shaft output to pass through. The third problem is the extra complication due to the two heat exchangers and the regenerator. Satisfactory performance of a Stirling engine is directly affected by how well the heat exchangers and, especially, the regenerator function. A Stirling engine with poorly designed heat exchangers and regenerator does not offer any advantage over other engine types. The main design problem of Stirling engines is that they do not scale linearly, making it more complicated to base a new design off of existing, proven designs. Economically, a Stirling engine of comparable power to a diesel engine is nearly twice as expensive to manufacture. (West, 1986)

The Stirling engine is composed of various components. The high-temperature thermal energy is received by one heat exchanger while another heat exchanger serves to reject the waste thermal energy. A third heat exchanger known as the regenerator is used to store thermal energy from the working fluid and return the same thermal energy to the working fluid during different parts of the cycle. There are two working spaces in the engine: one for high temperature expansion and another space for low temperature compression. A minimum of two pistons is necessary. One piston is the displacer that shuttles the fluid between the hot volume space to the cold volume space. The other piston known as the power piston compresses the working fluid or is moved as the working fluid expands. The pistons are usually connected to an output shaft through a kinematic linkage. Finally there is a rigid shell that contains all of the components.

The Stirling engine operates on a closed regenerative cycle, compressing and expanding cyclically the same working fluid, usually a gas. The movement of the working fluid into the compression and expansion spaces is controlled by volume changes due to the movement of pistons. Compression takes place at a lower temperature, while expansion takes place at a higher temperature. The difference in work between the high-temperature expansion and the low-temperature compression results in a net production of work. Thermal energy is supplied from an external source to heat the working fluid, while thermal energy is rejected to the environment to cool the working fluid. (Walker, 1973)

The Stirling thermodynamic cycle is the idealization of the Stirling engine cycle. Figure 2.1 shows the Stirling thermodynamic cycle. As shown in Figure 2.1b, the engine has two opposed pistons in the same cylinder with a regenerator between the pistons. The space to the right of the regenerator is called the compression space and it is maintained at the low temperature of the cycle, T_L. The space to the left of the regenerator is the expansion space at the high temperature of the cycle, T_H. The temperature gradient in the regenerator is assumed linear, from T_H to T_L, left to right. For the purposes of the ideal cycle, there is no conduction, no friction, and no leakage of the working fluid.

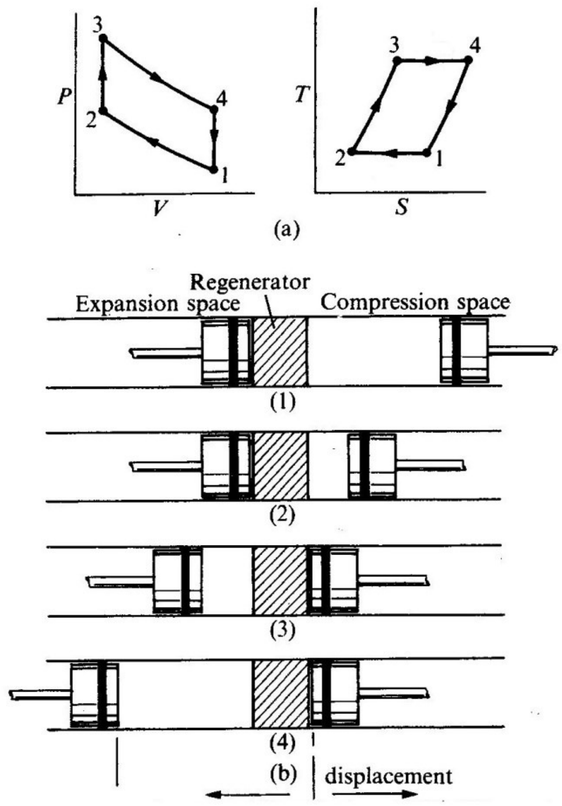

Figure 2.1
The Stirling Thermodynamic Cycle
(Walker, 1973)

The cycle starts at point 1 on the P-V and T-S diagrams of Figure 2.1a that corresponds to piston arrangement (1) of Figure 2.1b. The compression space volume is at its maximum, while the pressure and temperature are at their minimums for the cycle. The compression process 1→2 begins as the right piston moves toward the regenerator while the left piston is stationary. Work input is required to move the compression piston. As the working fluid in the compression space is compressed, the pressure increases, but the temperature remains constant at T_L as heat is removed from the compression space to the surrounds. The compression process stops when the volume reaches the value corresponding to point 2 on the P-V diagram.

The cycle continues from point 2. Process 2→3 occurs as both pistons move at the same velocity to the left, thereby keeping the volume constant. The working fluid is moved from the compression space, through the regenerator, to the expansion space. The fluid temperature increases from T_L to T_H since the regenerator is maintained at T_H on the left and at T_L on the right. The pressure increases due to the increase in temperature with the volume remaining constant. Both pistons stop moving simultaneously once the compression piston meets the regenerator, which is when the maximum cycle pressure is achieved.

The cycle continues from point 3. Process 3→4 begins when the compression piston has stopped, but the expansion piston continues moving to the left. Work is extracted as the expansion piston moves left. The volume increases while the pressure decreases with the temperature being held constant with the addition of thermal energy from the high temperature source. The expansion piston continues to move until the maximum cycle volume is reached as indicated by point 4.

The final part of the cycle continues from point 4. Process 4→1 starts after the expansion space is at its maximum volume. Both pistons move at the same velocity to the right, maintaining the volume between them. The working fluid is shuttled back to the compression space, through the regenerator, from the expansion space. As the fluid at T_H enters the regenerator, heat is transferred from the fluid to the regenerator and enters the compression space at T_L. The thermal energy is stored in the regenerator to be transferred to the working fluid during the next cycle. (Walker, 1973)

The thermal efficiency of the ideal Stirling cycle with a 100% effective regenerator can be shown to be the same as the thermal efficiency of the Carnot cycle, η, i.e.

$$\eta = 1 - \frac{T_L}{T_H} \tag{1}$$

using the same maximum and minimum temperatures, pressures and volumes for both cycles. Figure 2.2 shows the P-V and T-S diagrams for both the Stirling and Carnot cycles.

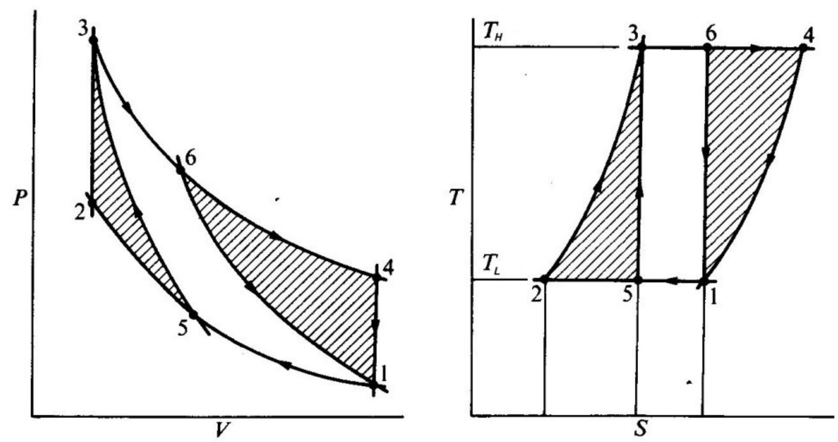

Figure 2.2
P-V and T-S Diagrams for the
Stirling and Carnot Cycles
(Walker, 1973)

The Carnot cycle is composed of processes 1-5-3-6 while the Stirling cycle is made up of processes 1-2-3-4. The heat supplied to and rejected from the Stirling cycle are larger than that for the Carnot cycle. The net work is also higher for the Stirling cycle, but the thermal efficiency is the same. The extra work and heat for the Stirling cycle are represented by the cross-hatched areas of Figure 2.2.

2.3 Stirling Engine Configurations

Stirling engines come in many different configurations, the number of possibilities being limited only by the designer's imagination. Since Stirling engines require at least two pistons, there are a variety of possible piston arrangements. Additionally, Stirling engines can have either single- or double-acting pistons. Besides the difference in piston arrangement, Stirling engines can either be kinematic, free piston, or hybrid. The kinematic Stirling engine uses a mechanical linkage connecting the pistons to the output shaft. The free piston Stirling engine has no direct linkage between the piston and output, whether the output is shaft work or electrical. A hybrid Stirling engine has one free piston and a linkage connected to the second piston. Finally, Stirling engines make use of different working fluids, most notably gases such as air, hydrogen, helium or nitrogen.

The three most common piston arrangements are the alpha, beta and gamma types. Figure 2.3 shows these three common arrangements.

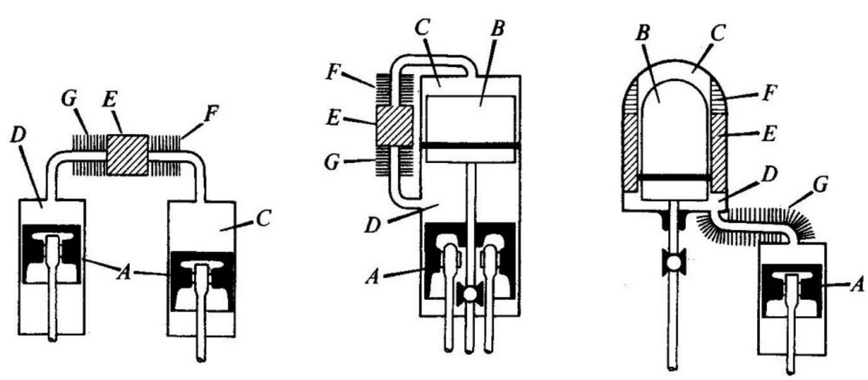

a) alpha b) beta c) gamma

A – piston, *B* – displacer, *C* – expansion space, *D* – compression space, *E* – regenerator, *F* – heater, *G* – cooler.

Figure 2.3
Alpha, Beta, and Gamma Configurations
(Walker, 1973)

Figure 2.3a shows what is known as the alpha engine. The engine of Figure 2.3b is the beta type. Figure 2.3c is the gamma type of Stirling engine. The beta and gamma types use a piston and a displacer. The displacer is a piston that does not have a gas-tight seal. The alpha type uses one piston in the high-temperature space and another piston in the low temperature space. Since the pressure variations of the working space act on only one side of the power piston, they are known as single-acting engines.

There are many more possible arrangements of the pistons and regenerator. Figure 2.4 shows some other possibilities for alpha type engines with the last name of the person most closely associated with that type. Figure 2.5 shows an assortment of beta engines. Figure 2.6 shows some other possibilities for gamma configurations.

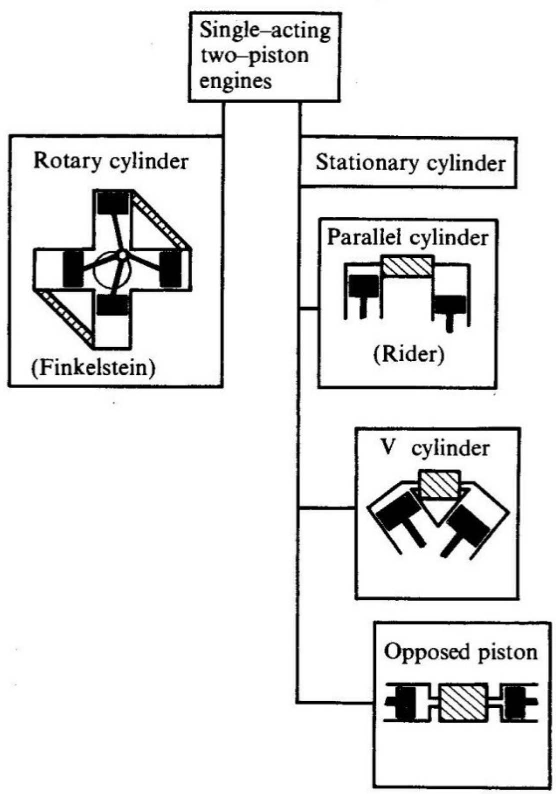

Figure 2.4
Various Alpha Configurations
(Walker, 1973)

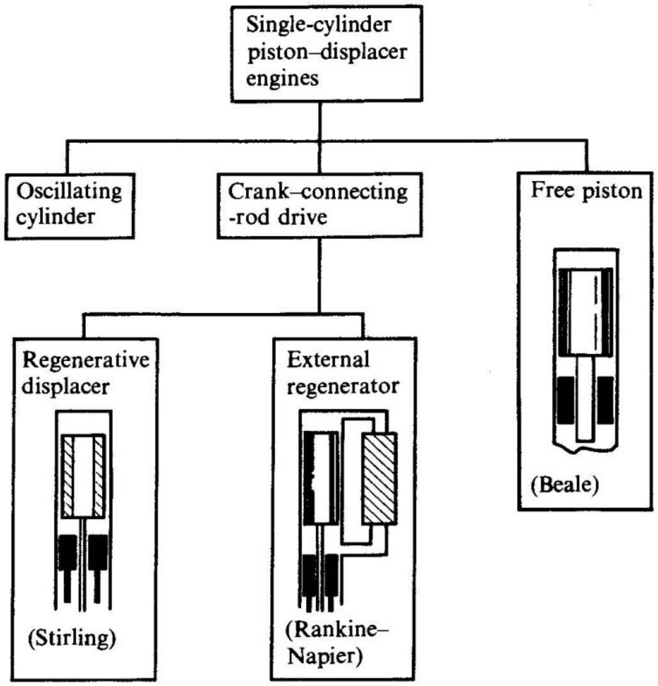

Figure 2.5
Various Beta Configurations
(Walker, 1973)

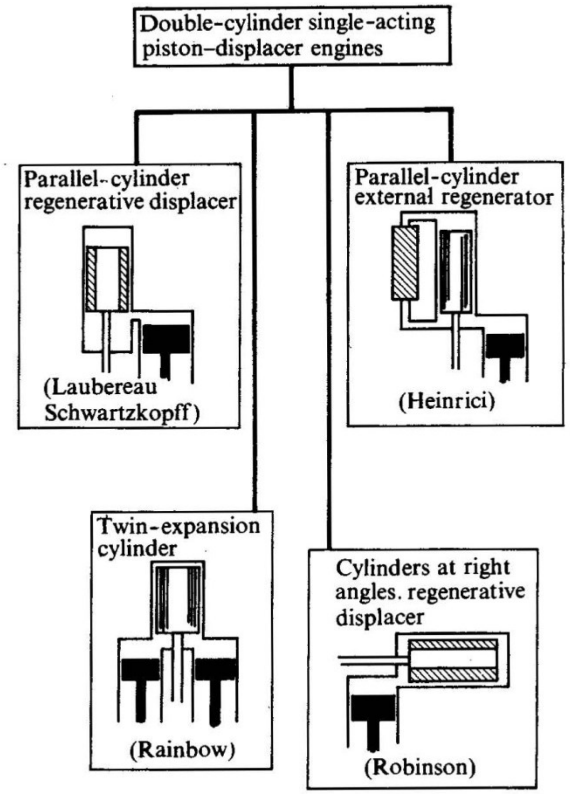

Figure 2.6
Various Gamma Configurations
(Walker, 1973)

Kinematic Stirling engines have a mechanical linkage connecting the piston to the output shaft. The most basic linkage is the simple crank-slider. This linkage is essentially the same as found in an internal combustion engine. While relatively cheap and simple, the crank-slider arrangement creates side-thrust on the piston, increasing friction and wear. Additionally, dynamic balance for single-cylinder engines is not possible. (West, 1986)

A variation of the crank-slider is the offset crank-slider or rhombic drive. Figure 2.7 shows the rhombic drive used with a beta type engine.

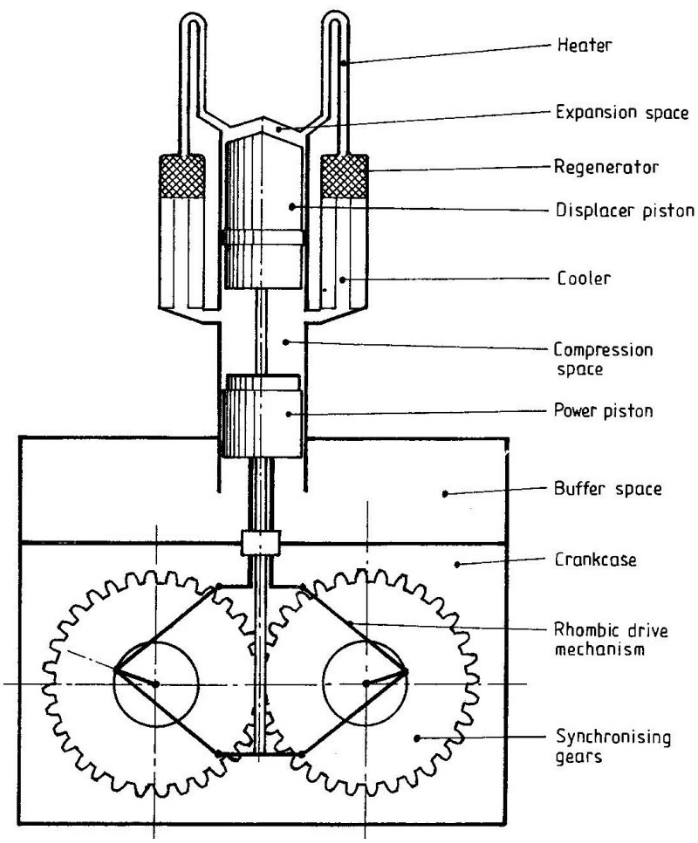

Figure 2.7
Beta Type Rhombic Drive Engine
(Urieli, 1984)

The axes of rotation of the crankshafts are offset from the centerline of the pistons. The effect of the offset is to increase the velocity of the piston in the center of the stroke and to increase the dwell time near the maximum and minimum limits of travel. The result is that the motion of the rhombic drive is not truly sinusoidal. Additionally, a beta type engine with rhombic drive would theoretically produce more power than the same engine using a simple crankshaft with sinusoidal motion. The two-cranks are geared together and counter-rotate, thereby making the engine statically and dynamically balanced. There are no net side forces on the pistons since the horizontal forces from each pair of connecting rods are balanced. This reduces the wear on the piston seal and reduces the complexity of the shaft seal since side-thrust has been eliminated. The major disadvantages are the increased part count, complexity and cost. (West, 1986)

Another type of compact linkage that converts linear piston motion to rotary motion is the Scotch yoke. Figure 2.8 shows an example of an inclined Scotch yoke used in conjunction with a beta type Stirling engine. It has the advantages of being simple and compact and it nearly eliminates side-thrust on the piston. However, friction and wear on the crankpin can be a concern.

Two other types of mechanical linkages that minimize side forces and provide balance are the Ross yoke and the swash plate. Figure 2.9 shows the Ross yoke linkage. The Ross yoke was invented by M.A. Ross in 1977. Figure 2.10 shows the swash plate. The swash plate is an angled circular disc that rotates with the output shaft. Both the Ross linkage and the swash plate have been used with multi-cylinder engines.

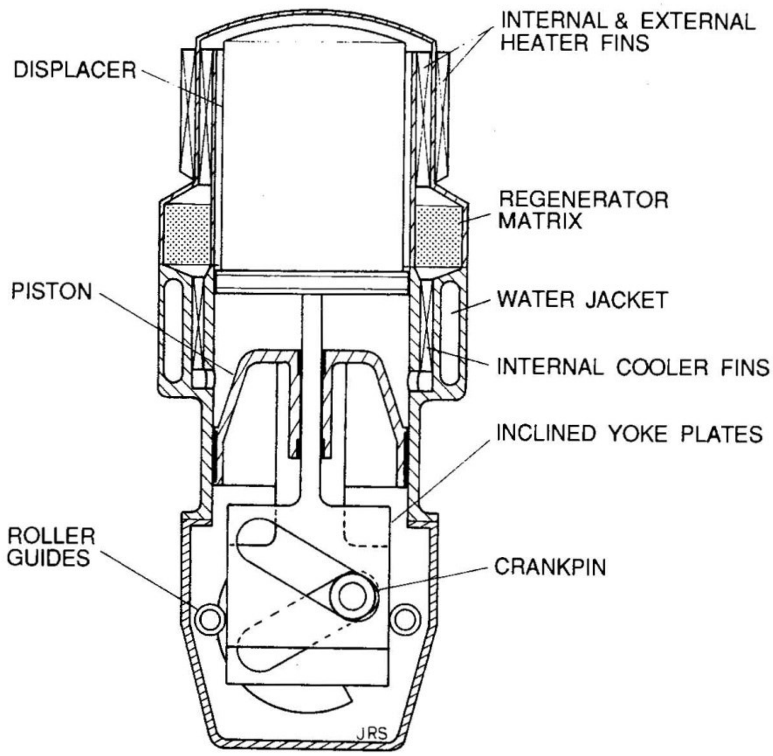

Figure 2.8
Beta Type Stirling Engine with inclined Scotch yoke
(Senft, 1993)

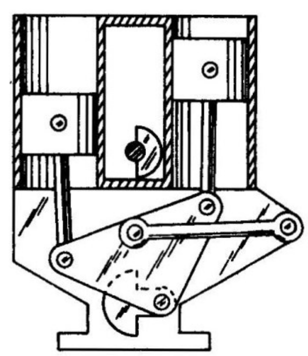

Figure 2.9
Alpha Type Engine with Ross Linkage
(West, 1986)

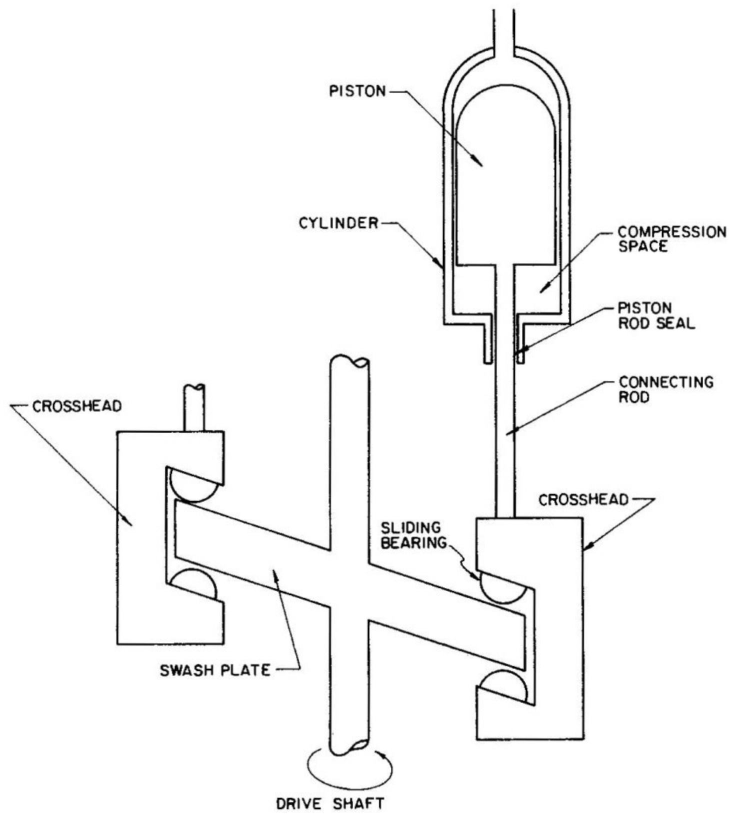

Figure 2.10
Swash Plate
(West, 1986)

Instead of connecting both pistons (piston and displacer) to the same drive mechanism, it is possible to drive the compression piston or displacer independently of the power piston. This configuration known as the Martini displacer was patented by W.R. Martini in 1968. The motion of the compression piston or displacer can be controlled mechanically using a mechanism like a crankshaft and cam or using an electric motor. This makes the Stirling engine essentially a thermo-mechanical amplifier.

In the early 1960s, the free-piston Stirling engine was invented. Figure 2.11 shows a beta type free piston Stirling engine.

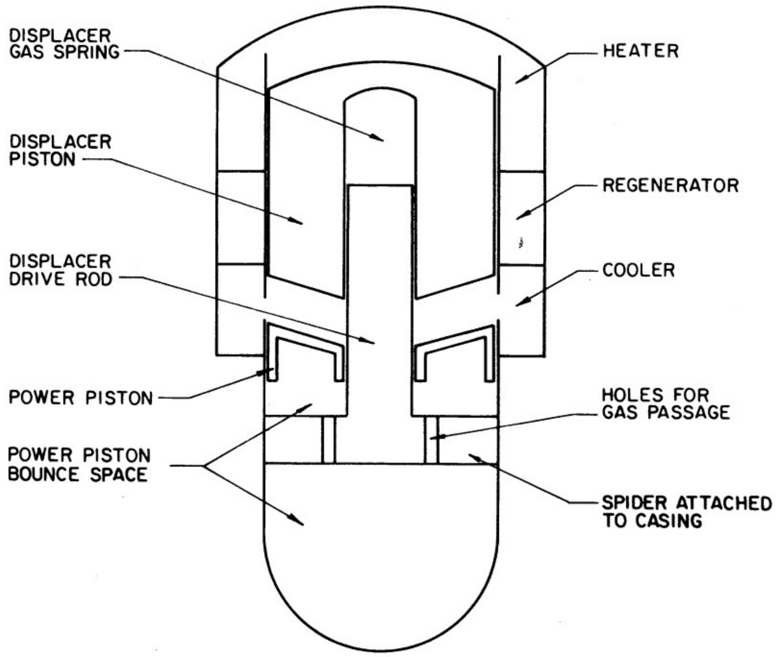

Figure 2.11
Beta Free Piston Stirling Engine
(West, 1986)

The major change introduced in the free-piston variant is that there is no direct link to a drive mechanism. The pistons move solely due to pressure differences. The piston contains a magnet that produces a current in a linear generator. The generator is contained within the pressure vessel, with only electrical connections passing through the pressure vessel. There are several advantages: no lubrication, self-starting, no side thrust on moving elements and no leakage. The two main disadvantages are no direct link to drive machinery and increased difficulty in designing a well-functioning engine. A variant of the free piston engine is the free cylinder engine. The piston is made significantly heavier than the cylinder resulting in the cylinder moving instead of the piston. The free cylinder Stirling engine can be used as a pump.

A combination of a free displacer piston and power piston connected to a kinematic linkage is known as the Ringbom Stirling engine or hybrid Stirling engine. O. Ringbom patented the idea in 1907. Figure 2.12 shows the original engine patented by Ringbom.

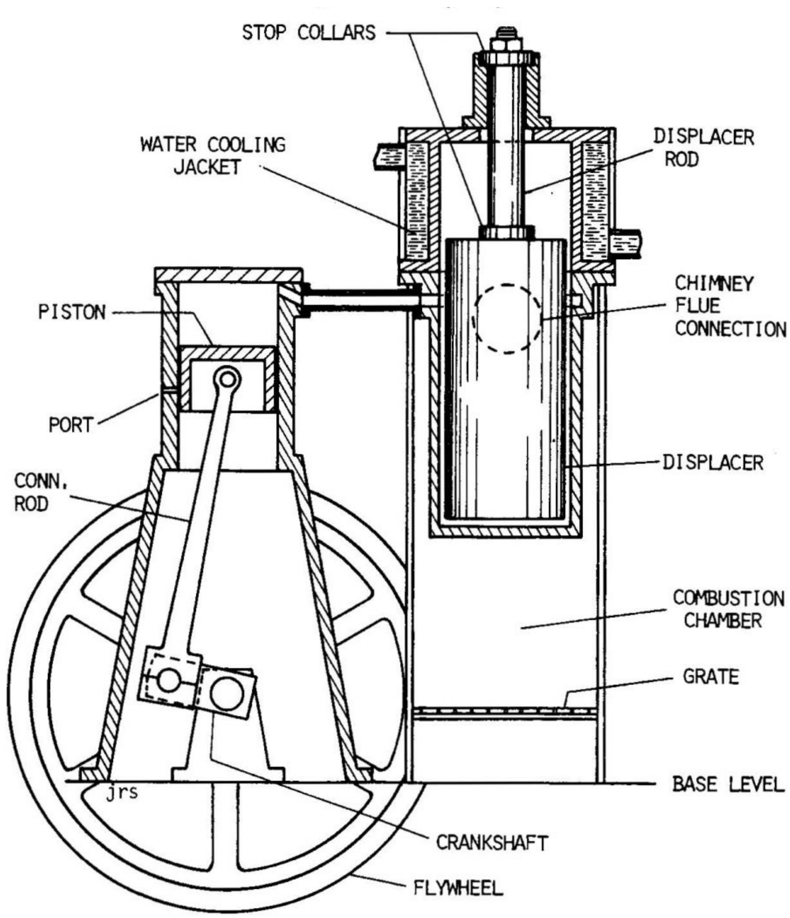

Figure 2.12
Ossian Ringbom's Stirling Engine
(Senft, 1993)

Ringbom's original concept used pressure along with gravity to affect displacer movement. Modern hybrid Stirling engines usually accomplish this by gas pressure alone. They offer the advantages of simpler mechanical design and smaller part count at the expense of more problematic design and a narrow range of operation. (Senft, 1993)

In addition to single-acting alpha type engines, double-acting alpha type engines are also possible, wherein the working fluid pressure acts on both sides of the piston. This increases efficiency and makes better use of multiple pistons. Figure 2.13 shows the two most common arrangements.

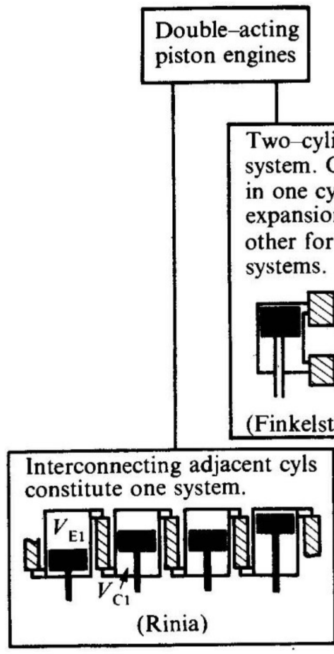

Figure 2.13
Double-Acting Alpha Engines
(Walker, 1973)

They can be used in conjunction with any of the other possible piston and linkage arrangements. The Rinia engine, or Siemens engine, was invented by Philips and has been used in research and development of Stirling engines employed as transportation prime movers where high- specific power is necessary.

Besides the different piston arrangements, various working fluids have been used in Stirling engines. The most common fluids are the gases hydrogen, helium, air, and nitrogen. Both hydrogen and helium are attractive due to the high specific heats and low viscosities, yielding high values of specific-work and smaller overall engines.

Unfortunately, their small molecular sizes make effective sealing problematic. Additionally, specialized equipment is needed for charging of the engine. Hydrogen has the added risk of flammability. Air is a convenient gas to use since no specialized equipment is needed and seals are more straightforward to design. The major disadvantages of air are the lower specific-work and the possibility of auto-ignition in the presence of petroleum based lubricants at high pressure. Nitrogen has all of the advantages of air without the possibility of auto-ignition since no oxygen is present. The only disadvantage is the need of specialized equipment for charging the working spaces of the engine. Attempts have been made to use either liquid or two-phase liquid-gas working fluids, but none have been especially successful.

2.4 Stirling Engine Examples

2.4.1 The Stirling Brothers' Engines

The original Stirling engine invented by Rev. Robert Stirling as described in the patent of 1816 is shown in Figure 2.14. It is a single cylinder beta type using air as the working fluid and employing a Watts type linkage.

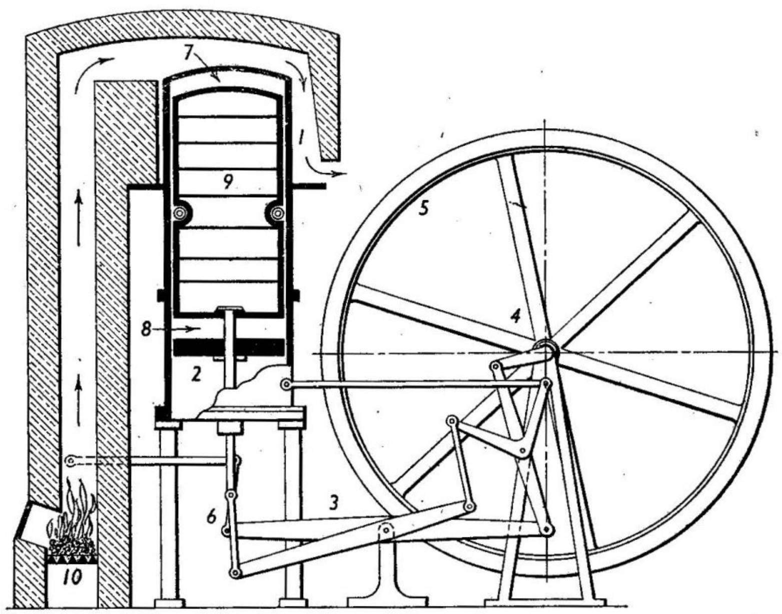

Figure 2.14
Drawing of Stirling's 1816 Engine
(Finkelstein, 1959)

Vertical cylinder (1) contains the working fluid. Piston (2) provides the means of varying the volume of cylinder (1). The mechanism that drives the piston consists of the flywheel (5) mounted on the crankshaft (4). The crankshaft is connected by beam (3) through a Watt's type linkage (6) to the piston. The space in cylinder (1) is divided into a hot space (7) and a cold space (8) by the displacer (9). The displacer has small wheels to keep it centered in the cylinder. The fire (10) provides the heat to keep the hot space (7) at elevated temperatures. Not shown on the drawing was provision for water cooling of space (8). Note that the piston is located in the low temperature part of the engine. The regenerator is located in the annular ring at the midway point of the displacer (9). The regenerator was made of thin wire wound in a spirals around the displacer body, with successive layers crisscrossed at right angles. The displacer (9) is actuated by a push rod that passes through the piston (2). A second beam moved the push rod out of phase with the main beam. Finally, a small cock near the cold space is used to vent to the atmosphere when the engine is running too fast on a light load.

The engine described in the patent was built and installed in 1818 at rock quarry to pump water. The engine was about 10 ft tall and the flywheel was 8 ft in diameter. It was reported to produce 2 hp. A modern analysis of this engine was undertaken by Organ (2000). Based off of the available information, the engine speed is estimated at around 30 rpm. The mean pressure is taken to be 100 kPa. The expansion space (7) temperature is estimated at 570 K while that of the compression space (8) is 303 K. The engine output is calculated to be 0.79 hp instead of the claimed 2 hp. The beta configuration, displacer located regenerator and compact heater and cooler are all beneficial in raising the compression ratio, pressure variation and temperature change.

Development of the original model was conducted by Robert Stirling with his brother James. An early improvement used a pump to increase the pressure of the engine. Other improvements were made and incorporated into further patents registered in 1827 and 1840. As shown in Figure 2.15, the 1827 patent had a stationary regenerator (R) moved to an annular space, not as part of the displacer. The regenerator was made of cylindrical metal sheets. The piston and displacer (D) were located in separate cylinders.

Figure 2.16 shows the 1840 patent. They had noticed in prior experiments that as the end of the displacer piston exposed to the hot fluid heated up, power dropped off. The regenerator (R) and the cooler (C) were moved to a separate enclosure outside of the main cylinder. The combustion flames were applied directly to the heater surface, raising the temperature of the expansion space. This in turn required more cooling capacity, leading to the use of water instead of air for cooling. The displacer was lengthened to reduce conduction losses which had increased due to the higher temperatures. Finally, dead space was minimized by using broken glass as filler. Most of the characteristics of a modern Stirling engine are present. The 1840 patent was used as the basis for an engine built in 1843. It produced 38 bhp at 30 rpm using coal as the fuel. The maximum and minimum cycle temperatures were 600°F and 100°F respectively. (Finkelstein, 1959)

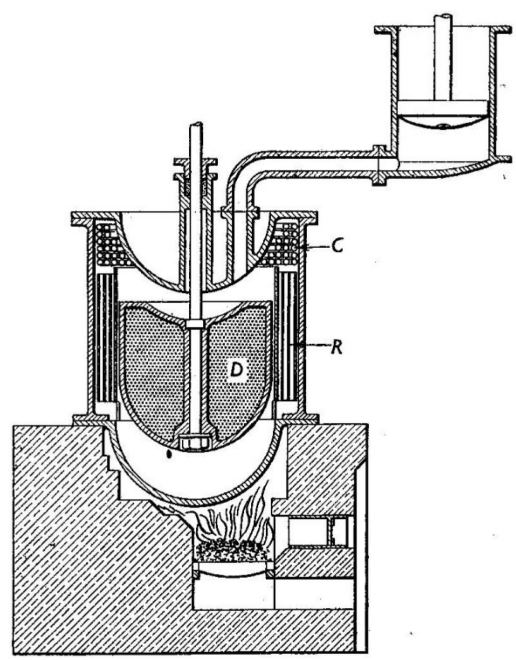

Figure 2.15
Engine Design of the 1827 Patent
(Finkelstein, 1959)

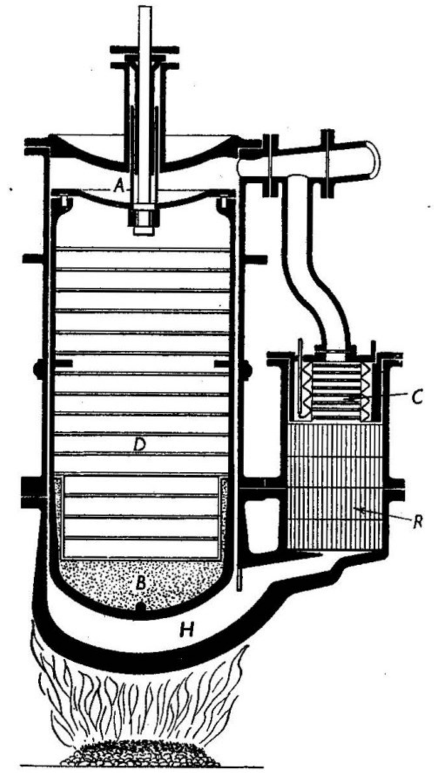

Figure 2.16
Engine Design of the 1840 Patent
(Finkelstein, 1959)

2.4.2 Philips Type 10

The work of Philips led to the development of the first modern Stirling engine, the Philips 1941 Type 10 Engine. Figure 2.17 shows the exterior of the Type 10 engine.

Figure 2.17
Exterior of the Philips 1941 Type 10 Engine
(Finkelstein and Organ, 2001)

From the picture, it has the same appearance and size as an air compressor or as a 2-cycle engine. It has essentially the same configuration as the Stirlings' 1818 engine except that the drive mechanism is incorporated inside of a crankcase. It was about 35 cm tall without the burner. In the picture, the burner is removed. It had a swept volume of 64 cm^3. It produced up to 1.5 hp at speeds of 2000 rpm with pressures around 5 atm running on hydrogen. Its efficiency was about 16%, which is comparable to internal combustion engines of the era.

Figure 2.18 shows a cross-section of the Philips 1941 Type 10 Engine.

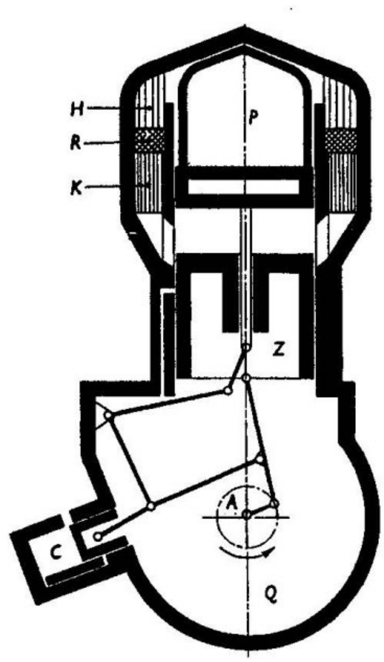

Figure 2.18
Cross-Section through the Philips 1941 Type 10 Engine
(Finkelstein and Organ, 2001)

The top of the cylinder is heated directly by a gas flame. Heat resistant alloy is used to make the thin-shelled dome that is provided with both external and internal fins to enhance heat transfer. The power piston (Z) is located in the bottom of the cylinder that is cooled by a water jacket. The displacer (P) has a thin sheet of nickel-chromium steel to reduce heat transfer losses. The displacer (P) is connected to the crankshaft (A) via a rod that passes through the piston. The heater (H), the cooler (K) and the regenerator (R) form an annular ring around the cylinder. The heater (H) is made of fins while the cooler (K) is a series of tubes going through the water jacket. The regenerator (R) is made of thin wires formed into a matrix. At the bottom of the engine is the crankshaft (A) which is entirely housed by the crankcase (Q). A small air pump (C) maintains the crankcase at the minimum cycle pressure. Leakage can only occur where the output shaft passes through the crankcase. The development of the Type 10 engine led to the MP102C portable generator set. It was rated at producing 200W and was powered by a version of the Type 10 engine. Figure 2.19 shows the complete electric power generator set. 150 sets were produced, but it was too expensive for the market.

Figure 2.19
Philips MP102C 200W Generator
(Finkelstein and Organ, 2001)

2.4.3 General Motors GPU-3

General Motors developed Stirling engines for use in many different applications. Some of these included satellite power generation, a bus prime mover and an electric generator set. The generator set was the Ground Power Unit 3 (GPU-3) developed for the U.S. Army. It was intended to be a silent generator set for use in Vietnam. It used a Stirling engine running on diesel fuel to turn an alternator. The complete GPU-3 is shown in Figure 2.20.

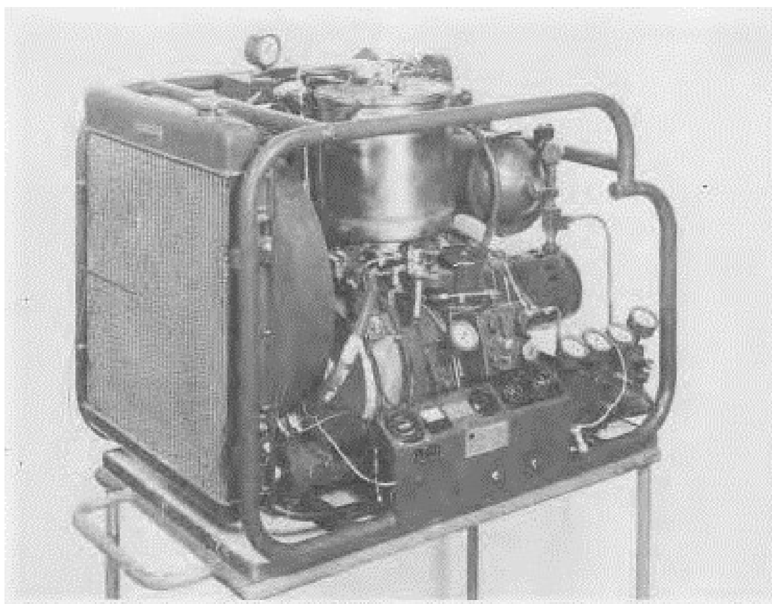

Figure 2.20
General Motors Ground Power Unit 3
(Urieli and Berchowitz, 1984)

The Stirling engine was a beta type, with a single piston and displacer. It is a development of the Philips 10-36 engine. Figure 2.7 shows a simplified cross-section. It used either hydrogen or helium as the working fluid. The pistons were connected to the output shaft via a rhombic drive mechanism. Operating at 3000 rpm on hydrogen, it produced 8 hp from a displacement of 7.175 in^3. A handful of prototypes were built and trialed but it was not accepted into service. After being rejected for service, two prototypes were extensively tested by NASA. As a result, the GPU-3 is one of the best documented Stirling engines that have been made.

2.4.4 Philips 4-235

Philips made a large in-line 4 cylinder Stirling engine called the 4-235. It was intended to be a replacement for diesel engines. Specifically it was to be used as a bus, marine and generator engine. Figure 2.21 shows a cut-away drawing of the 4-235. It is essentially four beta-type engines with rhombic drives combined into a single engine with a common crankcase. Each cylinder has its own fuel system and combustor. It was 1.25 m long and had a mass of 760 kg. Each cylinder had a swept volume of 235 cm^3. It was designed to produce a maximum of 156 kW at 3000 rpm at a mean pressure of 22 MPa. It had a brake efficiency of 26.2% at maximum power; maximum efficiency was 33% at 1300 rpm.

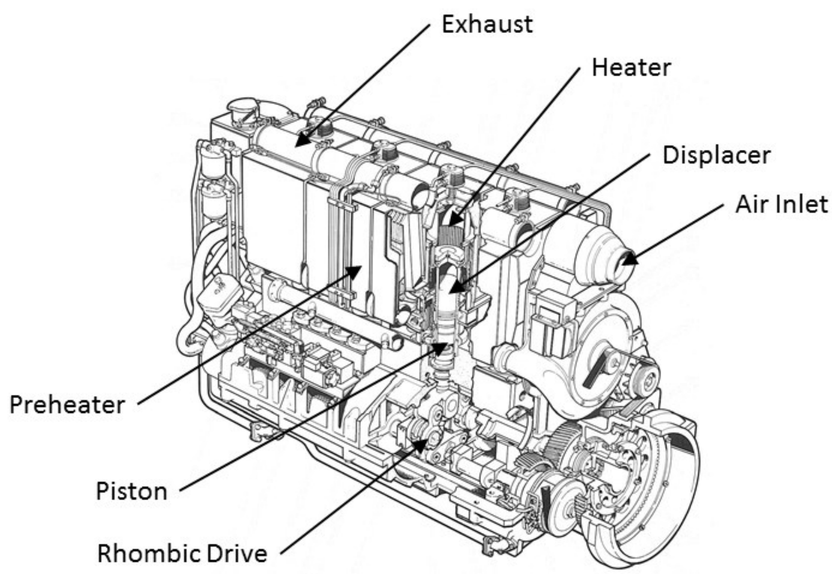

Figure 2.21
Cut-Away of Philips 4-235 Stirling Engine
(Hargreaves, 1991)

2.4.5 United Stirling of Sweden 4-95

United Stirling A.B of Sweden, a licensee of Philips, developed and tested engines intended as transportation prime movers, ranging in power from 40 kW to 150 kW. The 40 kW engine was the 4-95 aka P-40. Figure 2.22 shows the complete engine. It was a four cylinder Rinia configuration using double acting pistons. The pistons were placed in a square arrangement, with the pistons moving vertically. This is a U layout, i.e. a V layout with 0° between the cylinder banks. Figure 2.23 is a cross-section of the engine showing the U layout. The pistons were connected to two geared crankshafts via the crank-slider mechanism. The two crankshafts drove the main drive shaft. Each piston had a swept volume of 95 cm^3. Using hydrogen, it produced an indicated power of 55 kW at 4000 rpm with an indicated efficiency of 38%.

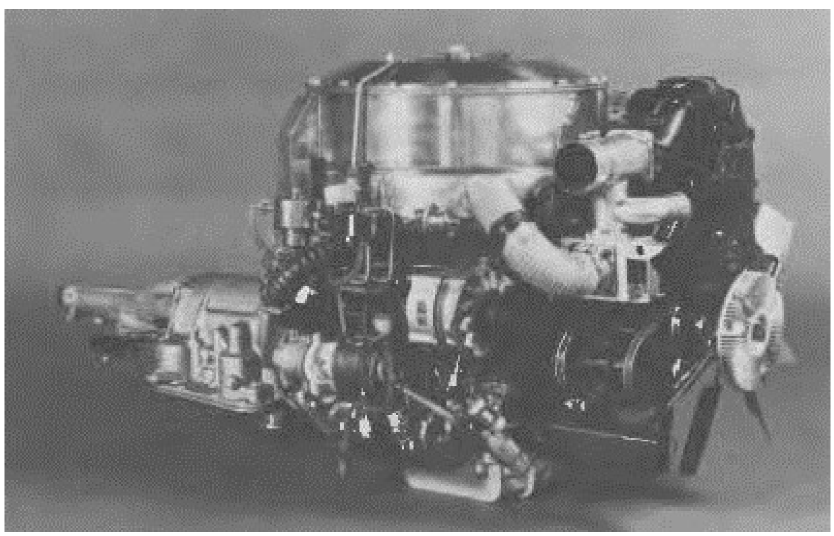

Figure 2.22
The United Stirling of Sweden 4-95
(West, 1986)

Besides being used as an automobile engine, the 4-95 has been used as a submarine power unit, a portable generator set, a heat pump motor and in dish-Stirling thermal-electric converters. (West, 1986)

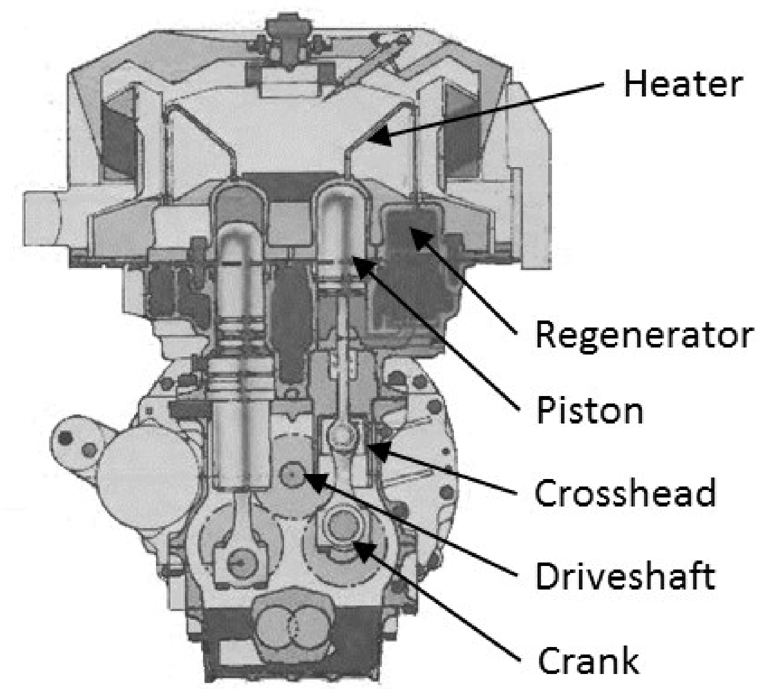

Figure 2.23
Cross-Section of the USS 4-95
(West, 1986)

2.4.6 United Stirling of Sweden V 160/SOLO 161

The USS V160 was conceived as a power pack for use in recreational vehicles, boats and military applications. It is a V alpha type Stirling engine using two pistons. It has been improved and modified for use in CSP systems by SOLO Kleinmotoren of Germany. The latest version produces 10 kW at 1500 rpm using helium. (Baumüller *et al*, 1999) Figure 2.24 shows the SOLO 161 as part of the Eurodish power unit. The engine is orange; the large hollow cylinder is the solar receiver.

Figure 2.24
The SOLO 161 as Part of the Eurodish
(Mancini, 2003)

Figure 2.25 shows a cross section through the engine. Having the two pistons in separate cylinders allows more room and possible configurations for the heater-regenerator-cooler. The alpha configuration also allows the use of the crank-slider-crosshead drive. The crosshead is a second piston that is directly connected to the connecting rod. It absorbs the side forces from the connecting rod and keeps the lubricated part of the drive from entering the compression/expansion spaces.

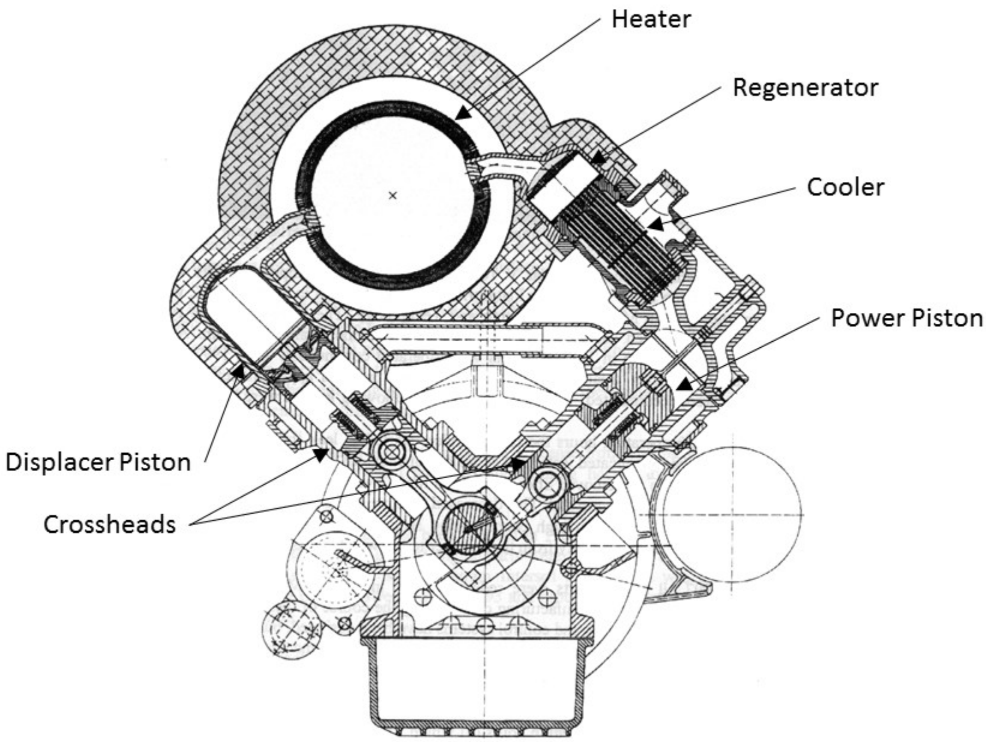

Figure 2.25
A Cross-Section of the SOLO 161
(Baumüller *et al*, 1999)

2.4.7 Sunpower SPIKE

An example of a free-piston Stirling engine is the SPIKE developed by Sunpower. Figure 2.26 shows the Sunpower SPIKE. It is a beta type with a swept volume of 215cm^3. The working fluid is helium. The piston drives a linear alternator which generates electricity. Figure 2.11 shows a simplified cross-section.

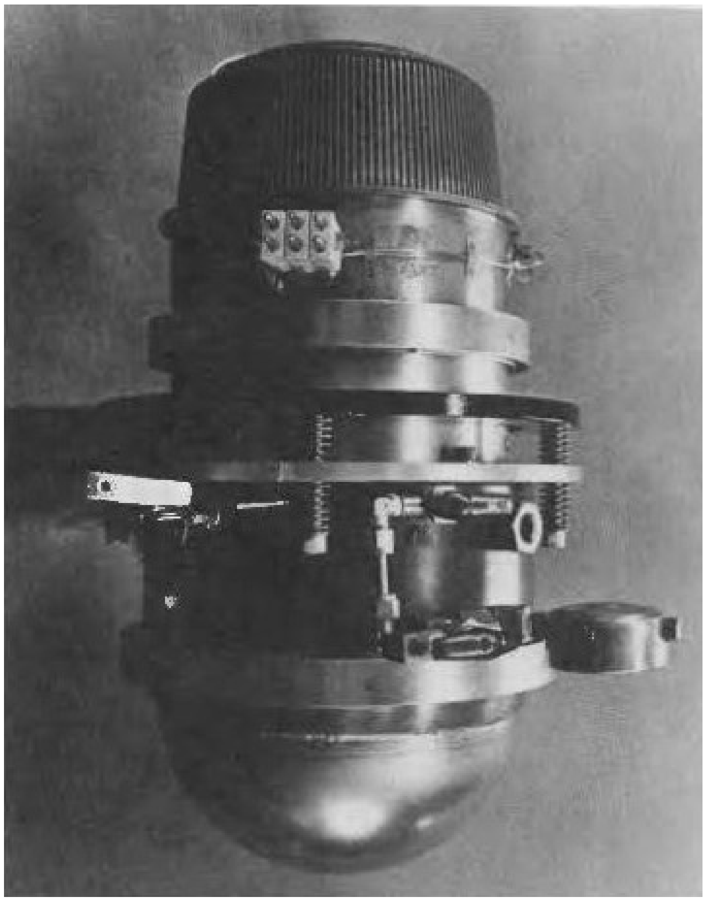

Figure 2.26
The Sunpower SPIKE
(West, 1986)

The SPIKE has an output of 1.3 kW using a heater temperature of 710ºC and a mean pressure of only 0.85 MPa. The SPIKE was powered by both coal and natural gas. The heater, which is located at the top of the engine in Figure 2.26, is an annular design with internal and external fins. This is the same type of design as the Philips Type 10. In contrast, the GPU-3 and 4-95 use expensive tube bundles. The advantages of the annular heater design are that it is cheaper to make and requires a low gas velocity to provide the necessary heat flux. The power to drive the combustion gas is then very low, about 10W for the SPIKE. (West, 1986)

2.5 Stirling Engine Applications

Stirling engines have been tried and used in a wide variety of applications. Stirling engines were used until the internal combustion engine had supplanted it by the beginning of the First World War. Before the First World War, Stirling engines were employed pumping water and providing shaft power to drive machines. (Finkelstein, 1959)

After World War Two, there have been many proposed applications of Stirling engines, but only in a few niches have they been successful. Stirling engines have been developed for use as automotive, bus and truck engines, none of which have been put into production due to economic and technical reasons. Additionally, attempts have been made to use them to drive electric generators, either in portable generator sets, or more recently in CSP dish-Stirling systems, none of which have been economically viable. Similarly to bus and truck engines, they have been tried as marine engines. Here their low noise and high efficiency have made them viable in submarines. Many small Stirling engines have been produced as toys and educational aids. They have also been developed to be artificial hearts. Another successful niche application is for space related applications. The most successful commercial use of Stirling cycle machines has been for reversed engines used as cryogenic coolers. In this role, the Stirling engine is able to achieve temperatures below -200ºC and liquefy gases much more quickly than other types of coolers. Besides liquefying gases, they are used in optical equipment to provide cooling for night vision, missile guidance systems and commercial cameras. (Walker *et al*, 1994)

CHAPTER 3

Current State of Study

3.1 Stirling Engines

The design of a well-functioning Stirling engine has been one of the major roadblocks on the way to the widespread use of Stirling engines. A new internal combustion engine design can be scaled from an existing, proven design in a straight forward manner, without having to resort to the use of fundamental principles. Traditionally, the Stirling engine, on the other hand, has not lent itself to scaling in the same manner. The only proven way of producing a well-functioning Stirling engine is by building, testing and modification. The advent of the computer promised a fairly quick and accurate method of designing a Stirling engine from fundamental principles, but this promise is fraught with difficulties.

Design methods for Stirling engines have been classified using three different levels of sophistication. According to Martini (1983), these are first order, second order and third order analysis, in increasing order of complexity. Walker *et al* (1994) use a more stratified hierarchy to describe the model differences in more detail. The differences are that a zero order analysis (Walker) is the same as a first order (Martini) one. A first order model (Walker) is a second order (Martini) analysis without the decoupled losses. Second order models with decoupled losses and third order ones are the same for both. Third order design methods involve solving the differential equations for mass, momentum and energy simultaneously in three dimensions using numerical methods. They lie outside of the scope of this dissertation.

3.1.1 First Order Models

Following Martini, first order analyses are simple, back-of-the envelope type calculations to get a quick idea of what a Stirling engine may produce. Typically, an ideal power output is calculated, and then multiplied by an "experience factor," to obtain an estimate of actual performance. The experience factor is a pseudo-efficiency, usually based off of the performance of an existing machine.

One way of finding the ideal power can be by doing a thermodynamic analysis of the ideal Stirling thermodynamic cycle as shown in Figures 2.1 and 2.2. The effect of dead spaces and non-ideal regeneration can be included to make it a little more realistic. See Martini (1983), for an in-depth discussion of the many variations. The amount of work per cycle is overestimated since the movement of real pistons almost never matches that of the ideal thermodynamic cycle.

Another way to estimate the ideal power output of a Stirling engine is to use an empirically based equation. One such equation (Walker, 1979) is:

$$\dot{W} = B_n \cdot P_{mean} \cdot f \cdot V_{PP} \tag{2}$$

where $\dot{W}$ = power

B_n = Beale Number

P_{mean} = mean pressure

f = cycle frequency

V_{PP} = power piston swept volume

This equation was based off of empirical data of several well developed engines. A variation of this equation which includes a temperature factor (West, 1981) is:

$$\dot{W} = W_n \cdot P_{mean} \cdot f \cdot V_{PP} \cdot \frac{T_e - T_c}{T_e + T_c} \tag{3}$$

where W_n = West Number

T_e = temperature in heater

T_c = temperature in cooler

Both of these equations take into account the engine's efficiency in the use of either B_n or W_n. Table 3.1 lists West numbers for a sample of Stirling engines. The West numbers are plotted in Figure 3.1. The slope of the dashed line in Figure 3.1 is 0.25, which is used as the standard West number. Similarly the standard Beale number is taken to be 0.15. If the specific type of Stirling engine is known, a more accurate Beale or West number can be used from an existing engine. The West Number correlation is probably the best of the first order design methods.

Engine	Power (W)	Mean Pressure (MPa)	Swept Volume (cm^3)	Heater Temp (°C)	Cooler Temp (°C)	Engine Speed (Hz)	West Number
1843	16000	1.3	316000	340	65	0.467	0.29
102C	480	1.2	67	900	15	26.7	0.37
GPU-3	4200	6.8	120	780	20	25	0.36
4-235	63000	11	940	630	37	50	0.25
4-95	52000	15	540	810	50	66.7	0.18
V 160	10700	13	226	930	50	30	0.24
SPIKE	1300	1.0	314	710	40	63.3	0.13

Table 3.1
West Numbers
(West, 1986)

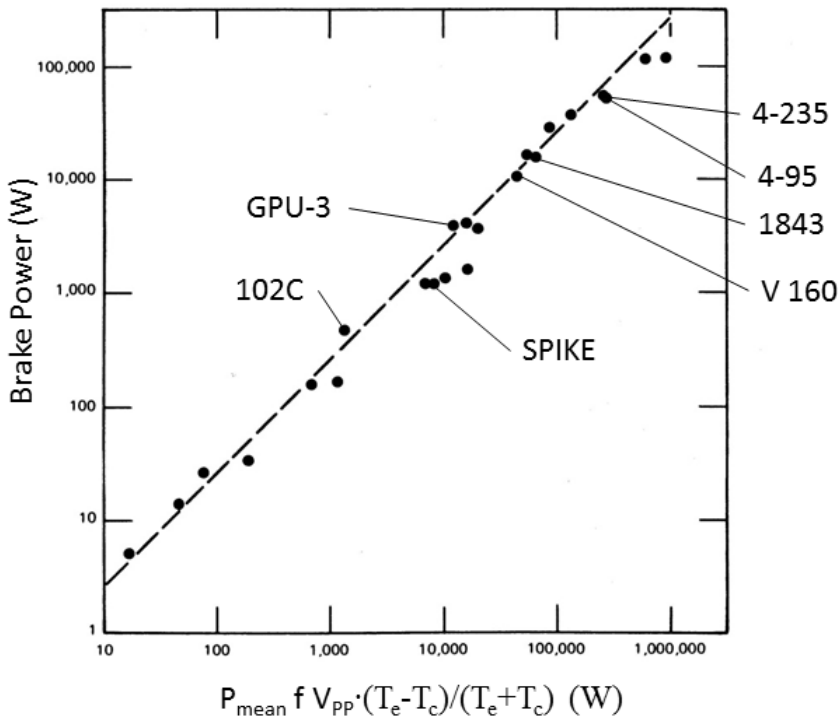

Figure 3.1
West Number Correlation
(West, 1986)

3.1.2 Second Order Models

Second order design methods start with a calculation of ideal power output then subtracting decoupled losses due to fluid friction and thermal shorting, and then subtracting power losses and adding losses to either the heat input or heat rejection. The model for predicting the ideal power is usually more complicated than that used for the first order analysis.

There are many possible methods of determining the power output of a Stirling engine for a second order analysis. The two most common analyses used are the isothermal (Eid, 2009) and adiabatic (Timoumi, 2007). Some others include the quasi-steady (Tlili, 2011), linear-harmonic analysis (LHA) (Choudhary, 2008), and finite-time-thermodynamics (FTT) (Cullen, 2011). More complicated models are 1-D nodal methods such as quasi 1-D compressible (Andersen, 2006) and method of characteristics (MOC) (Organ, 1982). For certain engine configurations, 2-D axisymmetric computational fluid dynamics (Tew, 2001) can be used.

The isothermal analysis is basically a finite volume solution of the mass and energy equations. (Urieli and Berchowitz, 1984) The engine is divided into a minimum of 5 volumes: expansion space, heater, regenerator, cooler, and compression space. Compression and expansion are assumed to take place isothermally, hence the name. The heater and cooler surfaces are assumed to be maintained at a constant temperature. The isothermal model assumes that the gas in each component is at the same temperature as the walls in the expansion and compression spaces, the heater, the cooler and the regenerator. Pressure is assumed constant throughout the engine and mass conservation is maintained. The first realistic analysis developed for a Stirling engine by Gustav Schmidt

(1871) was the ideal isothermal analysis using sinusoidal volume variation. The appeal of the isothermal analysis is that a closed-form solution is available for sinusoidally varying volumes as produced by the crank-slider mechanism. One major negative consequence of the assumption of isothermal working spaces is that the performance of the heat exchangers is not included.

The ideal adiabatic analysis was first developed by Finkelstein, (1960). The adiabatic analysis is very similar to the isothermal except that compression and expansion take place adiabatically. Pressure is assumed to be uniform spatially. The resulting set of equations does not have a closed form solution for any type of volume variation, so a numerical solution is required. The performance of the heat exchangers is included in the adiabatic analysis.

The quasi-steady model is a further refinement of the adiabatic model (Urieli and Berchowitz, 1984). It includes the effects of non-ideal heat exchangers and flow dissipation, i.e. pressure drop. Flow dissipation and finite rates of heat transfer are found using empirical friction factors and heat transfer coefficients. Compression and expansion are again assumed to occur adiabatically. As the name implies, the quasi-steady analysis assumes that the cycle can be divided into increments and that steady-flow conditions prevail during each increment. This significant assumption has not been verified. The major disadvantage of the quasi-steady model is the complexity of the resulting system of equations.

Urieli and Berchowitz (1984) developed a simplified refinement of the ideal adiabatic model that includes the effects of non-ideal heat exchangers. In this simple heat exchanger analysis, the ideal adiabatic results and empirical correlations for friction factor and heat transfer coefficient are used to find the heat transfer rates and pressure drop in the heater, cooler and regenerator. The finite heat transfer rates are used to determine new gas temperatures, and then the new gas temperatures are used in another iteration of the ideal adiabatic analysis. This is repeated until convergence is achieved, typically in a half-dozen steps. The results of this combined ideal adiabatic and simple heat exchanger analysis approaches the fidelity of the quasi-steady model without the complication.

Linear harmonic analysis (LHA) is another variation of the thermodynamic analyses of the isothermal/adiabatic types. The major change for LHA is that volume, pressure, etc. are represented by sinusoids. Nonlinear parameter combinations can be represented by series expansions such as binomial or Taylor's or by Fourier series. The resulting set of equations has a closed form algebraic solution, unlike the isothermal/adiabatic models which require numerical solutions. A simplified power equation using LHA which may be used for a first order analysis (West, 1986) is:

$$\dot{W} = f \cdot P_{mean} \cdot V_{PP} \cdot \frac{\pi}{2} \cdot \frac{V_e}{V_m} \cdot \frac{T_e - T_c}{T_e + T_c} \cdot \sin \phi \qquad (4)$$

where V_e = expansion space swept volume

V_m = total gas volume of engine

ϕ = phase angle between pistons

This equation is valid for a beta type engine with a sinusoidal drive mechanism, i.e. crank-slider.

Finite-time-thermodynamics (FTT) is a development of classical thermodynamics. The ideal thermodynamic cycle is the starting point. Following Cullen (2011), for Stirling engines, the Schmidt analysis is used to calculate the ideal cycle work. A finite time constraint is imposed on heat transfer to and from the system. Within the system, reversibility is assumed. All irreversibility generation of the cycle is assumed at the system heat transfer boundaries. The power from the reversible model is corrected using the loss terms that generate irreversibility. Loss terms include fluid losses, thermal shorting and the effect of non-ideal heat exchangers. Empirical friction factors and heat transfer coefficients are again used to find fluid losses and rates of heat transfer.

The quasi 1-D compressible CFD analysis is a one-dimensional simplification of a full three-dimensional CFD analysis. The quasi 1-D model uses either the finite-volume method or finite difference method of CFD to solve the mass, momentum and energy equations in one dimension. The mass, momentum and energy equations for the finite difference method are (Gedeon, 2012):

$$\frac{\partial(\rho A_x)}{\partial t} + \frac{\partial(\rho u A_x)}{\partial x} = 0 \qquad (5a)$$

$$\frac{\partial(\rho u A_x)}{\partial t} + \frac{\partial(u \rho u A_x)}{\partial x} + \frac{\partial P}{\partial x} A_x - F A_x = 0 \qquad (5b)$$

$$\frac{\partial(\rho e A_x)}{\partial t} + P\frac{\partial A_x}{\partial t} + \frac{\partial}{\partial x}\left(u \rho e A_x + u P A_x + \dot{Q}_x\right) - \dot{Q}'_w = 0 \qquad (5c)$$

where ρ = gas density

u = gas velocity

A_x = cross-section or flow area

A_w = area of wetted perimeter

P = gas pressure

F = force per unit length or per unit area

e = total gas energy per unit mass

$\dot{Q}_x$ = axial heat flux

$\dot{Q}'_w$ = film heat transfer per unit length

Forces, e.g. friction, and heat transfer effects are modeled using empirical correlations since they cannot be explicitly included in the 1-D equations. The quasi 1-D analysis offers the promise of predictions fairly close to the measured performance of engines, without unnecessary complexity or long processing times (Geng, 1992) and (Andersen, 2006). This quasi 1-D compressible CFD model is available in the software Sage which is used by NASA contractors in designing Stirling engines. For example, the Technology Demonstration Converter (TDC) Stirling engine has been modeled using Sage (Demko and Penswick, 2005).

The method of characteristics is a classical method of solving hyperbolic differential equations. The most basic form of this used with fluid mechanics is the application of it to the mass and momentum equations for homentropic flow. Organ (1982) used this method in regards to Stirling engines. The conservation equations used are:

$$\frac{\partial \rho}{\partial t} + \rho \frac{\partial u}{\partial x} = -\rho u \frac{1}{A_x} \frac{dA_x}{dx} \qquad (6a)$$

$$\frac{\partial u}{\partial t} + u \frac{\partial u}{\partial x} + \frac{1}{\rho} \frac{\partial P}{\partial x} = -\frac{f_f}{r_{hyd}} \frac{u^2}{2} \frac{u}{|u|} \qquad (6b)$$

where f_f = Fanning friction factor

r_{hyd} = hydraulic radius (cross-sectional area/wetted perimeter).

Equations 6a and 6b are essentially the same as 5a and 5b. They are recast into compatibility form for solving using velocity and pressure as state variables instead of the traditional MOC gas velocity and sonic velocity. If non-ideal heat exchangers are included, the addition of the energy equation results in a third compatibility equation, usually for entropy along a streamline (Poloni et al, 1987). Putting the conservation equations into compatibility form, changes the partial differentials into ordinary differentials. For 1-D unsteady, homentropic flow, an algebraic solution results. One appeal of MOC is the ability to more accurately predict the flow of information, e.g. pressure, than is possible with a straightforward numerical solution à la the quasi 1-D method. The flow of information in the quasi 1-D method is governed by the Courant-Friedrich-Lowry (CFL) stability criterion:

$$\frac{a + u}{C} = \frac{\Delta x}{\Delta t} \tag{7}$$

where a = sonic velocity

C = Courant number.

Since C is less than one to maintain stability, the propagation of pressure information is a fraction of the ratio of the space-to-time discretization ($\Delta x/\Delta t$).

Loss mechanisms have to be taken into account since these are not included. These losses are determined either from decoupled loss models and then subtracted from the work indicated by the model used to find the ideal power and either added to the heater or cooler as additional heat loads. Martini (1983) discusses this method of dealing with losses and provides many empirical models for estimating the losses. Some losses are conduction in the walls of the regenerator, cylinder and pistons, and heat loss in the regenerator due to non-ideal operation. Fluid losses can be due to friction, sudden contractions and expansions and bends. Since the loss mechanisms are accounted for assuming that they do not influence each other, the losses may very well be overestimated or underestimated depending on the nature of their interactions. The advantage of this method of accounting for losses is that it is easy to see which mechanisms have the most influence on the performance of the engine.

The isothermal/adiabatic/quasi-steady types of models all assume the pressure is uniform, i.e. that the pressure drops in the heater, cooler and regenerator are negligible. This can be justified by examining the momentum equation. The normalized momentum equation is usually given, neglecting gravity and without assuming Stokes hypothesis, as (Potter and Foss, 1982):

$$\tilde{\rho}\frac{D\tilde{\boldsymbol{u}}}{Dt} = -\frac{1}{\gamma M_o^2}\nabla\tilde{P} + \frac{1}{Re}\left[\nabla^2\tilde{\boldsymbol{u}} + \left(\frac{\beta}{\mu} + \frac{1}{3}\right)\nabla(\nabla\cdot\tilde{\boldsymbol{u}})\right] \tag{8a}$$

where μ is the dynamic, or shear viscosity and β is the bulk viscosity. Stokes hypothesis is usually invoked, setting β equal to zero. Solving for the pressure gradient yields:

$$\nabla\tilde{P} = -\gamma M_o^2\left(\tilde{\rho}\frac{D\tilde{\boldsymbol{u}}}{Dt}\right) + \frac{\gamma M_o^2}{Re}\left[\nabla^2\tilde{\boldsymbol{u}} + \left(\frac{\beta}{\mu} + \frac{1}{3}\right)\nabla(\nabla\cdot\tilde{\boldsymbol{u}})\right] \tag{8b}$$

or:

$$\nabla\tilde{P} \propto M_o^2 \tag{8c}$$

Since the Mach number is usually less than 0.1 in Stirling engines, the pressure gradient maybe assumed to be insignificant. Hence the pressure is assumed to depend only on time, and not location.

Equation 8b can provide further insight into the pressure loss mechanisms if Mach number (M_o) and Reynolds number (Re) are replaced by the following:

$$M_o^2 = \frac{(d_o\omega_o)^2}{\gamma\, P_o/\rho_o} \tag{9a}$$

$$Re = \frac{\rho_o(d_o\omega_o)L_o}{\mu} \tag{9b}$$

$$\rho_o = \frac{m_o}{V_o} \tag{9c}$$

where d_o = maximum displacement of drive

ω_o = engine speed (rad/s)

P_o = reference pressure (cycle average)

L_o = length of gas circuit

V_o = mean volume of gas circuit

m_o = mass of gas in engine.

Then Equation 8b becomes:

$$\nabla\tilde{P} = \left(\frac{d_o^2}{V_o}\right)\left(\omega_o^2 \frac{m_o}{P_o}\right)\left(-\tilde{\rho}\frac{D\tilde{\boldsymbol{u}}}{Dt}\right) + \mu\left(\frac{d_o}{L_o}\right)\left(\frac{\omega_o}{P_o}\right)\left[\nabla^2\tilde{\boldsymbol{u}} + \left(\frac{\beta}{\mu} + \frac{1}{3}\right)\nabla(\nabla\cdot\tilde{\boldsymbol{u}})\right] \tag{10}$$

d_o, L_o, and V_o do not vary with engine speed or pressure. The first term on the right only varies with engine speed if the heater and cooler tubes are maintained at the same temperatures using the Ideal gas law since the ratio m_o/P_o would be consant. The second term on the right indicates that viscous losses increase proportionally with engine speed and the inverse of pressure.

All of the second order models use friction factors to determine the pressure losses in the heater, cooler and regenerator. All friction factor correlations employed were developed for steady, incompressible flow. For regenerators and tube bundles, the method of Kays (1964) for evaluating pressure loss is used. The method of evaluating pressure losses as used by Kays (1964) assumed that the flow was steady and incompressible; See Kays, 1950. This means that the $\nabla(\nabla\cdot\tilde{\boldsymbol{u}})$ term from Equation 8 and the unsteady part of the material derivative of velocity, $D\tilde{\boldsymbol{u}}/Dt$, are neglected. For 1-D flow, a factor of 4/3 can be applied to the $\nabla^2\tilde{\boldsymbol{u}}$ term to better account for $\nabla(\nabla\cdot\tilde{\boldsymbol{u}})$. Models that employ only a small number of control volumes, e.g. adiabatic/quasi-steady, cannot account for this effect more accurately. The quasi 1-D models could evaluate the $\nabla(\nabla \cdot \tilde{\boldsymbol{u}})$ term and provide a more accurate estimate of its magnitude if this term were included in the model equations. For engines running on air or hydrogen, the effect of this term may even be greater since the bulk viscosity for both of these gases is not zero, unlike helium for which it is zero. (Graves, 1999)

Martini (1983) includes the performance of the GPU-3 calculated by GM as shown in his Figure 3-9. The model employed is the adiabatic and it uses empirical friction factors (Hargreaves, 1991). This model was developed by Philips and supplied to GM as part of the license agreement. Comparing Figures 3-8 and 3-9 of Martini, shows that this adiabatic model becomes increasingly inaccurate as the engine mean pressure is reduced for higher engine speeds. At the design point, the power is off by +5.4% and the efficiency is +14.6%. While at the lowest pressure (1.72 MPa), the power is off by 120% at 3000 rpm.

Rogdakis *et al* (2012) report on the analysis and experimental testing of the SOLO 161 Stirling engine. As tested, it ran on helium with mean pressures of 3.0 to 13.0 MPa at an engine speed of 1500 rpm. The model is a straightforward application of the Urieli and Berchowitz (1984) ideal adiabatic model. While the performance of the external components was measured, they were not modeled. The measurements were used to find the heater and cooler loads for comparison to those predicted by the adiabatic model. The model prediction for power at the lowest pressure of 3.0 MPa was off by 3.4%. Due to the modest engine speed, the steady, incompressible friction factors seem to account for the flow dissipation.

Demko and Penswick (2005) modeled the NASA Technology Demonstration Convertor (TDC) Stirling engine using Sage. The TDC is a small free-piston engine. The Sage software uses the quasi 1-D CFD finite difference model. The engine produces 50.7 W at a mean pressure of 2.5 MPa and engine speed of 81.2 Hz using helium. The completed, uncalibrated model overestimated power by 13.5% and efficiency by 5.9%. An artificial multiplier (1.4) was then applied to the pressure drop; the power was off by 3.6% and efficiency -1.5%. The low pressure and high frequency would indicate that the steady flow, incompressible friction factors need correcting and the $\nabla(\nabla \cdot \tilde{\boldsymbol{u}})$ term needs to be accounted for. The artificial multiplier used is close to the 4/3 as suggested. Note that this model does not include the external heat transfer.

Dyson *et al* (2005) report on the results of performing a 2-D axisymmetric CFD analysis on a complete Stirling engine. The engine modeled was the same NASA TDC as for Demko and Penswick (2005). The complete compressible momentum equation including the $\nabla(\nabla \cdot \tilde{\boldsymbol{u}})$ term can be properly calculated in this type of model. Engine power and efficiency were off by at most 1%. This illustrates that when the $\nabla^2 \tilde{u}$ and $\nabla(\nabla \cdot \tilde{\boldsymbol{u}})$ terms are correctly modeled, engine performance can be predicted accurately.

3.2 Systems Employing Stirling Engines

As already discussed, there have been many attempts at modeling the internal operation of the Stirling engine. When looking at applications of Stirling engines, there is only a limited amount of information available in the open literature about systems employing Stirling engines. This may help to explain the lack of success in finding a commercially viable use for Stirling engines. Most of the recent work is associated with dish-Stirling solar conversion systems, including solar-gas hybrids. There is a work on using a Stirling engine in combination with an Otto cycle (internal combustion) engine. Finally, one paper deals directly with the external heat transfer to the Stirling engine.

Some research has been published looking into the efficiency of dish-Stirling systems. One such paper is from Chen *et al*, (1998). This paper investigates the theoretical efficiency limit of dish-Stirling systems. Finite time thermodynamics are employed to model the Stirling engine. Only the effects of non-ideal heat exchangers are modeled; no fluid losses are included. Using a heat engine model, with the solar collector as the high-temperature heat source, the optimal operating temperature of the solar collector is determined by maximizing the efficiency of the system. More recent work by Yaqi *et al*, (2011) also provides a model for determining efficiency of dish-Stirling systems.

More complicated models of dish-Stirling systems have also been created. One such model was done by Howard and Harley, (2010). The focus of their model is the control system. The model is intended as a basis for more complete models. The concentrator model uses a single equation with a known mirror reflectivity. The receiver model is also basic, but it includes losses to the environment. The Stirling engine model used is the ideal adiabatic, but without any loss mechanisms. System controls are included in the model.

Another paper of interest on modeling dish-Stirling systems is from Nepveu *et al*, (2009). In this paper, a thermal model of the 10 kW Eurodish is presented. The thermal model of the Eurodish covers the complete solar receiver and Stirling engine. The entire Eurodish volume is divided into 40 volumes: 8 for the solar receiver and 32 for the Stirling engine. The Stirling engine heater is located within the solar receiver. The receiver model includes the effects of radiation, conduction and convection. The Stirling engine model employed is the quasi-steady model, which includes flow dissipation and non-ideal heat exchangers, but no thermal shorting losses. The results of the numerical model are compared to experimental measurements by Reinalter *et al*. (2006). Even though the efficiency is off by 15%, they claim good agreement between the model and the measured data. They attribute the differences to the Stirling engine model.

Another model of a dish-Stirling system is provided in a master's thesis which is used to predict the long term performance of dish-Stirling systems (Fraser, 2008). The main goal of this work was to provide a long term energy prediction model based on the location of the system. A detailed model of the collector and receiver accounts for the amount or radiation received and losses to the environment. The Stirling engine model is the West number correlation, but it does include parasitic power used by the cooling system. The results are compared to other dish-Stirling prediction models and to data collected from the Wilkinson, Goldberg and Associates, Inc. (WGA) Mod 2-2 dish-Stirling system operated by Sandia National Laboratory in Albuquerque, New Mexico.

The new model is claimed to have better fidelity with the measured data than the other models mentioned.

There is some material to be found in the open literature on solar-biogas hybrids, but a good portion of the research being done is being kept proprietary for commercial reasons. A paper by Kibaara *et al* (2012) provides a thermal analysis of a hybrid parabolic trough-biomass power system. It provides an energy balance model of both the solar collector and biomass systems, but does not include the electrical conversion system. Another work is by Kang *et al* (2009), wherein they experimentally measure the heat transfer characteristics of a hybrid solar dish-Stirling system, but do not provide any modeling.

The paper covering the use of a Stirling engine in conjunction with an Otto cycle engine is the PhD dissertation by Cullen, (2011). The Stirling engine model employed is the finite time thermodynamics model. Losses due to fluid friction, thermal shorting and non-ideal heat exchangers are included. As previously described, this model has to resort to using the Schmidt analysis to determine the reversible work output. The model for the combustion process is a simple first law of thermodynamics equation relating the change in gas enthalpy to the net rate of heat input into the engine. A thermal circuit is employed that contains the external convective heat transfer, the internal convective heat transfer and the conductive heat transfer through the heater tube walls. The GPU-3 is then modeled and compared to its published performance in Thieme (1979) and Martini (1983). The model is claimed to maintain good fidelity with the experimentally measured performance, except at high rpm. Unfortunately, the geometry of the heater was incorrectly modeled. Comparing Figure 6.4 (Cullen, 2011) with Figure 8 (Johnson *et al*, 1981), shows that the free-flow area for the combustion gases is significantly smaller than modeled. Additionally, the exhaust gas temperature was assumed to be equal to ambient, (§6.5.2 of Cullen, 2011), but it was over 200°C hotter per Appendix F of Thieme (1979). These would both lead to an erroneous estimate of combustion mass flowrate.

There is one paper by Johnson *et al*, (1981) dealing directly with the external heat transfer to the Stirling engine heater. Johnson *et al* investigate the possibility of improving the heat transfer to the heater by using jet impingement. They create models for the unmodified and modified GPU-3 and compare it to experimental results. But they do not describe the model details.

CHAPTER 4

Methodology

4.1 Engine Modeling

The model to be employed is the ideal adiabatic and simple heat exchanger model. (Urieli and Berchowitz, 1984) Adiabatic working spaces seem to be a little more realistic for a well-insulated engine than isothermal ones. The simple heat exchanger refinement is less complicated to implement than the quasi-steady. Since numerical integration for such a model is not time consuming, the LHA and FTT models main advantage, no need for numerical solution, is lost. Numerical integration can also deal with more complicated drive mechanisms like the offset-crank-slider or Ross yoke.

Some changes to the code include adding the rhombic drive equations, increasing the number of engine dimensions, an iterative procedure to adjust the mean cycle pressure by changing the mass of gas, adding three volumes, adding loss mechanisms and revising the energy balance.

The original code determined the mass of the working gas by applying the Schmidt analysis (isothermal with sinusoidal drive). The mass of gas from the Schmidt analysis is used as the initial value for an iterative scheme. The complete adiabatic model is run and the resulting cycle average pressure is found. The new mass of gas is adjusted based off of:

$$m_{new} = \left(1 + \frac{P_{mean} - \bar{P}}{P_{mean}}\right) \cdot m_{old} \tag{11}$$

where m_{new} = new mass value

P_{mean} = desired mean pressure

$\overline{P}$ = cycle averaged pressure

m_{old} = old mass value.

The adjusted mass of gas is found to be about 10% less than that found using the Schmidt analysis. This is primarily due to the offset-crank-slider mechanism. Reducing the mass of working gas reduces the power output of the adiabatic model accordingly.

The three volumes added to the model are shown in Figure 4.1. The volumes added are the cooler-regenerator manifold, regenerator-heater manifold, and the appendix gap. The two manifolds do not really impact the model. They were added just to better represent the geometry. The appendix gap was added to be able to include its losses. The temperature of the appendix gap (T_a) is the log-mean temperature difference using the expansion space temperature (T_e) and the compression space temperature (T_c). The revised set of equations is given in Appendix A.

The loss mechanisms are flow dissipation, non-ideal regenerator loss, appendix gap loss, regenerator wall thermal short, cylinder wall thermal short, displacer wall thermal short, displacer gas internal convection, displacer internal radiation thermal short, and gas circuit hysteresis.

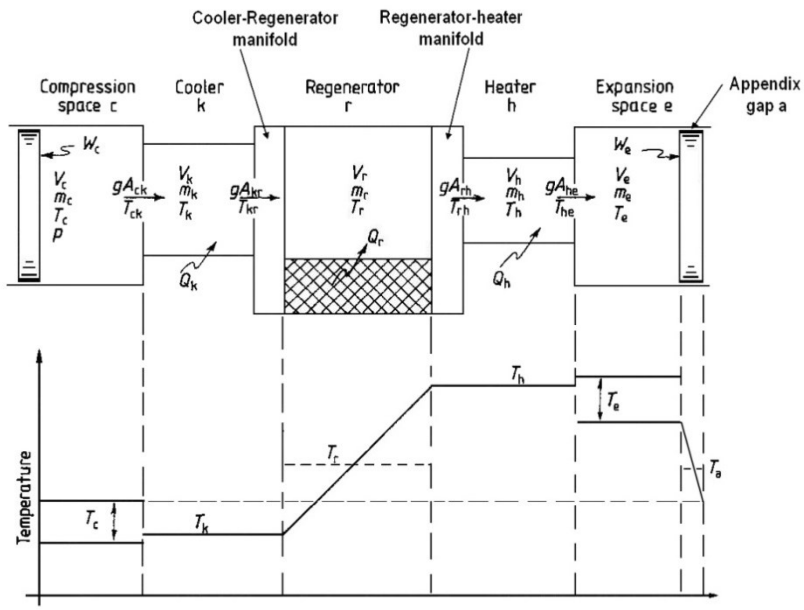

Figure 4.1
Adiabatic Model Volumes and Temperatures
(Adapted from Urieli and Berchowitz, 1984)

The flow dissipation was modeled starting with the loss model of Urieli (2012). The original loss model accounts for shear stress by using steady flow, incompressible friction factors. The Reynolds friction factor (f_r) for the heater and cooler tubes used is the Blasius relation assuming steady turbulent flow:

$$f_r = 0.0791Re^{0.75} \tag{12}$$

$$f_r = 24\ if\ Re < 2000$$

The steady flow Reynolds friction factor for the regenerator mesh taken from Kays and London (1964) is:

$$f_r = 54 + 1.43Re^{0.78} \tag{13}$$

Pressure losses due to sudden contraction, sudden expansion and acceleration were added following Kays and London (1964) for heat exchangers. Equation 14 is derived from Equation 2.26a (Kays, 1964), using the Fanning friction factor (f_f). It includes an unsteady term and losses due to bends:

$$\Delta P = \frac{(\rho u)^2}{2\rho_{in}}(K_{in} - 1 - \sigma_{in}^2) + \frac{(\rho u)^2}{2\rho_{out}}(K_{out} + 1 + \sigma_{out}^2)$$

$$+4f_f \frac{L\rho u^2}{D_{hyd}2} + L\omega \frac{\partial(\rho u)}{\partial\theta} + \sum K_b \frac{\rho u^2}{2} \tag{14}$$

where K_{in} = inlet contraction coefficient

K_{out} = outlet expansion coefficient

σ_{in} = inlet ratio of free-flow area to frontal area

σ_{out} = outlet ratio of free-flow area to frontal area

K_b = bend loss coefficient

L = length of component

ω = angular velocity of drive

θ = crank angle.

The partial derivative (∂/∂θ) is approximated by a first order backward finite difference.

The loss due to the non-ideal operation of the regenerator is modeled exactly as in Urieli (1984). The effectiveness (ε) of the regenerator is derived as:

$$\varepsilon = \frac{NTU}{NTU + 1} \tag{15}$$

where NTU = number of transfer units. The NTU is found using the Stanton number (St). The same empirical correlation for a mesh used by Urieli (1984) from Kays and London (1964) is used:

$$St = 0.46\frac{Re^{-0.4}}{Pr} \tag{16}$$

The appendix gap is modeled as a non-ideal regenerator as well. The effectiveness of the appendix gap functioning as an annular gap regenerator without a mesh is evaluated using the same ε-NTU relationship, Eq. 15, (Urieli, 2012). Other ε-NTU relationships have been proposed for the appendix gap. (Pfeiffer and Kuehl, 2014). Pfeiffer reports that Magee and Doering derived:

$$\varepsilon = \frac{1}{NTU} \tag{17}$$

while Martini (1983) derived:

$$\varepsilon = \frac{2}{NTU + 2} \tag{18}$$

Equation 15 behaves better, being equal to 0 at zero NTU and 1 at infinite NTU. The Reynolds friction factor (f_r) is found from Equation 12. The Stanton number for the appendix gap is found using the friction factor of the annular gap and then applying Reynolds simple analogy.

$$St = \frac{f_r}{2Re \cdot Pr} \tag{19}$$

The appendix gap loss is then the loss of heat due to the less-than-ideal effectiveness of the appendix gap.

The thermal shorting losses in the regenerator wall, cylinder wall, and displacer wall are estimated by assuming 1-D conduction through a constant thickness wall. The heater and cooler wall temperatures are used for the regenerator thermal short. The cooler and heater gas temperature are adjusted by ±10% for use with the displacer and cylinder walls to account for finite rates of heat transfer. The thermal conductivity of the walls is taken as the log-mean-temperature difference of the appropriate end temperatures.

The displacer gas internal convection loss is modeled as a thermal circuit from the expansion space gas, in through the displacer wall, to the internal gas, out through the displacer wall to the compression space gas. The Nu to/from the displacer ends is assumed to be 4.0, i.e. laminar. The gas in the core of the displacer is assumed to be stationary; therefore it only conducts the heat loss.

The displacer internal radiation thermal short models the radiation heat transfer that takes place in the displacer core, using the standard method for radiation heat transfer between surfaces (Incropera, 1990). View factors for the circular ends (coaxial parallel disks) and cylindrical side are calculated. The heat loss from the hot end to the cold end is then found assuming that the cylindrical side wall is reradiating. As with the cylinder and displacer wall thermal shorts, the displacer end temperatures are assumed to be ±10% of the compression and expansion space temperatures to account for finite heat transfer.

The gas circuit hysteresis loss is modeled following Bailey *et al* (2007). The hysteresis losses (Q_{hys}) are found using the following equations:

$$Q_{hys} = Q_o \frac{\pi}{2}\frac{1}{y}\left(\frac{\cosh y \sinh y - \sin y \cos y}{\cosh^2 y - \sin^2 y}\right) \qquad (20a)$$

$$Q_o = P_{avg} V_{avg} \left(\frac{P_{amp}}{P_{avg}}\right)^2 \frac{(\gamma - 1)}{\gamma} \qquad (20b)$$

$$y = 0.49 Pe_\omega^{0.43} \qquad (20c)$$

$$Pe_\omega = \frac{\omega D_{hyd}^2}{4\alpha_o} \qquad (20d)$$

$$D_{hyd} = \frac{4V_o}{A_o} \qquad (20e)$$

where P_{max} = maximum pressure of cycle

P_{min} = minimum pressure of cycle

$P_{avg} = (P_{max} + P_{min})/2$

$P_{amp} = (P_{max} - P_{min})/2$

V_{max} = maximum volume of cycle

V_{min} = minimum volume of cycle

$V_{avg} = (V_{max} + V_{min})/2$

α_{mid} = thermal diffusivity at mid-stroke

V_{mid} = volume at mid-stroke

$A_{w_{mid}}$= wetted area at mid-stroke.

Pe_ω is the Peclet number based on the angular velocity. D_{hyd} is the hydraulic diameter. Q_o is a normalizing term. Equation 20c is an adjustment of the original, theoretical result to better agree with experimental results. For this model, the compression space, compression space clearance volume and cooler are considered as one volume. The expansion space, expansion space clearance volume and heater are considered as a second volume.

The net work, heater heat absorption and cooler heat rejection as calculated by the adiabatic model are adjusted using the losses mentioned. The flow dissipation and hysteresis losses reduce the amount of work produced. The cylinder, displacer, and regenerator wall thermal shorts, the displacer internal radiation and gas convection losses, and appendix gap and regenerator losses are all added to both the heater and cooler as additional heat loads. The flow dissipation in the heater is subtracted from the heater load as a reheat affect. The flow dissipation in the cooler and regenerator is added to the cooler load.

4.2 System Modeling

The complete engine plus auxiliaries is shown in Figure 4.2. The components include the Stirling engine, a fan, a heat exchanger used as a preheater, a combustor, a combustion gas recirculation (CGR) system, and a fuel pump. Included within the Stirling engine are the alternator, heater, cooler, and water-to-air radiator (heat exchanger). The fan supplies the mass flow rate of atmospheric air to the system with a minimal pressure increase. The air is then heated in the preheater using the hot exhaust gases coming from the engine. The combustor burns the fuel increasing the air and CGR gas mixture temperature to its operating point. The resulting high temperature combustion gases pass over the heater of the Stirling engine, transferring the necessary energy to drive the engine. CGR is a variant of exhaust gas recirculation (EGR). (Walker, 1994) The CGR system returns part of the exhaust gases before going through the preheater to be reheated and reused in the combustor. The remaining exhaust goes through the preheater.

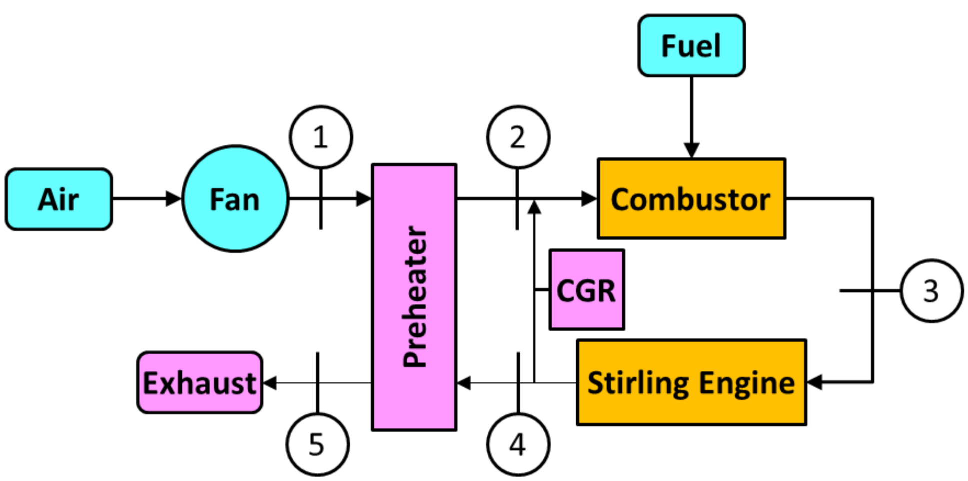

Figure 4.2
Complete System Including Fan, Preheater, Combustor, Stirling Engine and CGR

The overall thermal efficiency of the system is the net usable electric power divided by the total heat input to the system. The total heat input to the system is the amount energy released by the combustion of the fuel. The energy of the fuel is equal to the mass flow rate of fuel times the lower heating value (LHV) of the fuel.

The incoming air, fuel and products of combustion are modeled using the properties of air. The properties are assumed constant at an appropriate average temperature for each specific component. Due to the possible large temperature differences, the average specific heat at constant pressure (Cp) values are found once the inlet and exit temperatures are known. The new average Cp is then used to recalculate the inlet and exit temperatures. This is repeated until convergence, typically a few iterations.

4.2.1 Fan

The fan is modeled as an adiabatic compression process. Assuming constant specific heats through the compressor, the isentropic compressor work (specific), w, is given by:

$$w = \frac{\gamma R T_{in}}{\gamma - 1}\left[\left(\frac{P_{out}}{P_{in}}\right)^{\frac{\gamma-1}{\gamma}} - 1\right] + \frac{u_{out}^2}{2} \tag{21}$$

where T and P are the static values of temperature and pressure at the inlet and exit, respectively. R is the gas constant, γ is the ratio of specific heats and u is the velocity. The air enters at atmospheric pressure with negligible velocity. The pressure ratio of the fan is determined from the known atmospheric pressure and exit pressure which is the sum of the pressure losses through each component. The isentropic efficiency is assumed to be 80%.

4.2.2 Preheater

The preheater is modeled as a plate-fin heat exchanger of the form as shown in Figure 4.3.

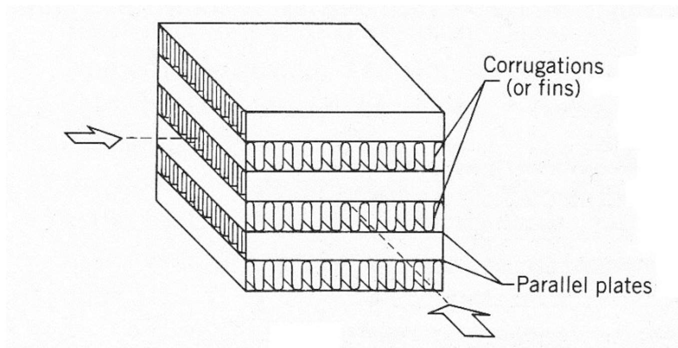

Figure 4.3
Plate-Fin Heat Exchanger
(Incropera, 1990)

Its size is determined by minimizing the pressure drop of both streams through it and maximizing the outlet temperature of the incoming air. It is assumed to be stainless steel.

4.2.3 Combustor

The combustor model simply uses the LHV of the fuel to find the energy input into the complete engine. The products of combustion are modeled using the properties of air and the mass of fuel burned is modeled as an equivalent mass of air. Starting with a simple control volume energy balance on the combustor:

$$\dot{Q}_{fuel} - \dot{Q}_{loss} = \dot{m}_{air}\Delta h_{air} + \dot{m}_{fuel}\Delta h_{fuel} + \dot{m}_{CGR}\Delta h_{CGR} \qquad (22a)$$

where $\dot{Q}_{fuel} = \dot{m}_{fuel} \cdot LHV$ (rate of energy from fuel)

$\dot{Q}_{loss}$ = various heat losses to environment

$\dot{m}_{air}$ = mass flow rate of air

$\dot{m}_{fuel}$ = mass flow rate of fuel

$\dot{m}_{CGR}$ = mass flow rate of CGR gas

Δh_{air} = enthalpy increase of air per mass

Δh_{fuel} = enthalpy increase of fuel per mass

Δh_{CGR} = enthalpy increase of CGR gas per mass

the mass flow rate of fuel is solved for:

$$\dot{m}_{fuel} = \frac{\dot{m}_{air}\Delta h_{air} + \dot{Q}_{loss} + \dot{m}_{CGR}\Delta h_{CGR}}{LHV - \Delta h_{fuel}} \qquad (22b)$$

The term $\dot{Q}_{loss}$ represents the heat loss to the ambient air in the form of radiation and convection as well as the heat absorbed by the fuel nozzle cooling system.

4.2.4 Stirling Engine Heater

The high temperature heat exchanger on the Stirling engine is configured as a bank of tubes in cross-flow. The tubes are arranged vertically in a radial pattern, similar to the heater of the GPU-3 shown in Figure 4.4a or as a radial volute of the 4-95 of Figure 4.4b. The combustion gases flow into the heater axially and exit radially. The flow is analogous to a shell-and-tube heat exchanger with one shell (combustion gases) and two tube passes (Stirling engine gas).

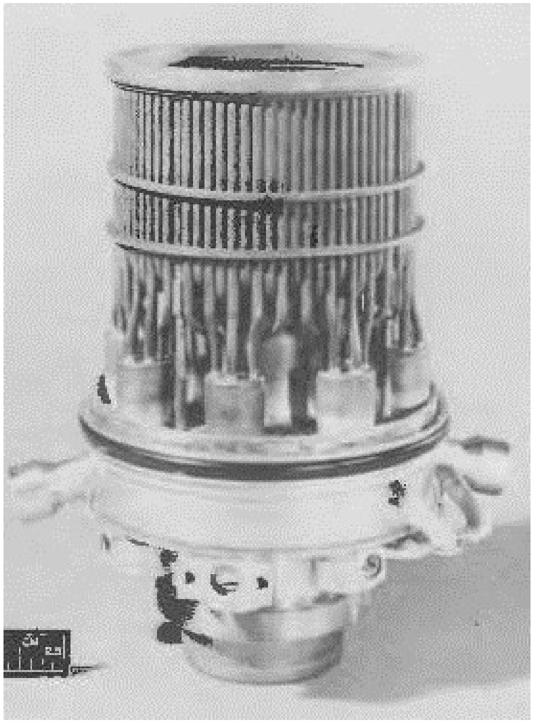

Figure 4.4a
GPU-3 Heater Tubes
(Urieli, 1984)

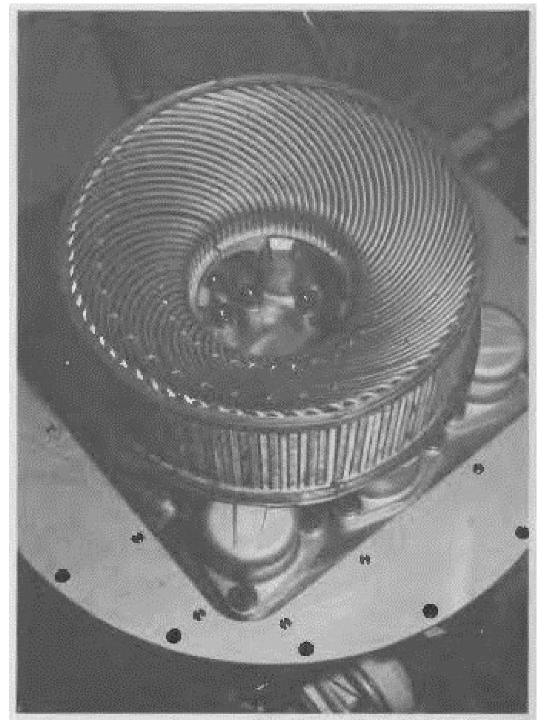

Figure 4.4b
4-95 Heater Tubes
(West, 1986)

The gas velocity over the heater tubes is initially found by determining the heat transfer coefficient (U) from Newton's law of heating since the surface area, gas and surface temperatures and the rate of heat transfer are known. The conduction resistance of the heater tube walls is also included. Since a large range of gas velocities is to be examined, the extra effect of heating due to high velocity viscous dissipation is accounted for by using the free-stream stagnation temperature instead of the free-stream static temperature (Kays, 2005). The velocity is extracted from the heat transfer coefficient using a Nu correlation for a single cylinder in cross-flow, which is recommended for flow over a bank of cylinders if the Reynolds number is no more than 1000. The correlation used is Equation 7.45 from Incropera (1990). It is of the form:

$$\overline{Nu}_D = cRe_D^n Pr^{\frac{1}{3}} \tag{23}$$

where c and n are based on the Reynolds number (Re). The velocity used for the Re is the mass averaged velocity in the gap between the heater tubes.

The temperature of the combustion products after flowing over the Stirling engine heater tubes is initially estimated by applying an energy balance to the fluid, given that the amount of heat transfer to the engine is known from the engine model. The net rate of heat transfer $(\dot{Q})$ is then calculated using Newton's law of heating and an appropriate form of the log-mean-temperature difference (LMTD):

$$\dot{Q} = U \cdot A_w \cdot LMTD \tag{24}$$

For the assumption of a constant heater tube surface temperature ($T_{h,s}$), the LMTD can be shown to be:

$$LMTD = \frac{\left(T_{h,out} - T_{h,in}\right)}{\ln\left(\frac{T_{h,out} - T_{h,s}}{T_{h,in} - T_{h,s}}\right)} \tag{25}$$

where $T_{h,out}$ and $T_{h,in}$ are the temperatures of the combustion gases exiting and entering the heater, respectively. The gas velocity and exit temperature are iterated until the rate of heat transfer using both the energy balance and LMTD methods is the same.

Radiation from the combustion products to the heater tubes is excluded. The products of combustion would contain N_2 and O_2 which can be ignored. CO_2 and H_2O do need to be accounted for, but at the partial pressures encountered in this system, their emissivities would be very low, resulting in very low amounts of radiative heat transfer (Incropera,1990).

4.2.5 79Stirling Engine Cooling System

The Stirling engine cooler is modeled as a compact heat exchanger arranged in a staggered tube bank. Figure 4.5 shows three of the eight canisters of the GPU-3 that contain the cooler tube bundles and the regenerator wire matrices.

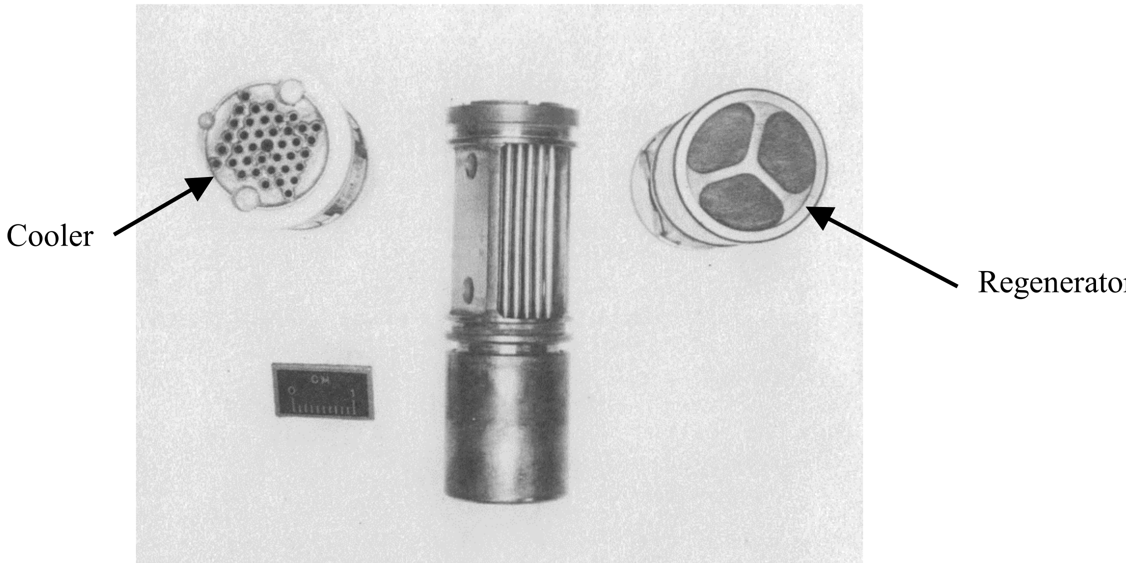

Figure 4.5
GPU-3 Cooler and Regenerator Canister
(Urieli, 1984)

A constant tube surface temperature is assumed. The thermal resistance of the cooler tubes is assumed negligible. The Nu correlation used is Equation 7.57 (Incropera, 1990):

$$\overline{Nu} = cRe_D^n Pr^{0.36}\left(\frac{Pr}{Pr_s}\right)^{1/4} \tag{26}$$

with c and n depending on Re and the tube bank configuration. The heat from the cooler is rejected to the atmosphere by the radiator, another compact heat exchanger. The ambient air temperature is assumed to be 25°C. The radiator configuration is a bundle of finned tubes (surface 8.0-3/8T) and its experimentally determined performance is shown in Figure 10-83 of Kays (1964). The amount of heat transfer, inlet water and inlet air temperatures are known from the engine model. The exit temperatures are calculated using the log-mean-temperature difference and overall heat transfer coefficient method for a thermal circuit from the cooler tube surface of the engine to the atmospheric air. The size of the finned tube heat exchanger is chosen by minimizing the power consumption of both the water pump and the fan for moving the air across the radiator.

4.2.6 Alternator

The alternator is modeled as having an efficiency of 90%. The fan and cooling system (water pump and radiator fan) are driven by electric motors, consuming part of the electricity produced.

4.2.7 Combustion Gas Recirculation (CGR)

The CGR system is modeled such that a specified percentage of the inlet mass flow rate (air plus fuel) is recirculated from the engine exhaust back into the combustor.

4.2.8 System Pressure Loss

The pressure losses through the preheater and over the Stirling engine heater are estimated using the method of Kays (1964). The external friction factor for the heater tube bundle is assumed to be 1. Losses due to sudden contraction and expansion are included at the inlet and exit of each component.

4.2.9 Solution

The system analysis is done numerically by assuming values for some variables and iterating to convergence. Due to the transcendental nature of Equation 25, it is not possible to get an analytical solution for the tube surface temperature directly. The analysis of an operating point is begun using an assumed heater tube inner surface temperature, an assumed cooler tube temperature, and the engine speed. The temperature of the products of combustion and the air and fuel mass flow rates are not known à priori. The adiabatic plus simple heat exchanger model is run, and the average heater and cooler gas temperatures, heater and cooler heat loads, and indicated power and efficiency of the engine are found. Next the temperature of the products of combustion and the static fan pressure ratio are assumed. The fuel and air mass flow rates, temperature of the gas after passing over the Stirling engine heater, and the performance of the preheater and cooler are found. The combustion gas temperature and gas velocity through the heater tube gap are adjusted until the desired air/fuel mass ratio, heater tube surface temperatures, and cooler water flow rate are attained. The assumed heater tube inner surface temperature and cooler tube temperature used in the adiabatic model may have to be fine-tuned to achieve the known tube surface temperature and the heater gas temperature.

CHAPTER 5

Model Validation

The model is validated by analyzing a specific engine and comparing the model results to the experimentally measured results. The specific engine modeled is the General Motors Ground Power Unit-3 (GPU-3). Its dimensions and performance have been extensively documented in the literature, Thieme, 1979 and 1981, Johnson, 1981, and Martini, 1983.

Some changes to the system model are necessary to match the test conditions. A source of constant temperature water was used during testing, so the cooling system water-air radiator is not included. The GPU-3 did not use any CGR systems, so there is no CGR. The actual preheater was a bundle of fined tubes, but no dimensions were found in the literature. Instead the preheater configuration used is the plain plate-fin surface 46.46T and its measured performance is given in Figure 10-37 of Kays (1964). Its size is determined by taking measurements from the known drawings. It is assumed to be stainless steel. The dimensions including preheater, as used in the model, are given in Appendix B.

5.1 External Components of System

The performance of the model of the external components of the engine is compared to the experimentally determined performance as given in Johnson (1981). The data used is from Figure 14. The engine was run using hydrogen at a mean pressure of 6.9 MPa, at an engine speed of 3000 rpm with an air/fuel ratio of 26:1. The measured heat into the engine (22454 W) was used instead of running the engine model to eliminate any error introduced by the engine model. Table 5.1 shows the results. The preheater exhaust temperature is a little high, but given the unknown configuration of the original, 17% difference is acceptable. The heat transfer coefficient is low. Still it is within 20% of the measured value which is reasonable. As a result of the lower heat transfer coefficient, the combustion temperature is higher. The rest of the quantities agree within 10% of the measured values. The ersatz preheater configuration seems to be a reasonable choice considering that the preheater temperatures (T_2 and T_5) and effectiveness are acceptably close.

The variable with the largest amount of uncertainty in the modeling of the external system is the heat transfer coefficient to the heater. Hargreaves (1991) reports that Philips while developing the 1-98 engine created heat transfer correlations similar to Equation 23 that uses a different empirical constant and exponent but without the Pr correction. The Philips 1-98 engine is the forerunner of the 10-36 engine on which the GPU-3 is based. The values in Table 5.1 in brackets are found using the Philips correlation. While the temperatures are significantly in error, the flow rates (which are the most important) are still within 10% of the measured values.

Quantity	Model	Experimental	Error (%)
Air Preheat Temperature T_2 (°C)	1047 [741]	1037	0.96 [-28.5]
Combustion Temperature T_3 (°C)	2297 [1997]	2108	8.97 [-5.3]
Engine Exhaust Temperature T_4 (°C)	1285 [910]	1191	7.89 [-23.6]
Preheater Exhaust Temperature T_5 (°C)	343 [243]	293	17.1 [-17.1]
Heat transfer coefficient (W/m^2-°C)	253 [462]	301	-15.9 [53.2]
Fuel Flow Rate (g/s)	0.68 [0.63]	0.66	3.03 [-4.5]
Air Flow Rate (g/s)	17.83 [16.39]	17.51	1.83 [-6.4]
Preheater effectiveness	0.81	0.80	1.25

Table 5.1
External Model Comparison to Experimental
(Numbered temperatures refer to Figure 4.2)

5.2 Complete System with Stirling Engine

The performance of the GPU-3 was measured during tests that General Motors performed in 1969. This experimentally measured performance is shown in Figure 3-8 of Martini (1983). The engine tests used Number 1 diesel fuel which has an LHV of 18590 BTU/lb (43236 kJ/kg). The power consumption of the fan and fuel pump is not included since they were not measured during testing. The measured combustor pressure drop is 3 kPa which is used to find the pressure at the exit of the fan.

The engine power % error ranges from -1.9% to +40.9%. The brake specific fuel consumption (bsfc) % error ranges from -35.1% to -1.8%. The drive efficiency is calculated using the brake and indicated power measurements from Figures 6 and 15 of Thieme, 1981. The drive efficiency varied from 69% (at 1.72 MPa) to 84% (at 6.9 MPa), while Organ (1978) estimated the efficiency of the rhombic drive to be about 80%. Comparing the power and bsfc for each pressure, the model performance at the lowest pressure has significant error. On the other hand, for the three higher pressures, the engine power % error ranges from -1.9% to +6.1% and the bsfc % error ranges from -9.7% to -1.8%. This suggests that the steady, incompressible friction factors are adequate at higher pressures. If the measured power values at 1.72 MPa are used instead of the model power values, the model bsfc becomes significantly better, with an error range of -11.0% to -1.5%. This indicates that the engine model is not calculating the power output correctly at the lowest pressure, but the heat input to the engine is reasonable, albeit low. Some heat losses maybe underestimated or not included.

One possible cause of the model over predicting the engine power at low mean pressures, could be the use of steady flow friction factors instead of ones for oscillating flow. According to Ju *et al*, 1998, the regenerator friction factor for oscillating flow is significantly higher than that of steady flow. Ju *et al* measured the pressure drop in a regenerator of a pulse tube cryocooler. The working gas was helium, the operating frequency was 50 Hz and the mean pressure varied from 0.6 to 0.9 MPa. The resulting cycle-averaged oscillating flow friction factor was compared with a steady flow friction factor. The pressure drop was found to be 2-3 times larger using the cycle averaged oscillating friction factor than the pressure drop from the steady flow friction factor.

The complete engine simulation for all engine speeds and pressures was repeated using a regenerator pressure drop multiplied by a correction factor of two. For the three higher pressures, the engine power % error ranges from -7.8% to +3.3% and the bsfc % error ranges from -7.6% to +6.2%. For the lowest pressure, the engine power % error improves to +2.2% to +15.8%. The bsfc % error also improves to a range of -13.4% to -21.5%. This is an improvement, but there is still too much power at the lowest engine pressure; something is still missing from the engine model.

The complete engine simulation for all engine speeds and pressures was run again with the shear stress pressure drop multiplied by a factor of 4/3 to account for the $\nabla(\nabla \cdot \tilde{\boldsymbol{u}})$ term of Equation 8. The engine power % error ranges from -14.1% to +12.7% and the bsfc % error ranges from -12.7% to +13.4% for all pressures. Figures 5.1a-d show the engine output and the bsfc as a function of engine speed for the four mean pressures. Most of the power predictions are lower than the measured values at the three highest pressures, while at the lowest pressure the power predictions straddle the experimental values. This would indicate that the decoupled loss mechanisms are actually less than predicted. Specifically, the 4/3 correction to the flow dissipation for compressibility is probably overestimating this effect. Also, flow dissipation and hysteresis losses may be coupled. The notable exception to the less than expected power is at an engine speed of 10 Hz and a pressure of 1.72 MPa. It is 12.7% higher. Considering the small amount of power produced, smaller loss mechanisms that have been ignored may be the difference for this operating condition. Two of these might be the flow dissipation in the appendix gap and the leakage past the displacer seal. The bsfc model values for the three higher pressures are higher than the experimental ones. This is due in large part to the model engine power being lower than the experimental values. At the lowest pressure, the model bsfc is lower but the engine power is similar. This most likely indicates that there is a heat loss mechanism that is missing or underestimated.

Figure 5.2a shows that the coefficient ($\omega_o^2 \cdot m_o/P_o$) of Equation 8 increases as engine speed varies for 6.9 MPa and 1.72 MPa. For the same engine speed, this term does not vary with pressure. P_o is a function of the drive geometry, gas circuit geometry, heater and cooler temperatures and mass of the gas, m_o, but the ratio (m_o/P_o) does not change. Figure 5.2a indicates that the contribution of the unsteady and acceleration ($\tilde{\rho}\, D\widetilde{\boldsymbol{u}}/Dt$) effects does not change since its coefficient does not change as pressure is lowered.

Figure 5.2b shows the coefficient (ω_o/P_o) of Equation 8 as the engine speed varies for all four pressures. As pressure decreases, the magnitude of this ratio increases. This reveals that the contribution of dissipation ($\nabla^2\widetilde{\boldsymbol{u}}$) and compressibility $\left(\nabla(\nabla \cdot \widetilde{\boldsymbol{u}})\right)$ to the pressure gradient increases as pressure is reduced. Comparing the values for this coefficient at 50 Hz shows the increasing magnitude of the dissipation and compressibility term as pressure is decreased.

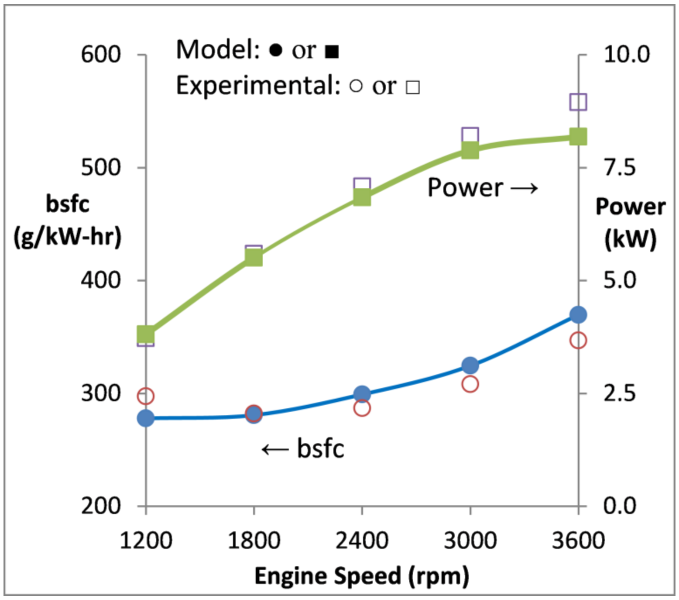

Figure 5.1a
GPU-3 Power and bsfc as Engine Speed Varies
(6.9 MPa Mean Engine Pressure)

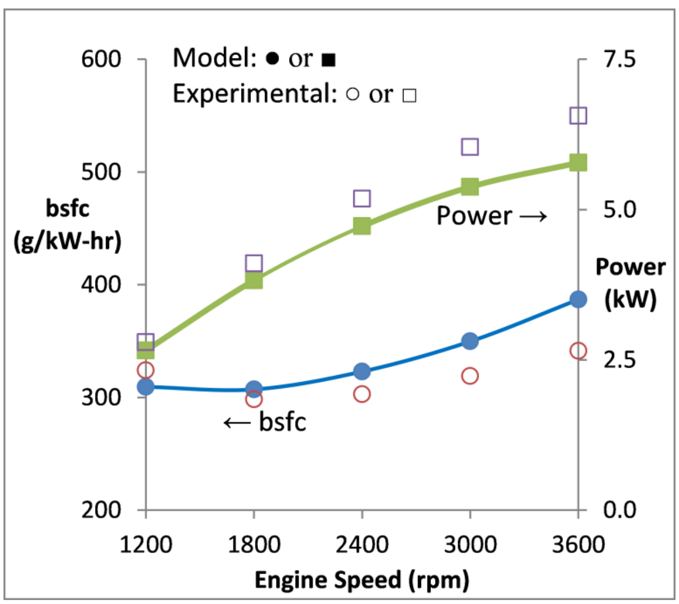

Figure 5.1b
GPU-3 Power and bsfc as Engine Speed Varies
(5.17 MPa Mean Engine Pressure)

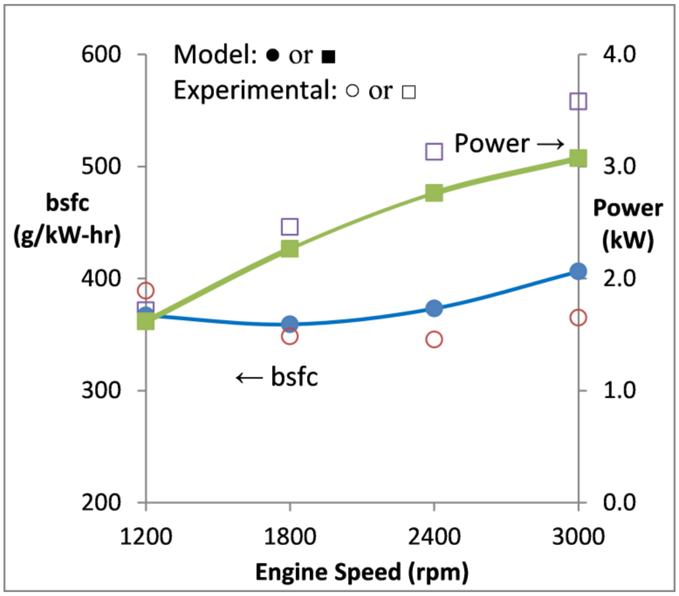

Figure 5.1c
GPU-3 Power and bsfc as Engine Speed Varies
(3.45 MPa Mean Engine Pressure)

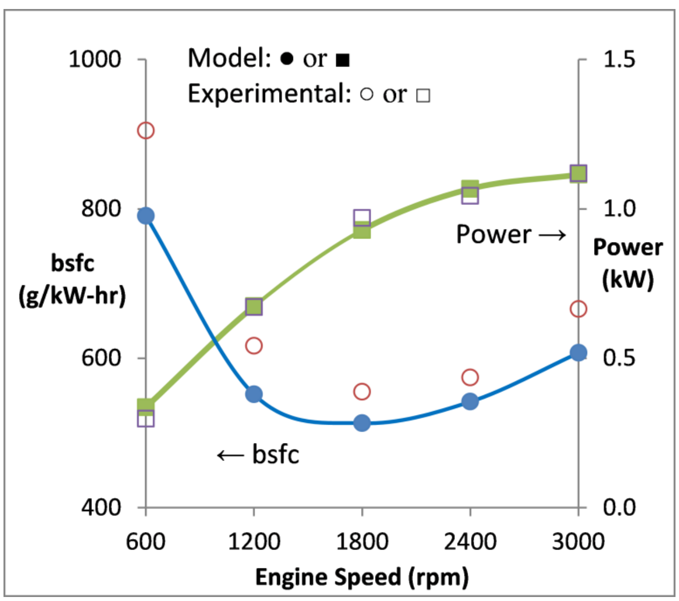

Figure 5.1d
GPU-3 Power and bsfc as Engine Speed Varies
(1.72 MPa Mean Engine Pressure)

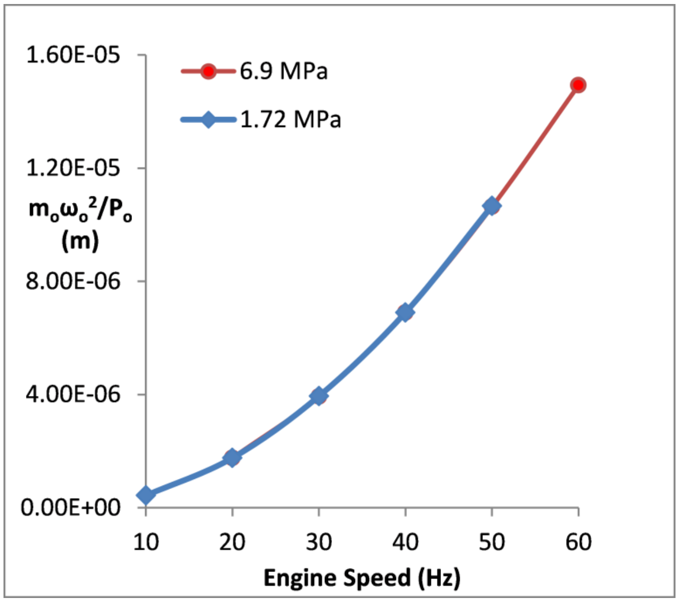

Figure 5.2a
Coefficient of Unsteady and Acceleration Term in Momentum Equation

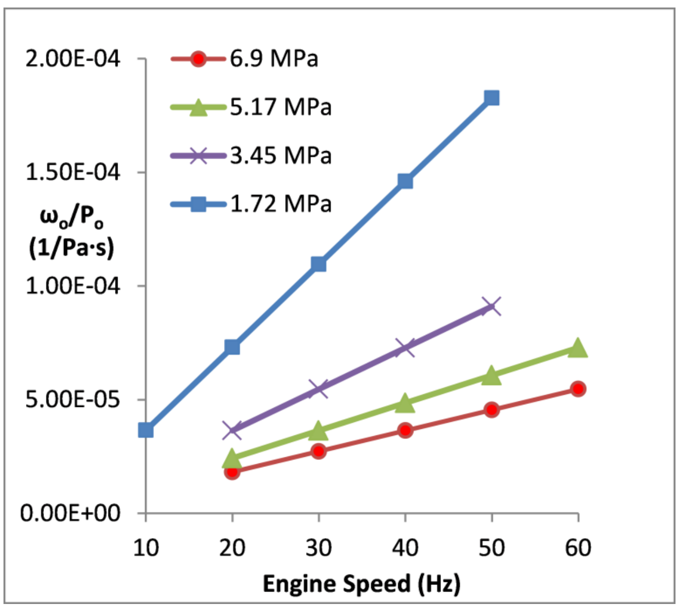

Figure 5.2b
Coefficient of Dissipation and Compressibility Term in Momentum Equation

The modeling of the GPU-3 indicates that flow dissipation losses increase significantly below a mean engine pressure of 3.45 MPa. Figure 5.3 shows the engine output and bsfc for 3.45 MPa and 1.72 MPa mean pressures with and without the corrections for compressibility and oscialltory flow. For all engine speeds, the uncorrected model is sufficiently accurate at 3.45 MPa. At 1.72 MPa, the uncorrected model is reasonably accurate below 1500 rpm, but it is off by as much as 35% for power and 41% for bsfc at higher speeds. When corrected, the model is off by at most 13% at 1.72 MPa. The analysis of the SOLO 161 (Rogdakis *et al*, 2012) also shows that the steady, incompressible friction factors adequately account for flow dissipation for pressures of at least 3.0 MPa at an engine speed of 25 Hz. No correction was necessary to account for compressibility or oscillating flow in modeling the SOLO 161. On the other hand, the modeling of the TDC (Demko and Penswick, 2005) implies that a correction for compressibility is needed at 2.5 MPa and 81 Hz engine speed. This suggests a rule of thumb that for engines operating below a mean pressure of 3.0 MPa *and* at engine speeds above 25 Hz, the effects of unsteady, compressible flow need accounting for. For models of the isothermal/adiabatic type multiplying the steady, incompressible friction factor by 4/3 seems to be an adequate correction. For models that can evaluate the $\nabla(\nabla \cdot \tilde{\boldsymbol{u}})$ term from Equation 8, this term needs to be included. A more rigorous criterion should be developed by evaluating the $\mu\left(\frac{d_o}{L_o}\right)\left(\frac{\omega_o}{P_o}\right)$ coefficient and the $\left(\nabla(\nabla \cdot \tilde{\boldsymbol{u}})\right)$ term of Equation 8 for a variety of Stirling engines to determine when these effects warrant inclusion.

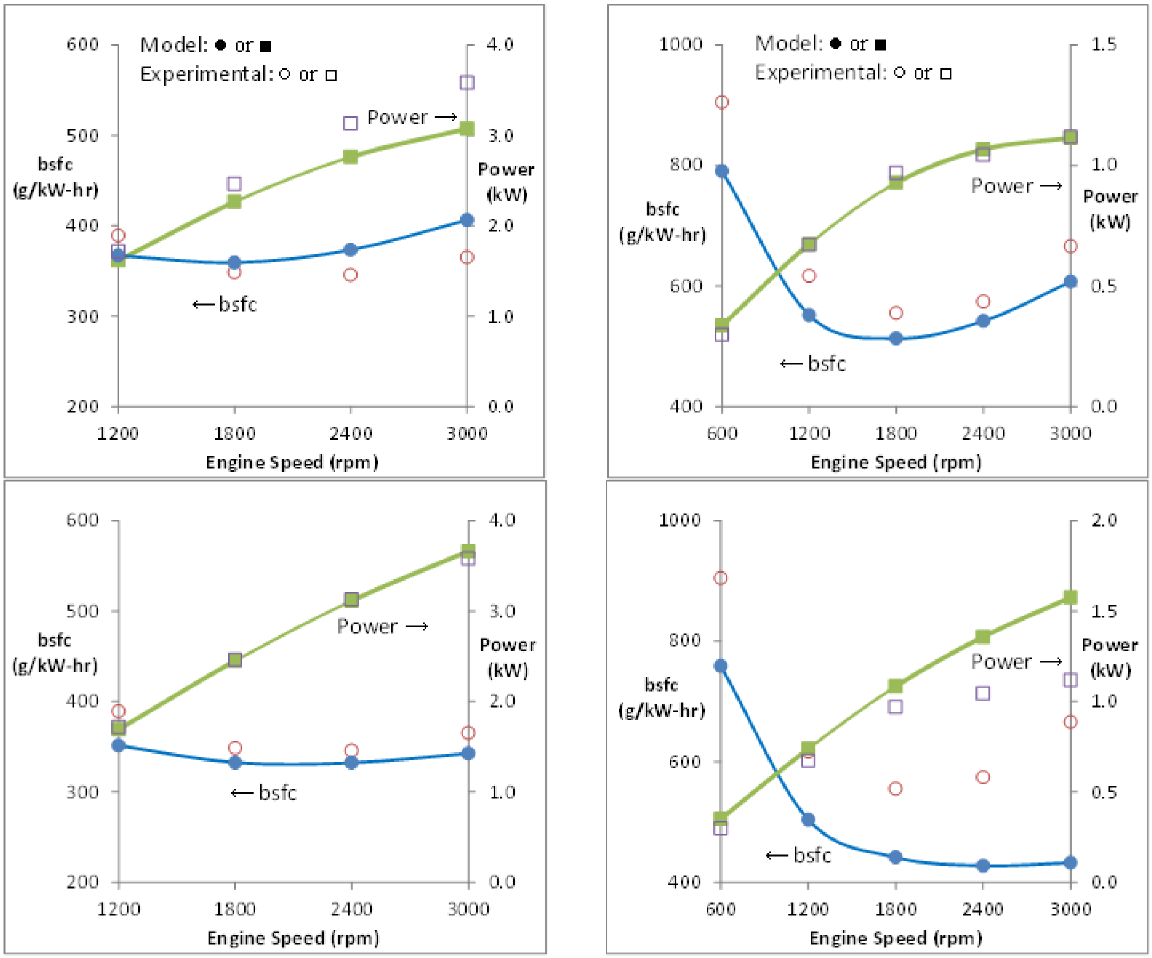

Figure 5.3
Comparison of power and bsfc for models with and without pressure corrections
Left column: 3.45 MPa mean engine pressure
Right column: 1.72 MPa mean engine pressue
Top row: With compressibility and oscillatory flow corrections
Bottom row: No corrections

Figures 5.4a and 5.4b show the decoupled losses as a percentage of the total loss for 6.9 MPa and 1.72 MPa. At 6.9 MPa, regenerator ineffectiveness, flow dissipation, and regenerator wall losses are the largest. At 1.72 MPa, the regenerator wall conduction and flow dissipation are the two biggest losses. The wall conduction losses are constant over all pressures and engine speeds since they are mainly dependent on temperature and geometry, but become a larger percentage of the total loss as engine speed and pressure are reduced. For example, at 1.72 MPa and 10 Hz, the regenerator wall conduction is still the same magnitude (800 W), but is 69% of the losses. The loss due to non-ideal regenerator operation is more significant at higher pressures due to the resulting larger mass flow rates that reduce the amount of time for heat transfer. Not shown in Figures 5.4a and 5.4b are the displacer internal heat losses which were much less than 1% of the total loss.

Figures 5.5a and 5.5b show the external energy balance as a function of engine speed for 6.9 MPa and 1.72 MPa. At 6.9 MPa, the engine output decreases as a fraction of the total energy input, while the cycle heat rejection remains fairly steady as engine speed increases. The exhaust losses increase from 15% to over 23%. For 1.72 MPa, the engine output peaks at an engine speed of 30 Hz (1800 rpm). The cycle heat rejection increases as engine speed increases, while exhaust losses are constant. The losses to the environment become significant at low pressures and low engine speeds, being more than 20% at 10 Hz. These trends are similar to those from Figure 11 of Thieme, 1979.

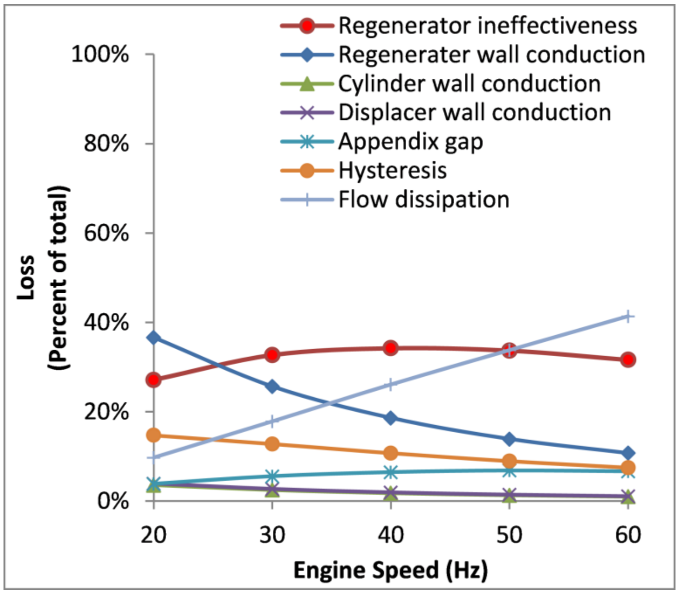

Figure 5.4a
GPU-3 Decoupled Losses
(6.9 MPa Mean Pressure)

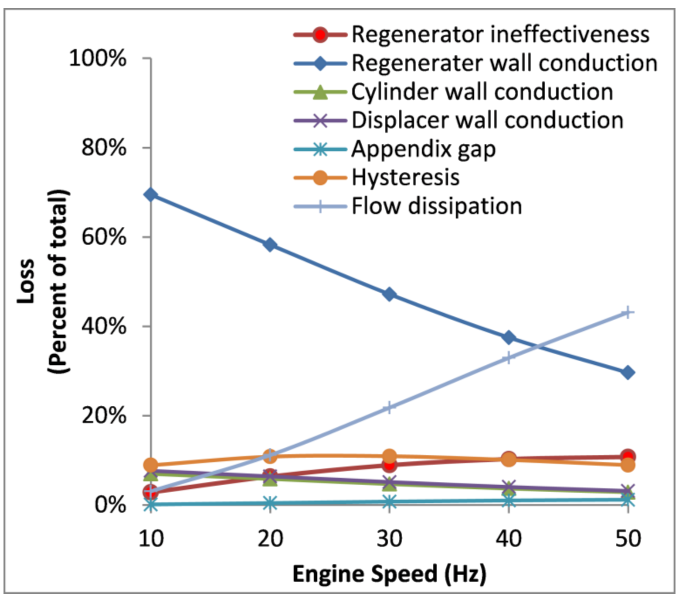

Figure 5.4b
GPU-3 Decoupled Losses
(1.72 MPa Mean Pressure)

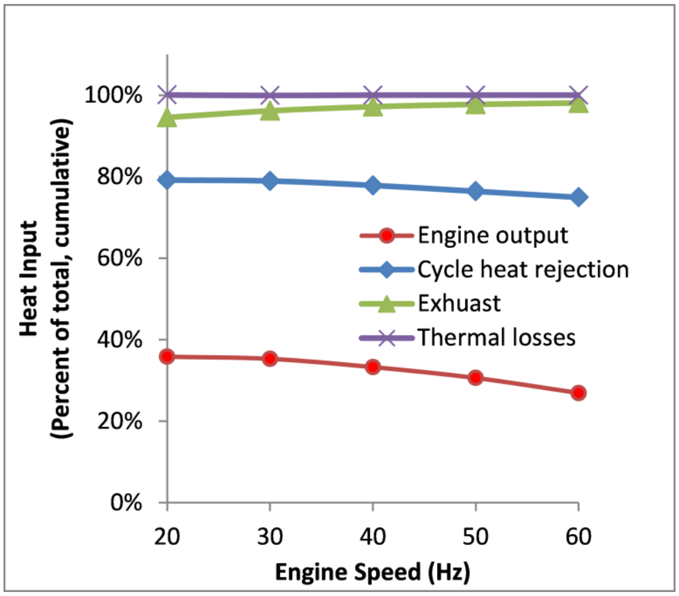

Figure 5.5a
GPU-3 Energy Balance
(6.9 MPa Mean Pressure)

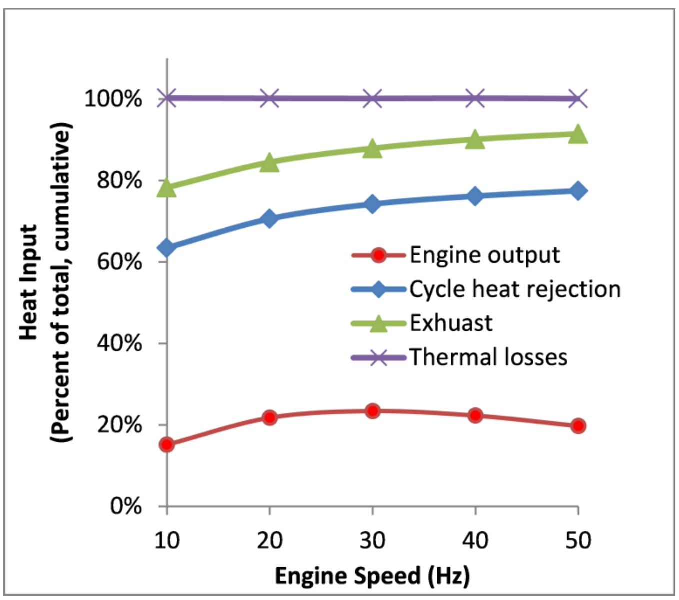

Figure 5.5b
GPU-3 Energy Balance
(1.72 MPa Mean Pressure)

CHAPTER 6

System Analysis

The complete system needs to produce a net 5 kWe. The specific engine to be used is a derivative of the GM GPU-3.The temperature of the products of combustion exiting the combustor is to be 900°C. The adiabatic flame temperature needs to be below the point at which ash begins to melt (1250°C) if such fuels as wood and garbage are used (Pålsson, 2003). The dimensions of the GPU-3 engine are changed to better suit the lower heater temperatures. Two-cylinder versions are investigated as well, being either in parallel like the Philips 4-235 or in series, staged in a simplified Fauvel-Stirling arrangement (Walker, 1992). To increase the thermal efficiency and reduce NOx emission, a combustion gas recirculation (CGR) system is added.

The fuel for this particular analysis is biogas produced from digestion of food and human waste. It consists of 55% methane, 43% carbon dioxide, and 2% water vapor by volume. The lower heating value (LHV) of this biogas is 15705 kJ/kg fuel. The presence of the carbon dioxide and water vapor may be beneficial in reducing NOx emissions. See Lee *et al* (2001) and Zhao *et al* (2002). Using NASA's Chemical Equilibrium with Applications (CEA) program and an equivalence ratio,   air-fuel mass ratio/stoichiometric air-fuel mass ratio, (λ) of 1.1, the adiabatic flame temperature is calculated to be 2005 K. The amount of CGR is estimated to be at least 233% of inlet mass flow rate to keep the adiabatic flame temperature below 1250°C, using a CGR gas temperature of 650°C.

6.1 Single Cylinder Engine

The performance of the GPU-3 was investigated as the combustor gas temperature was reduced. Figure 6.1 shows the engine indicated efficiency and the total system efficiency. The mean pressure was 6.9 MPa; the engine speed was 30 Hz using hydrogen. The heater tube temperature was adjusted so that the system produced the maximum amount of power. The system has an efficiency of 5.9% at the desired temperature of 900°C. The indicated engine efficiency is 27.0%.

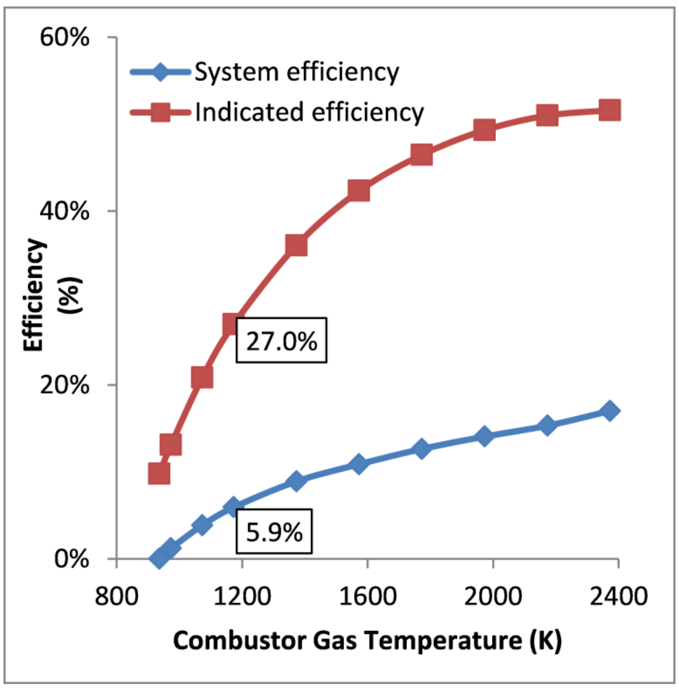

Figure 6.1
GPU-3 Efficiencies as Combustor Gas Temperature is Reduced

Figure 6.2 shows the net usable power produced by the system, the power consumed by the fans and water pump, the heat supplied to the heater, the cycle heat rejection and the amount of heat added from the fuel. At 1173K, 1600 W net are produced and 644 W are consumed to drive the fans and pump. The lowest possible temperature at which the GPU-3 would run is estimated to be 936 K.

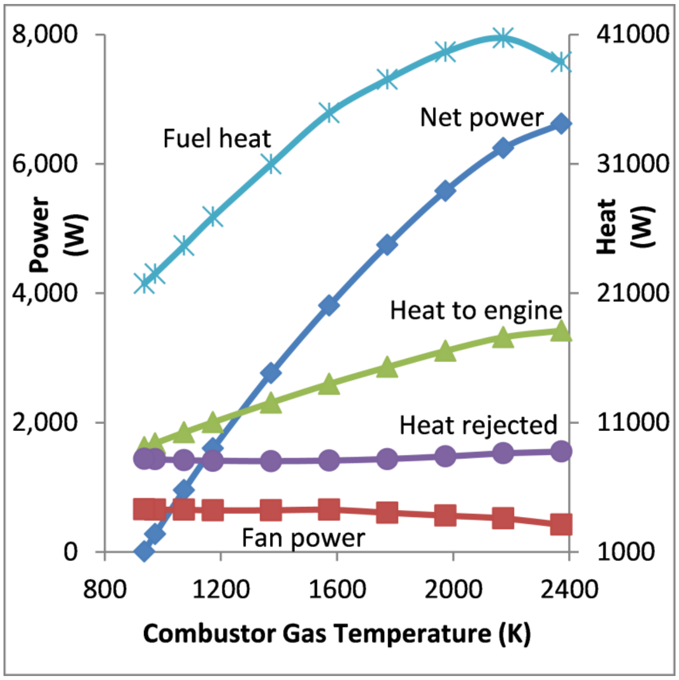

Figure 6.2
GPU-3 Power and Heat as Combustor Gas Temperature is Reduced

Figure 6.3 shows the pressure drop through the system, heater and preheater. The pressure drop is 8.5 kPa and the mass flow rate is 3644 g/min at a combustor temperature of 1173K. This estimate of pressure loss seems reasonable since Thieme (1979) reported a pressure drop of 3.85 kPa at a mass flow rate of 1238 g/min while (1981) a pressure drop of 3.23 kPa at a mass flow rate of 762 g/min was recorded.

Figure 6.4 shows the mass flow rate, the density and velocity squared through the heater. The density increases as the temperature drops. The velocity squared peaks then decreases with temperature faster than the density increases. The net result is that the pressure drop through the heater follows the velocity.

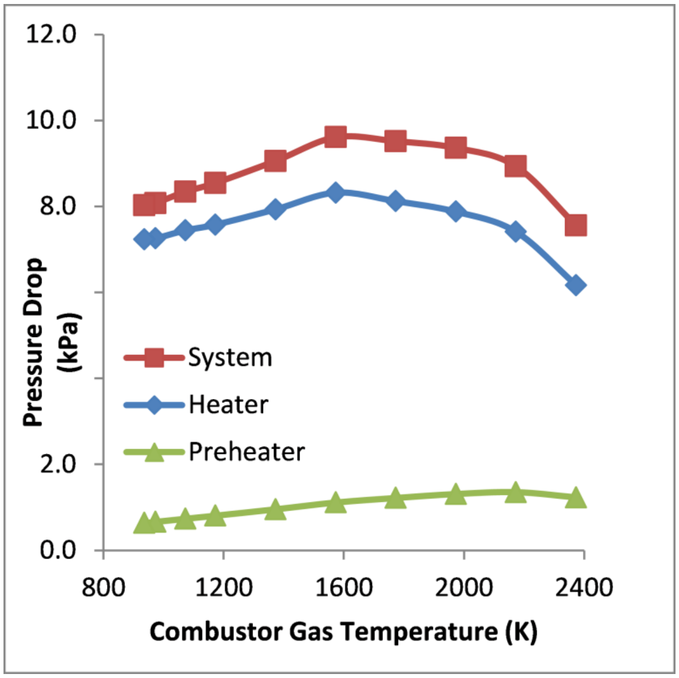

Figure 6.3
GPU-3 Pressure Drop as Combustor Gas Temperature is Reduced

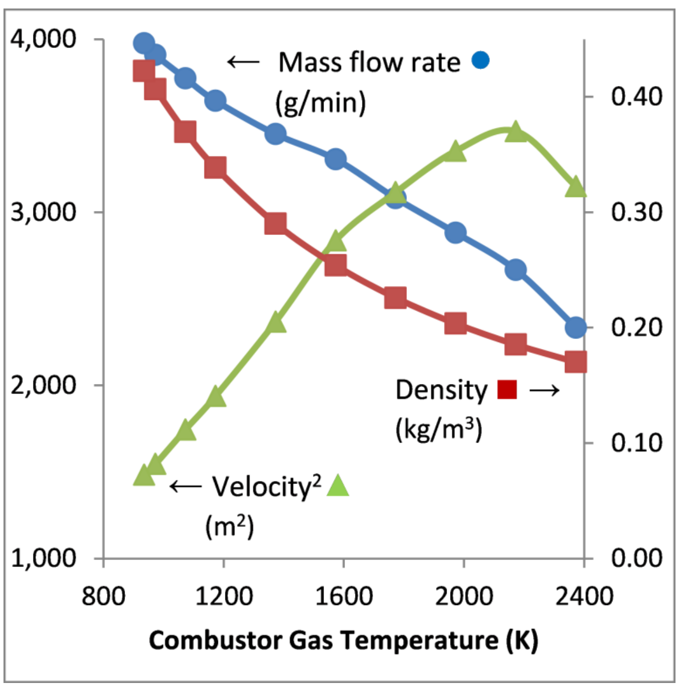

Figure 6.4
GPU-3 Mass Flow Rate, Density and Velocity^2 as Combustor Gas Temperature is Reduced

Figure 6.5 shows the energy balance as a percent of the total heat input. The exhaust losses increase from 50% then level off. Drivetrain losses decrease slightly, while heat loss to the environment increases slightly. Power drops off, more rapidly as the temperature decreases. Cycle heat rejection goes down a small amount then increases. The amount of heat rejection is fairly constant, but as a fraction of the amount of energy added, it increases due to the decreasing engine efficiency and decreasing heat input to the engine.

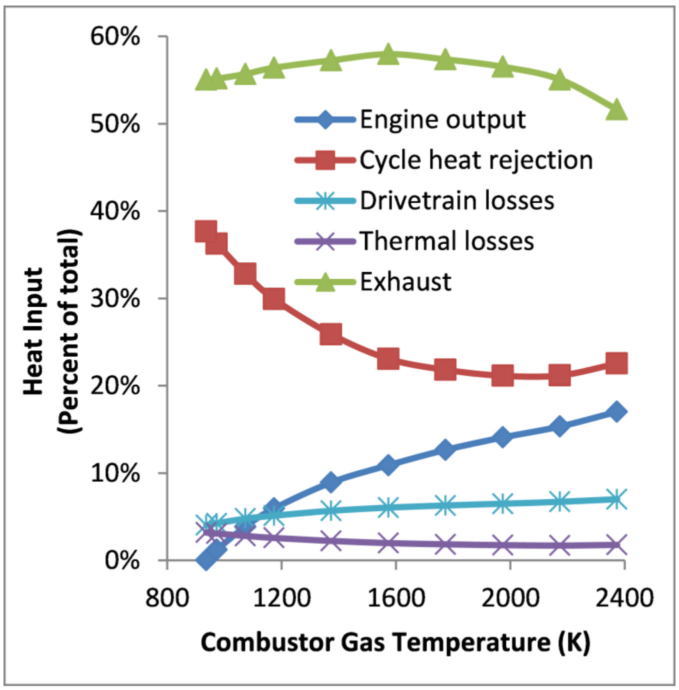

Figure 6.5
GPU-3 Energy Balance as Combustor Gas Temperature is Reduced

The performance of the unmodified GPU-3 at 900°C is 1600 W. From Figure 6.2, it is evident that the engine is being choked from a lack of heat input. Due to the decreasing engine efficiency, the heat input needs to increase as temperature drops to achieve the necessary power output. From Equation (24), the convection coefficient (U) is a function of the fluid velocity. It is limited by the need to keep fan power consumption reasonable. The log-mean-temperature-difference (LMTD) is determined by the gas temperature and tube temperature, which in turn is a function of the fluid velocity. Only the surface area (A) can be increased.

Figure 6.6 shows the effect of increasing the heater surface area on net power, power consumed by the fans and pump, and the heat input to the engine. The surface area was increased by lengthening the heat transfer section of the heater tubes from 15.54 cm to 26.0 cm and by increasing the number of heater tubes from 40 to 60. The maximum tube length is set at 26.0 cm which is the length as used in the USS 4-95 engine without significant problems running on hydrogen at 30 Hz. (West, 1986)

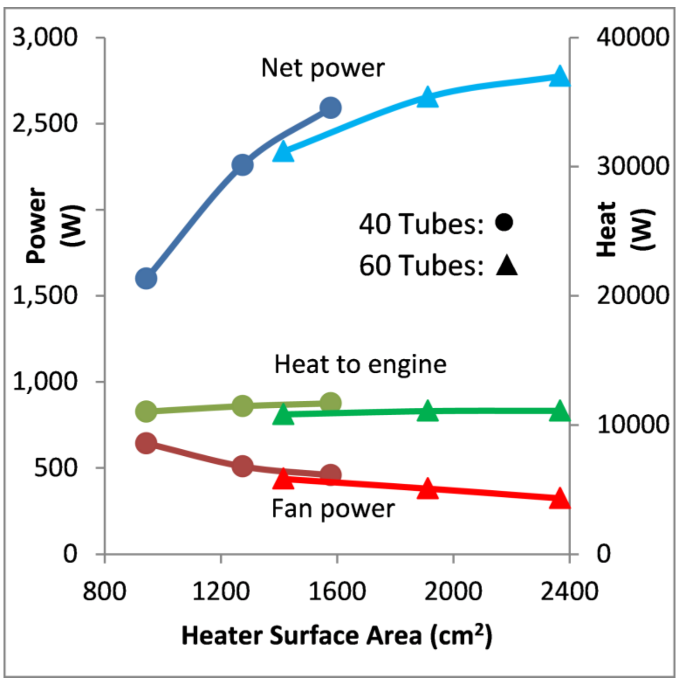

Figure 6.6
Effect of Increased Heater Surface Area on Engine Performance

The length of the cylinder is increased to accommodate an extra row of heater tubes. The heater tubes of the GPU-3 are arranged in two staggered rows where they meet the cylinder. A third staggered row is needed for additional tubes to be used with the same diameter cylinder. Also, the height of the preheater is increased to match the extra length of the heater tubes. The maximum net power increased to 2775 W from 1600 W. The system efficiency went from 5.9% to 9.1% while the engine's indicated efficiency increased from 27.0% to 37.1% due to the ability to maintain the heater tubes at a higher temperature, from 672 K to 878 K. Despite the increase in dead volume, the system power and efficiency both improve. At the same tube temperature (766 K), the indicated efficiency decreases from 33.17% for 40 tubes at 15.54 cm to 32.83% for 60 tubes at 26.0 cm length. A further increase in heater tubes by a fourth row decreased the maximum power attainable.

To meet the 5 kWe power requirement, the engine must be increased in size. Since the original engine was designed to produce approximately the same power level, the dimensions of the drive mechanism are not changed. The diameter of the cylinder is increased. This allows the number of heater tubes to increase. As the number of tubes increases, the vertical heat transfer section must be located further away from the cylinder, thereby increasing the total unheated length of the tubes. The size of the preheater surrounding the heater tubes is enlarged to fit over the heater tubes and optimized to minimize the total pressure loss of both streams. The size of the regenerator canisters is also increased, maintaining the same engine-swept-volume-to-regenerator-volume ratio. The length of the cooler tubes is increased to 9.0 cm as used in the USS 4-95 and the number of cooler tubes is increased; maintaining the same ratio of cooler tubes-to-engine swept volume.

Figure 6.7 shows the net electrical power produced by the system as the piston and cylinder diameters are increased. Engines using three rows of heater tubes are able to reach the power requirement. Engines using two rows of heater tubes are not able to meet the power requirement; the maximum is 4.8 kWe. The gross power of the engine using 2 rows of heater tubes increases but at a rate that decreases with diameter, while the power consumed by the fan increases nearly linearly. The result is that the extra power produced by the engine is less than the power consumed by the fan as the engine becomes larger.

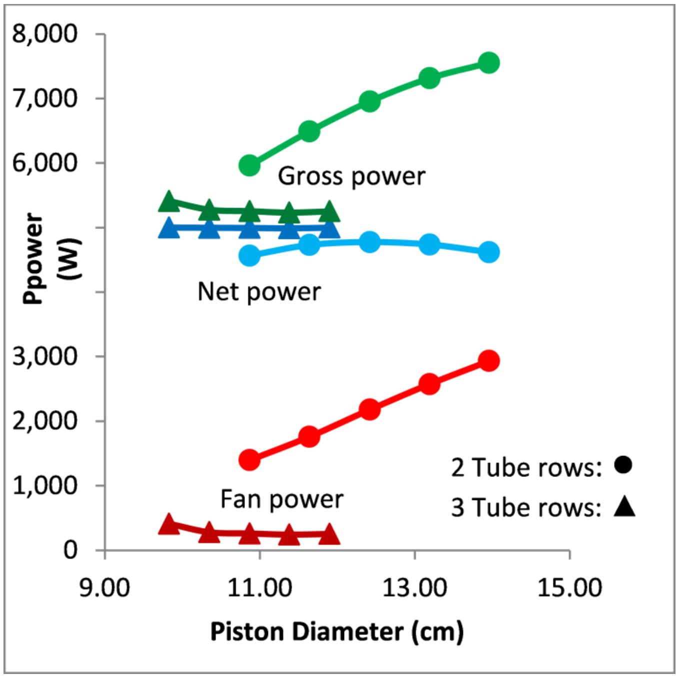

Figure 6.7
Effect of Increased Piston Diameter on Engine Power

Figure 6.8 shows the overall system efficiency. The engine using 3 tube rows (piston diameter of 10.87 cm; expansion space swept volume 292 cm^3) produces 5.0 kWe at a system efficiency of 12.4%. The maximum system efficiency occurs where the heat added to the incoming air is at a minimum. The engine using 2 tube rows (piston diameter of 12.42 cm; expansion space swept volume 382 cm^3) produces 4.8 kWe at a system efficiency of 5.8%. The higher efficiency of the engine with 3 tube rows is due primarily to the lower gas velocity over the heater tubes, lowering the mass flow rate

(5422 g/min v. 11137 g/min), the exhaust losses and the fan power consumption. The system using the engine with 2 tube rows can achieve 5.0 kWe by removing the preheater thereby reducing the fan power consumption and the system efficiency (2.9%). It may also be possible to reach the power requirement using the engine with two tube rows if the engine were better optimized. Timoumi *et al* (2008) report that the GPU-3 may produce up to 20% more power by choosing more optimal engine dimensions; the GPU-3 derivative used here may well respond similarly.

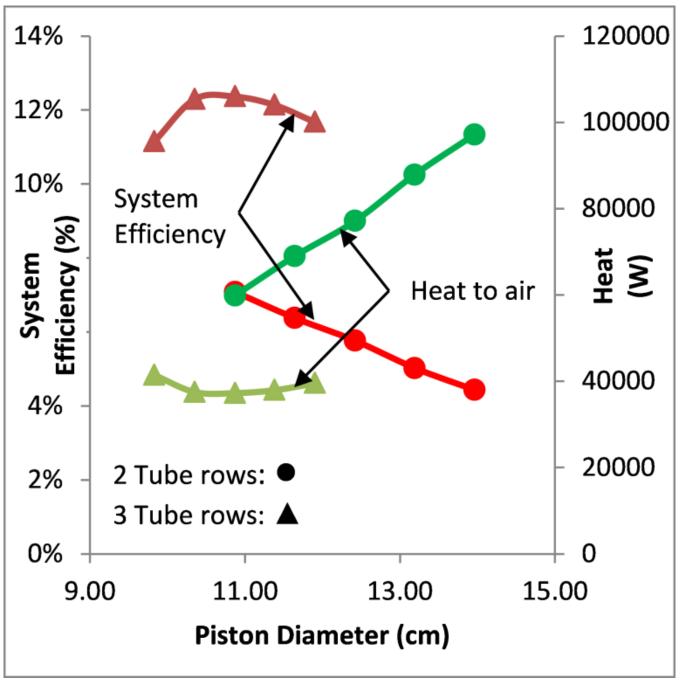

Figure 6.8
Effect of Increased Piston Diameter on Engine Efficiency

Figure 6.9 shows the effect the gap between the heater tubes has on the system power and efficiency for the engine that uses 2 rows of heater tubes with a piston diameter of 12.42 cm. Maximum efficiency occurs at the lowest possible tube gap. There is a heater tube gap that minimizes fan power consumption thereby maximizing system power. The net power increases to 4.9 kWe at 4.9% when the gap is 0.088 cm versus the 0.067cm gap used on the GPU-3.

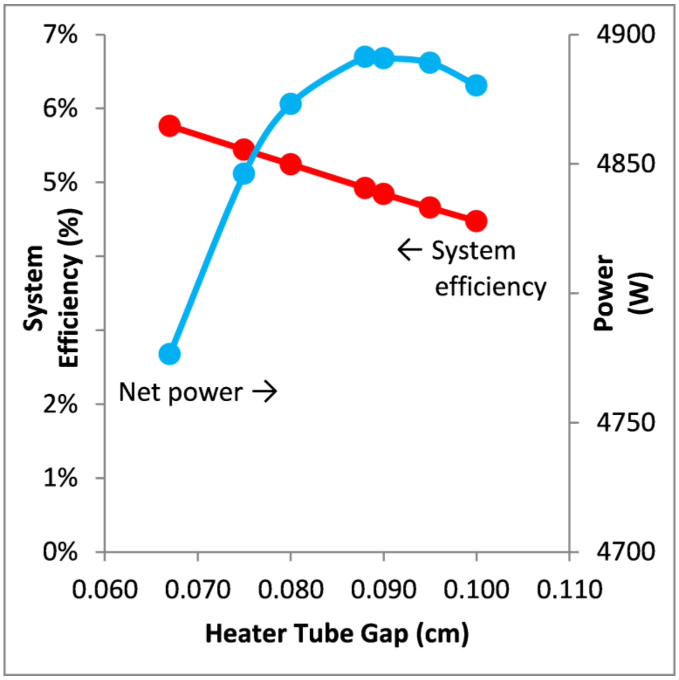

Figure 6.9
Effect of Heater Tube Gap on System Power and Efficiency

6.2 Multiple Cylinder Engine – Parallel Configuration

Two single cylinder engines could be combined to produce the necessary power. Two GPU-3s with 40 heater tubes of 26 cm length would produce 5.0 kW at an efficiency of 10.4%. Combining the engines together in a single crankcase and using a single preheater and radiator would produce the same performance and reduce the number of components. The complication is the extra tubing needed to route the gas to-and-from the preheater. There have been a few such engines: Philips 4-235 (Hargreaves, 1991) and the GM 4L23 (Martini, 1983). Both were large, 4 cylinder high power transportation prime movers. The 4-235 used four separate displacer-piston pairs and a rhombic drive, while the 4L23 used four interconnected double acting pistons and the crank-slider mechanism.

Figure 6.10 shows the power and efficiency for an engine using two cylinders in parallel. The maximum system efficiency is 15.4% for an engine using three tube rows (64 tubes) per cylinder with a piston diameter of 7.51 cm (139 cm^3 swept volume). The maximum efficiency for two tube rows (40 tubes) is 13.7%.

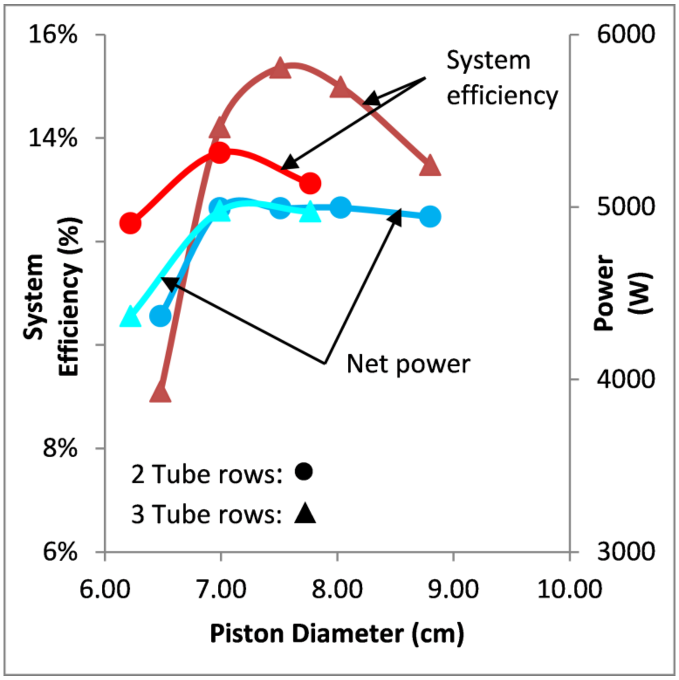

Figure 6.10
Performance of Two-Cylinder Engines – Parallel as Engine Size Varies

6.3 Multiple Cylinder Engine – Series Configuration

Instead of having two-cylinders in parallel, the two cylinders can be used in series, i.e. the second uses the exhaust from the first. While the engine used here is a beta configuration, having the pistons in separate cylinders as in an alpha or gamma type, e.g. SOLO 161, allows a better heater configuration that facilitates routing the exhaust from the first to the second engine. Figure 6.11 shows the performance of the two-cylinder-series engine as the heater tube gap of the first engine is varied. The engine used is the same one for the two-cylinder-parallel arrangement (piston diameter 7.51 cm; 64 heater tubes) except that the heater tube gap for the 1st engine is varied. For a 1st engine heater tube gap of 0.204 cm, both engines produce 50% of the power. The second cylinder produces the same amount of power despite the lower gas temperature because the gas is squeezed through the smaller tube gap of the second cylinder, increasing the gas velocity and the convection coefficient. When both cylinders have the same heater tube gap (0.067 cm), the second cylinder produces 40.7% of the power. Maximum system efficiency occurs when both engines have the same minimum heater tube gap. The system efficiency is now 17.1% compared to 15.4% in parallel for essentially the same amount of hardware.

Figure 6.12 shows the fan consumption and the exhaust losses as the 1st tube gap is varied. The power consumption of the fan first reaches a minimum, and then increases as the gap is increased from 0.067 cm to 0.204 cm, while exhaust losses increase as the first engine heater tube gap is increased. Minimizing exhaust losses maximizes system efficiency. The exhaust losses decrease due to the mass flow rate of gas decreasing. As for the single cylinder engine, there is a heater tube gap for the first cylinder that minimizes fan consumption and maximizes net power; in this case 0.115 cm.

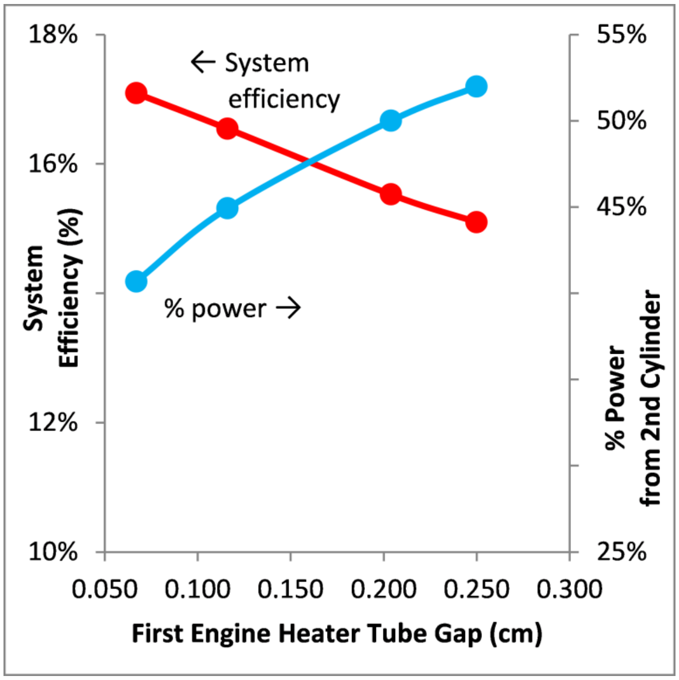

Figure 6.11
Effect of First Engine Heater Tube Gap on System Efficiency and Power Produced from 2nd Engine

Figure 6.13 shows the system efficiency as the size of the two cylinders is varied. The maximum efficiency occurs when the heat absorbed by the air is at a minimum. The engine with a piston diameter of 6.48 cm was only able to produce a maximum of 4.35 kW, not the necessary 5 kWe. Since the system efficiency improved by having the 1st cylinder produce more power, the size of the 1st cylinder was increased and the 2nd was decreased. The efficiency did improve on the order of 0.1% but that is not significant enough to be important.

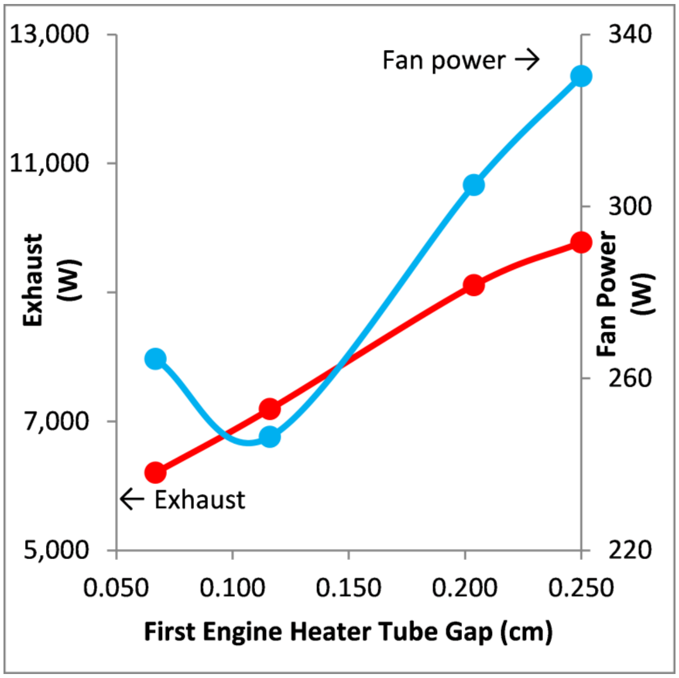

Figure 6.12
Effect of First Engine Heater Tube Gap on Exhaust Losses and Fan Power Consumption

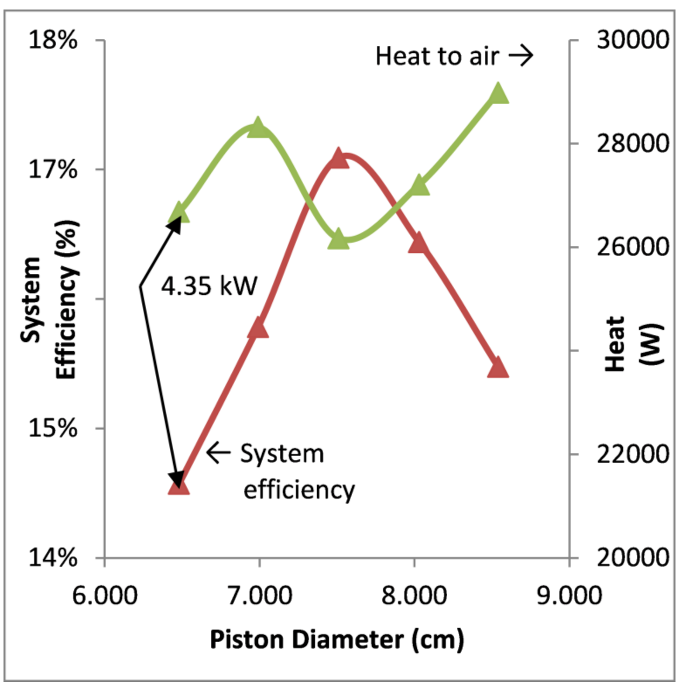

Figure 6.13
Performance of Two-Cylinder Engines – Series as Engine Size Varies

All of the engines modeled have had regenerators sized so that the ratio of the swept volume-to-regenerator volume has been kept the same as the original GPU-3. From Figure 5.4, the regenerator is the largest source of loss. Figure 6.14 shows the effect of increasing the regenerator volume on the system efficiency. The maximum system efficiencie for all engines increases. The largest increase is for the single-cylinder, two-tube-row engine, from 5.7% to 12.7%. The highest efficiency is now 19.8% for the two-cylinder series engine. As the regenerator diameter increases, the engine and system efficiencies increase but the power output decreases due to the increase in dead volume. The power output is maintained by increasing the mass flow rate of combustion gas over the heater thereby adding to the heat transferred to the engine. Beyond a certain point, the system efficiency peaks as the fan power consumption increases faster than the engine output.

Organ (1997) suggested that the GPU-3 regenerator was too small, on the order of 50% of the ideal size, while the USS 4-95 was nearly ideal. Using the swept volume-to-regenerator void volume of the 4-95 as a guide limits the size of the regenerators for the single cylinder engines. The maximum efficiencies for the two-cylinder engines occur before the limit. The maximum efficiency is now 15.9% and 11.4% for the 3-tube and 2-tube single-cylinder engines respectively.

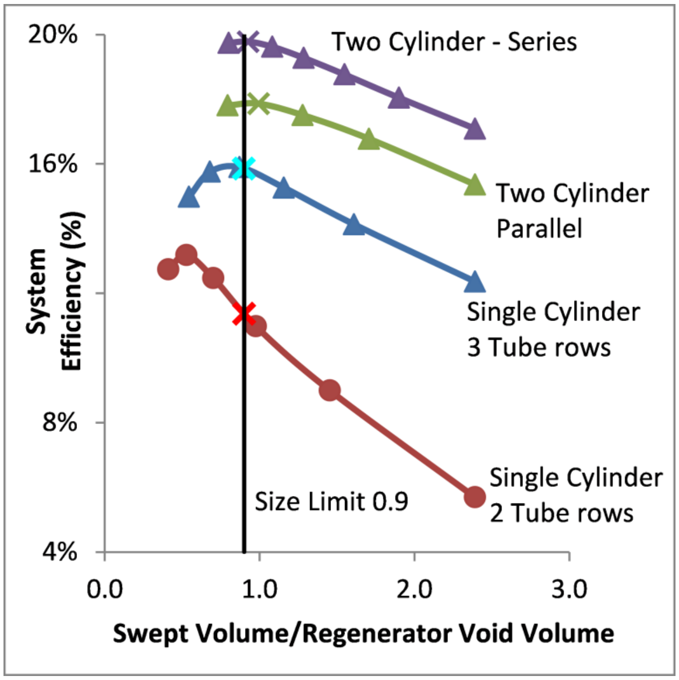

Figure 6.14
System Efficiency as Regenerator Volume Increases

6.4 Combustion Gas Recirculation

All of the engine/system combinations thus far have used a preheater but no combustion gas recirculation system. Table 6.1 shows the effect of adding CGR (% of inlet mass flow rate) to the single-cylinder and two-cylinder engines. The amount of CGR is the maximum possible while keeping λ at 1.1. Adding CGR increases system efficiency to a maximum of 24.7% for the two-cylinder series engine. CGR has a larger effect on systems with larger mass flow rates; hence the larger increase in efficiency for the two-cylinder parallel system compared to the two-cylinder series system. If the single-cylinder, two-tube row engine had its regenerator at the size that maximized system efficiency, the increase due to CGR would be larger than for the single-cylinder three-tube row engine. The main effect of the CGR is to reduce the amount of fuel needed and the exhaust losses. The reduction in fan power consumption is due to the pressure drop being reduced since the mass flow rate through the preheater is smaller.

Engine	Mass Flow Rate (g/min)	System Efficiency (%)	Fan (W)	Fuel Heat (W)	Exhaust Losses (W)
1-Cylinder (2 tube rows)	5935	11.4	456	44238	18975
+ CGR (669%)	5797	18.3	371	27342	2220
1-Cylinder (3 tube rows)	4258	15.9	155	31542	12047
+ CGR (614%)	4217	23.6	132	21206	1750
2-Cylinder Parallel	4025	17.9	166	28052	8044
+ CGR (614%)	3935	24.4	111	20636	1394
2-Cylinder Series	3093	19.8	215	25237	5373
+ CGR (456%)	3056	24.7	169	20286	1178

Table 6.1
The Effect of Adding CGR on System Performance for One- and Two-Cylinder Engines

6.5 System Design

The performances of the systems using engines with three-heater tube rows per cylinder are similar. The two-cylinder configurations offer a small advantage efficiency wise but the engine would cost nearly twice as much. The single-cylinder, three-heater-tube row engine offers the best compromise between performance and manufacturing cost and is therefore the better choice.

Table 6.2 shows the system operating point. The dimensions for the single-cylinder, three-heater-tube row engine are given in Appendix C.

	Mass Flow Rate (g/min)	Temperature (K)
Inlet air ①	509	298
Preheated air ②	509	853
Fuel	81	298
Combustor exit ③	4217	1173
Heater exit ④	4217	940
CGR	3627	940
Exhaust ⑤	590	473
Heater pressure drop (kPa)	0.672	
Preheater pressure drop, both streams (kPa)	0.138	

Table 6.2
System Operating Point
(① refer to Figure 4.2)

CHAPTER 7

Conclusions

7.1 Summary

The goal of this research is to develop a Stirling engine based generator set running off of alternative, lower quality fuel sources. Lower quality fuel sources have higher levels of impurities and lower energy content. One such application is part of a system to produce potable water to forward operating bases (FOB) in an energy self-sufficient manner. The history, theory, and configurations of Stirling engines were reviewed, along with some representative engines described in detail. The modeling of Stirling engines and systems employing Stirling engines was examined. A generator set employing a derivative of an existing, proven Stirling engine was analyzed and specified.

Second order models of Stirling engines were reviewed and a model was developed for use in designing the generator set. The ideal adiabatic model plus simple heat exchanger was developed in detail. Decoupled loss mechanisms were incorporated including thermal shorts, flow dissipation, gas hysteresis, regenerator loss and appendix gap loss.

System models using Stirling engines were reviewed and a model of the complete system was developed. The fan was modeled as an adiabatic compression process. The combustor was modeled as a steady flow device using a control volume formulation. The external heat transfer to the engine was modeled using a heat transfer convection coefficient and a log-mean-temperature difference. The preheater and cooling systems were modeled as compact heat exchangers using thermal circuits and an overall heat transfer coefficient. The system and engine models were validated using experimental data for the General Motors GPU-3 Stirling engine based generator set.

A derivative of the General Motors GPU-3 Stirling engine was specified. The effect of lower combustion gas temperatures on the operation of the GPU-3 was analyzed. The dimensions of the GPU-3 were modified to produce the necessary power while operating at a significantly lower temperature. The diameter of the cylinder was increased to produce the power requirement, while the rhombic drive was kept unchanged from the original GPU-3. The length and number of heater tubes were increased dramatically to allow a higher rate of heat transfer to provide the energy to drive the engine. The length and number of cooler tubes were increased as well to provide more cooling capacity to improve engine efficiency. The size of the regenerator was increased as well. The increased heater and cooler surface areas and regenerator size improved performance of the system at the lower operating temperature despite the significant increase in engine dead volume.

Multiple cylinder Stirling engines were investigated as well as the single-cylinder GPU-3 based derivative. Two smaller single-cylinder engines were combined into an engine with a single crankcase, combustor, preheater and cooling system. Parallel and series (simplified Stirling-Fauvel) engines improved efficiency over single-cylinder ones. The series configuration had the highest efficiency of all possible engines. But at the small scale of this generator set, the increase in efficiency was not significant enough to justify the extra manufacturing cost.

Combustion gas recirculation (CGR) was added to the system. The addition of CGR to the single cylinder and two-cylinder engines significantly increased system efficiency. The main effect of CGR is to reduce the mass flow rate of the exhaust gases. The system efficiency improves since less energy is lost through the exhaust. The pressure drop through the preheater is reduced as well, decreasing the power consumption of the fan.

7.2 Contributions

The review of the second order models revealed that all of them, including the more basic thermodynamic type analyses that maintain mass and energy conservation and the more complex types that include momentum, use friction factors developed for steady, incompressible flow. A non-dimensional parameter grouping was identified that shows that losses due to flow dissipation increase dramatically at lower mean pressures and higher engine speeds. By providing simple corrections to the flow dissipation models to account for the non-steady, compressible flow, the ideal adiabatic model can be reasonably accurate over a wide range of engine pressures and speeds.

A simple yet effective model was developed to include the external heat transfer to the Stirling engine heater that can be used with any of the second order Stirling engine models that assume the heater tube temperature is constant. Using the heat transfer correlation for a single tube in cross-flow, but specifying the mass average velocity between the tubes in defining the Reynolds number, the heat transfer convection coefficient can be estimated with acceptable accuracy. The rate of heat transfer to the engine can then be determined by employing a log-mean-temperature-difference along with the convection heat transfer coefficient.

The development of the GPU-3 based Stirling engine revealed that the standard practice of minimizing dead volume may not lead to the best engine. At the lower temperatures of this system, engine and system performance both increased significantly by enlarging the heater and cooler. Increasing the size of the regenerator was also shown to improve the performance of the engine and system. The improvement in heat transfer to the engine and increased efficiency more than offset the effect of the increase in dead volume.

7.3 Recommendations

The Stirling engine based generator set specified needs to be manufactured. While the models were validated using GPU-3 data, the specified system should be built and tested to verify the models developed for use at the lower temperatures.

A rigorous criterion to determine when compressibility and unsteady effects in a Stirling engine are significant should be developed. The evaluation of the $\mu\left(\frac{d_o}{L_o}\right)\left(\frac{\omega_o}{P_o}\right)$ coefficient and the $\left(\nabla(\nabla\cdot\tilde{\boldsymbol{u}})\right)$ term of the momentum equation for a range of engines and operating conditions would provide this.

While the performance of a Stirling engine can be reasonably predicted using one of the second order models, these models do not provide enough information to properly describe the fluid flow in the engine components. Flow dissipation losses are one of the largest in a Stirling engine; reducing them would allow the engine efficiency to increase. Currently, only a full 3-D transient CFD analysis can provide such knowledge of the internal flow characteristics for Stirling engines using tubular heaters and coolers. For Stirling engines that use annular heaters and coolers, a 2-D axisymmetric CFD analysis can be employed. A pseudo 3-D CFD method needs to be developed that can provide internal flow information without the cost and time of a full 3-D simulation.

The development of the derivative engine shows the importance of the heater in determining the performance of the engine and system, especially at lower combustion gas temperatures. Heater surface area was increased by using more, longer tubes. Surface area may also be increased by using fins or using tubes of non-circular cross-sectional shape. Other means of augmenting heat transfer could also lead to increased rates of heat transfer such as using impinging jets, coiled heater tubes or turbulence generators.

The analysis of the two-cylinder engines suggests that they may provide improved performance over single cylinder engines. Multiple-cylinder Stirling engines are necessary to reach high power densities, but they may offer significant advantages in efficiency at lower temperatures and higher power requirements. At the low power requirements of the system, the increased performance was too small to be justified considering the extra manufacturing costs. Developing a larger system on the order of 25 kW might show that the multiple-cylinder engines enhance performance enough to justify the expense.

APPENDICES

APPENDIX A

Equation Set
Ideal Adiabatic plus Simple Heat Exchanger including cooler-regenerator manifold, regenerator-heater manifold and appendix gap (Based off of Urieli, 1984)

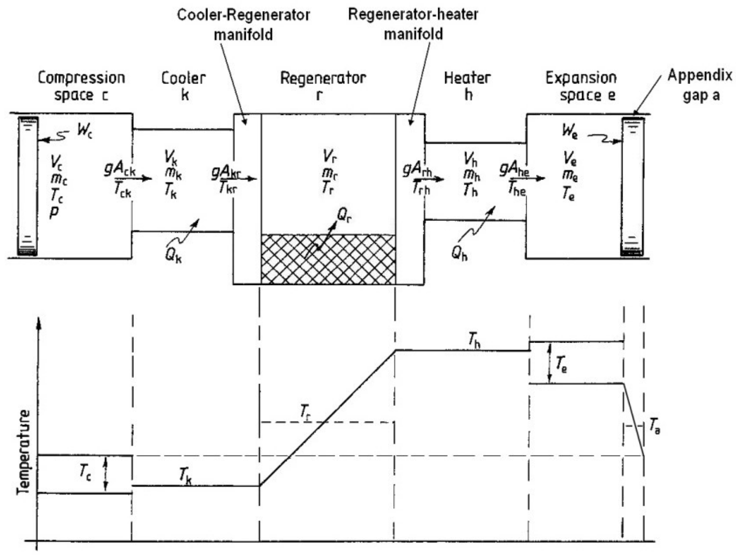

Figure A1
Adiabatic Model Volumes and Temperatures

Pressure, P

$$dP = \frac{-\gamma P\left(\frac{dV_c}{T_{ck}} + \frac{dV_e}{T_{he}}\right)}{\left[\frac{V_c}{T_{ck}} + \frac{V_e}{T_{he}} + \gamma\left(\frac{V_k}{T_k} + \frac{V_{ri}}{T_{ri}} + \frac{V_r}{T_r} + \frac{V_{ro}}{T_{ro}} + \frac{V_a}{T_a}\right)\right]}$$

$$P = \frac{MR}{\left(\frac{V_c}{T_c} + \frac{V_k}{T_k} + \frac{V_{ri}}{T_{ri}} + \frac{V_r}{T_r} + \frac{V_{ro}}{T_{ro}} + \frac{V_h}{T_h} + \frac{V_e}{T_e} + \frac{V_a}{T_a}\right)}$$

Mass, m

$$dm_c = \frac{1}{RT_{ck}}\left(PdV_c + \frac{dV_c dP}{\gamma}\right)$$

$$dm_e = \frac{1}{RT_{he}}\left(PdV_e + \frac{dV_e dP}{\gamma}\right)$$

$$dm_k = \frac{m_k}{P}dP$$

$$dm_r = \frac{m_r}{P}dP$$

$$dm_h = \frac{m_h}{P}dP$$

$$dm_{ri} = \frac{m_{ri}}{P}dP$$

$$dm_{ro} = \frac{m_{ro}}{P} dP$$

$$dm_a = \frac{m_a}{P} dP$$

$$m_c = \frac{PV_c}{RT_c}$$

$$m_e = \frac{PV_e}{RT_e}$$

$$m_k = \frac{PV_k}{RT_k}$$

$$m_r = \frac{PV_r}{RT_r}$$

$$m_h = \frac{PV_h}{RT_h}$$

$$m_{ri} = \frac{PV_{ri}}{RT_{ri}}$$

$$m_{ro} = \frac{PV_{ro}}{RT_{ro}}$$

$$m_a = \frac{PV_a}{RT_a}$$

Mass Flows, ṁ

$$\dot{m}_{ck} = -dm_c$$

$$\dot{m}_{kr} = \dot{m}_{ck} - dm_k$$

$$\dot{m}_{rir} = \dot{m}_{kr} - dm_{ri}$$

$$\dot{m}_{rro} = \dot{m}_{rir} - dm_r$$

$$\dot{m}_{rh} = \dot{m}_{rro} - dm_{ro}$$

$$\dot{m}_{he} = \dot{m}_{rh} - dm_h$$

$$\dot{m}_{ea} = dm_a$$

Temperatures, T

$$dT_c = T_c\left(\frac{dP}{P} + \frac{dV_c}{V_c} - \frac{dm_c}{m_c}\right)$$

$$dT_e = T_e\left(\frac{dP}{P} + \frac{dV_e}{V_e} - \frac{dm_e}{m_e}\right)$$

$$T_r = \frac{(T_h - T_k)}{\ln\left({}^{T_h}/_{T_k}\right)}$$

$$T_a = \frac{(T_e - T_c)}{\ln\left({}^{T_e}/_{T_c}\right)}$$

Conditional Temperatures

$$if\ \dot{m}_{ck} > 0\ then\ T_{ck} = T_c, else\ T_{ck} = T_k$$

$$if\ \dot{m}_{he} > 0\ then\ T_{he} = T_h, else\ T_{he} = T_e$$

Energy, Q

$$dQ_k = \frac{C_v V_k dP}{R} - C_p(T_{ck}\dot{m}_{ck} - T_k\dot{m}_{kr})$$

$$dQ_r = \frac{C_v V_r dP}{R} - C_p(T_k\dot{m}_{rir} - T_h\dot{m}_{rro})$$

$$dQ_h = \frac{C_v V_h dP}{R} - C_p(T_h\dot{m}_{rh} - T_{he}\dot{m}_{he})$$

$$dQ_a = \frac{C_v V_a dP}{R} - C_p T_e \dot{m}_{ea}$$

Work, W

$$dW = dW_c + dW_e$$

$$W = W_c + W_e$$

Subscripts

c – compression space

k – cooler

ri – cooler-regenerator manifold

r – regenerator

ro – regenerator-heater manifold

h – heater

e – expansion space

a – appendix gap

ck – compression space to cooler

kr – cooler to cooler-regenerator manifold

rir – cooler-regenerator manifold to regenerator

rro – regenerator to regenerator-heater manifold

rh – regenerator-heater manifold to heater

he – heater to expansion space

ea – expansion space to appendix gap

APPENDIX B

Parameter	Value
connecting rod length (m)	4.600e-002
eccentricity (m)	2.080e-002
crank radius (m)	1.380e-002
piston diameter (m)	6.990e-002
piston length (m)	5.370e-002
compression clearance volume (m^3)	21.47e-006
expansion clearance volume (m^3)	21.04e-006
buffer space volume (m^3)	400.0e-006
cylinder wall thickness (m)	3.800e-003
displacer length (m)	4.350e-002
displacer rod diameter (m)	0.952e-002
displacer wall thickness (m)	1.590e-003
cylinder bore clearance (m)	1.000e-004
appendix gap width (m)	2.500e-004
cooler inner pipe diameter (m)	1.080e-003
cooler heat transfer length (m)	3.550e-002
cooler total pipe length (m)	4.610e-002
number of cooler tubes	312
regenerator housing outer diameter (m)	2.646e-002
regenerator housing inner diameter (m)	2.260e-002
regenerator length (m)	2.260e-002
number of regenerators	8
cooler-to-regenerator manifold length (m)	0.0807e-002
regenerator-to-heater manifold length (m)	0.2293e-002
regenerator void volume (m^3)	5.030e-006
regenerator matrix void factor	0.697
wire diameter (m)	4.000e-005
heater tube inner diameter (m)	3.020e-003
heater heat transfer length (m)	15.54e-002
heater total pipe length (m)	24.53e-002
number of heater tubes	40
preheater height (m)	0.094
preheater thickness (m)	0.035
preheater center diameter (m)	0.232

Table B1
GPU-3 Engine Dimensions

APPENDIX C

Parameter	Value
connecting rod length (m)	4.600e-002
eccentricity (m)	2.080e-002
crank radius (m)	1.380e-002
piston diameter (m)	10.870e-002
piston length (m)	5.370e-002
compression clearance volume (m^3)	21.47e-006
expansion clearance volume (m^3)	202.50e-006
cylinder wall thickness (m)	3.800e-003
displacer length (m)	4.350e-002
displacer rod diameter (m)	0.952e-002
displacer wall thickness (m)	1.590e-003
cylinder bore clearance (m)	1.000e-004
appendix gap width (m)	2.500e-004
cooler inner pipe diameter (m)	1.080e-003
cooler heat transfer length (m)	9.000e-002
cooler total pipe length (m)	10.060e-002
number of cooler tubes	752
regenerator housing outer diameter (m)	6.140e-002
regenerator housing inner diameter (m)	5.740e-002
regenerator length (m)	2.260e-002
number of regenerators	8
cooler-to-regenerator manifold length (m)	0.0807e-002
regenerator-to-heater manifold length (m)	0.2293e-002
regenerator void volume (m^3)	5.030e-006
regenerator matrix void factor	0.697
wire diameter (m)	4.000e-005
heater tube inner diameter (m)	3.020e-003
heater heat transfer length (m)	26.00e-002
heater total pipe length (m)	40.08e-002
number of heater tubes	90

Table C1
Final Engine Dimensions

REFERENCES

REFERENCES

1. Andersen, S.K., Carlsen, H., and Thomsen, P.G. 2006. Control volume based modeling in a one space dimension of oscillating, compressible flow in reciprocating machines. *Simulation Modelling Practice and Theory*. 14. 1073-1086.

2. Bailey, P.B., Dadd, M.W., Reed, J.S., and Stone, C.R. 2007. Gas Spring Losses in Linear Clearance Seal Compressors. *Int. Cryocooler Conf. Cryocoolers* 14. 345-352.

3. Baumüller, A., Lundholm, G., Lundström, L., and Schiel, W. 1999. The Development History of the V 160 and SOLO Stirling 161 Engines. *Proc. 9th ISEC,* 23-32.

4. Chen, J., Yan, Z., Chen, L., and Andresen, B. 1998. Efficiency Bound of a Solar-Driven Stirling Heat Engine System. *Int. J. Energy Res*. 22. 805-812.

5. Choudhary, F. 2009. Dynamics of Free Piston Stirling Engines. MS Thesis. University of Maryland.

6. Cleanergy, 2014. http://cleanergy.com/.

7. Cullen, B. 2011. The Combined Otto and Stirling Cycle Prime-Mover-Based Power Plant. PhD Thesis. Dublin Institute of Technology.

8. Demko, R. and Penswick, L.B. 2005. Sage Simulation Model for Technology Demonstration Convertor by a Step-by-Step Approach. *3rd International Energy Conversion Conference.*

9. Dyson, R.W., Wilson, S.D., Tew, R.C., and Demko, R. 2005. Fast Whole-Engine Stirling Analysis. NASA-TM-2005-213960.

10. Easterly, J.L. and Burnham, M. 1996. Overview of Biomass and Waste Fuel Resources for Power Production. *Biomass and Bioenergy*, 10(2-3):79-92.

11. Eid, E. 2009. Performance of a beta-configuration heat engine having a regenerative displacer. *Renewable Energy*. 34. 2404-2413.

12. Ernst, W.D. and Shaltens, R.K., 1997. Automotive Stirling Engine Development Project. NASA CR-190780.

13. Ferreira, S.B. and Pilidis, P. 2001. Comparison of Externally Fired and Internal Combustion Gas Turbines Using Biomass Fuel. *J. Energy Res. Tech.* 123:291-296.

14. Finkelstein, T. 1959. Air Engines. *The Engineer*. 207. 522-527 and 720-23.

15. Finkelstein, T. 1960. Generalized Thermodynamic Analysis of Stirling Engines. SAE Paper 118 B.

16. Finkelstein, T. and Organ, A. J. 2001. Air Engines. The History, Science, and Reality of the Perfect Engine. ASME Press, New York.

17. Fraser, P.R. 2008. Stirling Dish System Performance Prediction Model. Masters Thesis. University of Wisconsin, Madison.

18. Gaderer, M., Gallmetzer, G., and Spliethoff, H. 2010. Biomass Fired Hot Air Gas Turbine With Fluidized Bed Combustion. *J. Applied Thermal Energy.* 30:1594-1600.

19. Gedeon, D. 2012. Sage Software for Engineering Modeling and Optimization. http://www.sageofathens.com/.

20. Geng, S.M. and Tew, R.C. 1992. Comparison of GLIMPS and HFAST Stirling Engine Code Predictions With Experimental Data. *Proc. 27th IECEC.*

21. Graves, R.E., and Argrow, B.M. 1999. Bulk Viscosity: Past to Present. *J. Thermophysics and Heat Transfer*, 13(3) 337-342.

22. Hargreaves, C.M., 1991. The Philips Stirling Engine. Elsevier, New York.

23. Howard, D., and Harley, R. 2010. Modeling of dish-Stirling solar thermal power generation. *Power and Energy Society General Meeting*, *IEEE*

24. Incropera, F.P., and DeWitt, D.P. 1990. Introduction to Heat Transfer. 2nd Ed. John Wiley & Sons, New York.

25. Johnson, D.C., Congdon, C.W., Begg, L.L., Britt, E.J., and Thieme, L.G. 1981. Jet Impingement Heat Transfer Enhancement for the GPU-3 Stirling Engine. NASA-TM-82727.

26. Ju, Y., Jiang, Y., and Zhou, Y. 1998. Experimental study of the oscillating flow characteristics for a regenerator in a pulse tube cryocooler. *Cryogenics* 38(06) 649-656.

27. Kang, M.C., Kang, Y.H., Kim, J.H., Kim, J.S., Kim, N.J., and Yoo, S.Y. 2009. An experimental study on the heat transfer characteristics of the hybrid solar receiver for a dish concentrating system. *Proc. ISES World Congress 2007 Vol.I-Vol.V,* 689-693.

28. Kays, W.M. 1950. Loss Coefficients for Abrupt Changes in Flow Cross Section With Low Reynolds Number Flow in Single and Multiple-Tube Systems. *Trans. ASME* 72:1067-1074.

29. Kays, W., Crawford, M., and Weigand, B. 2005. Convective Heat and Mass Transfer. 4th Ed. McGraw-Hill. New York.

30. Kays, W., and London, A.L. 1964. Compact Heat Exchangers. 2nd Ed. McGraw-Hill. New York.

31. Kibaara, S., Chowdhury, S., and Chowdhury, SP. A Thermal Analysis of Parabolic Trough CSP and Biomass Hybrid Power System. 2012 *Proc. IEEE PES*. 1-6.

32. Lee, C.E., Lee, S.R., Han, J.W., and Park, J., 2001. Numerical Study on effect of CO_2 addition in flame structure and NO_x formation of CH_4-air counterflow diffusion flames. *Int. J. Energy Res*., 25:343-354.

33. Liao, W. 2012. A Self-Sustaining Solar-Bio-Nano Based Wastewater Treatment System for Forward Operating Bases. Michigan State University. Presentation.

34. Mancini, T., Heller, P., Butler, B., Osborn, B., Schiel, W., Goldberg, V., Buck, R., Diver, R., Andraka, C., and Moreno, J. 2003. Dish-Stirling Systems: An Overview of Development and Status. *Journal of Solar Energy Engineering*. 125. 135-151.

35. Martini, W.R. 1983. Stirling Engine Design Manual, 2nd Ed. NASA CR-168088. DOE/NASA, Washington D.C.

36. NASA Chemical Equilibrium with Applications (CEA). 2014. http://www.grc.nasa.gov/WWW/CEAWeb/

37. Nepveu, F., Ferriere, A., and Bataille, F. 2009. Thermal model of a dish/Stirling systems. *Solar Energy*. 83. 81-89

38. Organ, A.J. 1978. Mechanical Efficiency of the Stirling Cycle Machine with Rhombic Drive. *Proc. 13th Intersociety Energy Conversion Engineering Conference* 1841-1852.

39. Organ, A.J. 1982. Gas Dynamics of the Temperature Determined Stirling Cycle. *Journal Mech. Eng. Science*, 23(04), 207-216.

40. Organ, A.J. 1997. The Regenerator and the Stirling Engine. Mechanical Engineering Publications Ltd, London.

41. Organ, A.J. 2000. Stirling's air engine – a thermodynamic appreciation. *Journal Mech. Eng. Science*, 234(C4), 511-536.

42. Pålsson, M. and Henrik, C., 2003. Development of a Wood Powder Fuelled 35 kW Stirling CHP Unit. *Proc. 11th Int. Stirling Engine Conf.*, 221-230.

43. Pfeiffer, J. and Kuehl, H.D. 2014. Review of Models for Appendix Gap Losses in Stirling Cycle Machines. *J. Propulsion Power*, 30(5): 1419-1432.

44. Poloni, M, Winterbone, D.E., and Nichols, J.R. 1987. Comparison of Unsteady Flow Calculations in a Pipe by the Method of Characteristics and the Two-Step Differential Lax-Wendroff Method. *Int. J. Mech. Sci.*, 29(05), 367-378.

45. Potter, M.C. and Foss, J.F. 1982. Fluid Mechanics. Great Lakes Press, Inc, Okemos, MI.

46. Reinalter, W., Ulmer, S., Heller, P., Rauch, T., Gineste, J.-M., Ferriere, A., and Nepveu, F. 2006. Detailed performance analysis of the 10kW CNRS-PROMES dish/stirling system. *13th SolarPACES International Symposium*.

47. Rogdakis, E.D., Antonakos, G.D., and Koronaki, I.P., 2012. Thermodynamic Analysis and Experimental Investigation of a Solo V161 Stirling Cogeneration Unit. *Energy* 45. 503-511.

48. Saab AB, 2014. http://www.saabgroup.com/kockums.

49. Schmidt, G. 1871. Theorie der Lehmannschen calorischen Maschine. *Zeit. Des Vereins deutscher Ing*. 15. 1-12 (January), 98-112 (February).

50. Senft, J.R. 1993. Ringbom Stirling Engines. Oxford University Press, New York

51. Tew, R.C. and Ibrahim, M.B. 2001. Study of Two-Dimensional Compressible Non-Acoustic Modeling of Stirling Machine Type Components. *Proc. 36th IECEC*.

52. Thieme, L.G. 1979. Low-Power Baseline Test Results for the GPU-3 Stirling Engine. NASA-TM-79103.

53. Thieme, L.G. 1981. High-Power Baseline and Motoring Test Results for the GPU-3 Stirling Engine. NASA-TM-82646.

54. Timoumi, Y. Tlili, I. and Nasrallah, S.B. 2007. Design and performance optimization of GPU-3 Stirling Engines. *Energy* 33. 1100-1114.

55. Tlili, I. 2011. Numerical Model for Predicting Thermodynamic Cycle and Thermal Efficiency of an Alpha-type Stirling Engine with Ross Yoke Mechanism. *SATRESET* 1(3) 102-115.

56. Turns, S. 2000. An Introduction to Combustion. 3rd Ed. McGrall Hill, New York.

57. Urieli, I. and Berchowitz, D.M. 1984. Stirling Cycle Engine Analysis. Adam Hilger Ltd, Bristol.

58. Urieli, I. 2012. Stirling Cycle Machine Analysis. http://www.ohio.edu/mechanical/stirling/me422.html. Ohio University.

59. Walker, G. 1973. Stirling-cycle machines. Clarendon Press, Oxford.

60. Walker, G. 1979. Elementary Design Guidelines for Stirling Engines. *Proc. 14th IECEC*.

61. Walker, G. and Senft, J.R. 1985. Free Piston Stirling Engines. Springer-Verlag, Berlin.

62. Walker, G., Reader, G., Fauvel, O.R., and Bingham, E.R. 1994. The Stirling Alternative. Gordon and Breach, Yverdon, Switzerland.

63. West, C.D. 1981. Theoretical Basis for the Beale Number. *Proc. 16th IECEC*.

64. West, C.D. 1986. Principals and Applications of Stirling Engines. Van Nostrand Reinhold Company, Ltd, New York.

65. Wiltsee, G.A. Jr, Easterly, J., Vence, T. *et al*. 1993. Strategic Analysis of Biomass and Waste Fuels for Electrical Power Generation. Electric Power Research Institute, EPRI-TR-10277.

66. Yaqi, L., Yaling, H., and Weiwei, W. 2011. Optimization of solar-powered Stirling heat engine with finite-time thermodynamics. *Renewable Energy*. 36. 421-427.

67. Zhao, D., Yamashita, H., Kitagawa, K., Arai, N., and Furuhata, T. 2002. Behavior and Effect of NO_x Formation of OH Radical in Methane-Air Diffusion Flame with Steam Addition. *Combustion and Flame*, 130:352-360.